# Geochemical Characterization and Assessment of Stabilization Mechanisms for Mercury-Contaminated Riverbank Sediments from the South River, Virginia (USA)

by

Krista Desrochers

A thesis
presented to the University of Waterloo
in fulfillment of the
thesis requirement for the degree of
Master of Science
in
Earth Sciences

Waterloo, Ontario, Canada, 2013

## AUTHOR'S DECLARATION

I hereby declare that I am the sole author of this thesis.

This is a true copy of this thesis, including any final required revisions, as accepted by my examiners.

I understand that this thesis may be made electronically available to the public.

Krista Desrochers

# ABSTRACT

Elevated concentrations of mercury (Hg) in aquatic systems can be a threat to ecosystems and human health. Mercury-bearing sediment particles from eroding riverbanks can be an ongoing source of bioavailable Hg to aquatic ecosystems. Hyporheic zones in particular can be important sources of both inorganic and organic-complexed Hg, which can be rapidly transported to adjacent surface waters. The objective of this study was to investigate the release and treatment of dissolved and particle-bound Hg in water derived from the riverbank sediments of the South River, Virginia. The solid-phase forms of Hg in riverbank sediment samples were characterized by sequential extraction and synchrotron based techniques. The analyses suggest that 79-93% of Hg in the sediment samples is in the form of insoluble sulfides (βHgS metacinnabar); however significant masses of more-soluble Hg phases (0.4-33 μg $g^{-1}$) are also present.

Simulated erosion events resulted in elevated concentrations of Hg in the river water up to 80 μg $L^{-1}$. There was no correlation between the mass of water-soluble Hg in the sediment and the concentrations of Hg released in the river water following sediment suspension. Column transport experiments were conducted to assess Hg release from the sediment under water:sediment ratios typical of those that might occur at the bottom or in the banks of the river. Concentrations of Hg in the 0.45 μm-filtered fraction of the effluent varied from 0.15 μg $L^{-1}$ for samples collected from the base of the riverbank to 8 μg $L^{-1}$ for samples collected from the top of the riverbank. Filter size-fractionation of water column effluent suggested approximately 50% of the leached Hg was present in the dissolved phase, with the remainder in particulate form.

Riverbank sediments were amended with various types of reactive material including complexing agents, reductants and charcoals. Batch experiments indicate that the mass of Hg released from the sediment could be lessened by 64-99% with the addition of reactive media, and that aerating and re-wetting the sediment amendments resulted in equal or greater removal of Hg from the water. The greatest

removal of Hg was observed when more amendment was added to the sediment, however the greatest Hg uptake capacity (Hg captured per mass of material) was observed for the lowest doses of reactive media. The Hg uptake capacities ranged from 35-500 ng $g^{-1}$ and were greatest for treatment of water with elevated concentrations of Hg. The Hg uptake capacities were a function of the Hg concentrations in the untreated water, and were generally lower relative to values reported in the literature.

Column studies were used to simulate the flow of river water containing elevated concentrations of Hg through a reactive zone containing a charred hardwood material. The concentration of filtered Hg was < 120 ng $L^{-1}$ for treated effluent from columns, resulting in > 98% removal of Hg from the water. Assuming that the majority of removal occurred within the initial 2-3 cm along the length of the column, the calculated uptake of $Hg^{2+}$ ranged from 1.2-7.7 μg $g^{-1}$. The uptake capacity for charred hardwood material was much greater for the column experiments relative to the batch experiments, suggesting that the uptake capacity is limited by Hg loading. The chemical composition of the treated column effluent was similar to the South River water, and suggests the material did not add or remove significant constituents during the course of these experiments.

# ACKNOWLEDGEMENTS

I would like to give many thanks and my sincerest appreciation to my thesis advisor and mentor, Dr. Carol Ptacek. Your guidance and support over the past few years was invaluable, and I am very grateful to have had the opportunity to study under your supervision. I would also like to extend my thanks and appreciation to Dr. David Blowes, for sharing your valuable input, and occasional comic relief. I would also like to thank Doug Gould, for his insight into this thesis.

I would like to extend my appreciation to Richard Landis, James Dyer, William Berti and Nancy Grosso for their interest and support in this research project, and for their enthusiastic encouragement along the way. Many thanks to all of the members of the GGR Group, especially those who contributed to this research including Blair Gibson, Matthew Lindsay, Peng Liu, Laura Groza, Jeff Bain, Krista Paulson, Alana Wang, and James Tordiff. Special thanks to friends for sharing your own experiences, especially Brenda Bailey, Julia Jamieson-Hanes, Stacey Hannam, Corina McDonald, Nicholas Flinn, Jutta Hoppe, Lionel Sequeira and Heather Shrimpton.

I would like to extend my sincerest gratitude to my family and friends for all of their love and support. Greatest thanks to my loving husband, David, for your friendship, patience, and encouragement.

Funding for this research was provided by NSERC Canada and E.I. du Pont De Nemours and Company. Synchrotron-based techniques were performed at GeoSoilEnviroCARS, Advanced Photon Source, Argonne National Laboratory, on beamline 13BMD.

# DEDICATION

For David.

# TABLE OF CONTENTS

# LIST OF TABLES

# LIST OF FIGURES

# LIST OF ABBREVIATIONS

| | |
|---|---|
| ATP | Attapulgite clay |
| CL2 | Hardwood charcoal |
| CSE | Chemical sequential extraction |
| CVAFS | Cold vapour atomic fluorescence |
| DI | Deionized water |
| DOM | Dissolved organic matter |
| EPA | Environmental Protection Agency |
| GAC | Granular activated carbon |
| IC | Ion chromatography |
| ICP-MS | Inductively Coupled Plasma Mass Spectrometer |
| IRB | Iron reducing bacteria |
| MeHg | Methyl mercury |
| MRM | Organically modified bentonite clay |
| MWCO | Molecular weight cut-off |
| PV | Pore volume |
| rpm | Rotations per minute |
| RRM | Relative river mile |
| S | Elemental sulfur |
| SR | South River |
| SRB | Sulfur reducing bacteria |
| SRW | South River water |
| TEA | Terminal electron acceptor |
| THg | Total mercury |
| Thiol II | 2,5-dimercapto-1,2,4-thiadiazole |
| XANES | X-ray absorption near edge structure |
| XAS | X-ray adsorption spectroscopy |
| XRF | X-ray Fluorescence |
| ZVI | Zero-valent iron |
| $\theta$ | Theta; moisture content |

# Chapter 1: *Introduction*

## *1.1 Introduction*

Mercury (Hg) is a hazardous environmental contaminant, and can exist in three forms in the natural environment: elemental ($Hg^0$), organic, and inorganic ($Hg^{2+}$, $Hg^{1+}$). The valance state of $Hg^{2+}$ is the most common form in both free form and in complexes including chlorides, sulphides, and dissolved organic matter (Morel et al., 1998). The organic forms of Hg, methylmercury or dimethylmercury (MeHg), are lipid soluble, allowing these forms to cross biological membranes. Elevated levels of MeHg in surface water can result in accumulation in low trophic-level organisms such as phytoplankton and zooplankton, and can magnify up the food chain. Mercury is primarily a neurotoxin (Clarkson & Magos, 2006), but can also cause biochemical, enzymatic, immunological, genetic, and reproductive effects on biota, and is particularly harmful to the development of human embryos and fetuses.

Bioaccumulation of Hg in the food chain is dependent on the availability of Hg to biota as a result of absolute Hg methylation rates (methylation and demethylation processes). The extent of MeHg formation is dependent on the physiochemical properties of the Hg species, and the availability/solubility of the Hg to potentially methylating bacteria (primarily sulfur and iron reducing bacteria). Less soluble Hg complexes (such as mercuric sulfides) may also be available for methylation (Drott et al., 2007, Benoit et al., 2001).

There are many sources that contribute to elevated Hg concentrations in aquatic environments, including atmospheric deposition, degassing from natural mineral deposits, erosion of Hg-bearing rock and sediments, agricultural use of pesticides and fungicides, as well as industrial releases including mining, chlor-alkali, pulp and paper, coal and oil combustion (Fitzgerald and Lamborg, 2003). However, industrial activities have greatly contributed to increased Hg accumulation in soils and sediment within the past 100 years. Mercury has a strong affinity for organic matter and sulphur functional groups, and

often accumulates in the organic-rich upper layer of the soil horizon (Schuster, 1991). Due to the association of Hg with soil particles, erosion of Hg contaminated sediments and soils can be a dominant mode of entry of Hg to aquatic systems (Gabriel & Williamson, 2004).

### *1.2 Site description*

The study area encompasses approximately 3.5 km of riverbank adjacent to the South River near Waynesboro, Virginia, USA (Figure 1.1). The South River is a tributary to the headwater of the South Fork of the Shenandoah River which flows northeast within the Shenandoah Valley of Augusta County. The geologic material in the study area consists of Cambrian carbonate rocks, sandstone, quartzite and shale. The average width of the river is approximately 26 m and the average depth of the riverbank is approximately 1.9 m (Pizzuto, 2012). The South River contains elevated concentrations of Hg in the sediments and floodplain soils as a result of historical industrial operations. A textile manufacturing facility in Waynesboro utilized Hg-$SO_4$ as a catalyst for the production of acetate fibers. Thousands of kilograms of Hg were released into the soil, sewer system, groundwater and river water between 1929 and 1950 (Carter, 1977). Elevated concentrations of Hg are now observed in the riverbanks and floodplain soils up to 25 miles downstream from the point source, with the most elevated concentrations within 5 miles of the historical plant release site. Monitoring of concentrations of Hg in fish species has shown no decrease in the past 30 years (Wang et al., 2004).

Current studies have suggested that frequent inundations of the riverbanks and regular erosion events are a potential source of Hg and Hg-bound particulates to the river water (Pizzuto, 2012, Flanders et al., 2010, Rhoades et al., 2009). During periods of flooding, river water can overtop the banks of the South River and Hg can be deposited on floodplain soils. Contaminated floodplain soils can also be transported back into the river via bank erosion processes. Additionally, a rise in river level can result in water infiltrating a previously unsaturated region, which may not exhibit the same Hg removal properties as the permanently saturated sediment, resulting in release of Hg into the river

### *1.3 Research objectives*

The primary objectives of this research is to enhance the understanding of the solid-phase composition and geochemical characteristics of Hg in riverbank sediments collected from the South River, near Waynesboro, Virginia. Stored Hg in the riverbank sediments can be remobilized during storm driven runoff events, and may lead to elevated sediment transport and a continuing source of contamination to the river system. To effectively apply mitigation measures to reduce the overall Hg load into the river, the physical and chemical properties of the contaminant must be understood. The specific objectives of this thesis include:

- Characterize the geochemical associations of Hg in the sediment,
- Understand the role of particle-size Hg transport,
- Investigate the potential for Hg stabilization/immobilization by amending sediment with a variety of reactive materials.

### *1.4 Thesis organization*

This thesis is presented as two research papers related to the described research objectives. The first paper, presented in Chapter 2, describes the solid-phase characterization of Hg in the riverbank sediment samples, and results of batch and column experiments conducted to evaluate Hg release from the sediment. The second paper, presented in Chapter 3, describes a series of batch and column experiments to determine the effect of reactive amendments on the release of Hg from sediment.

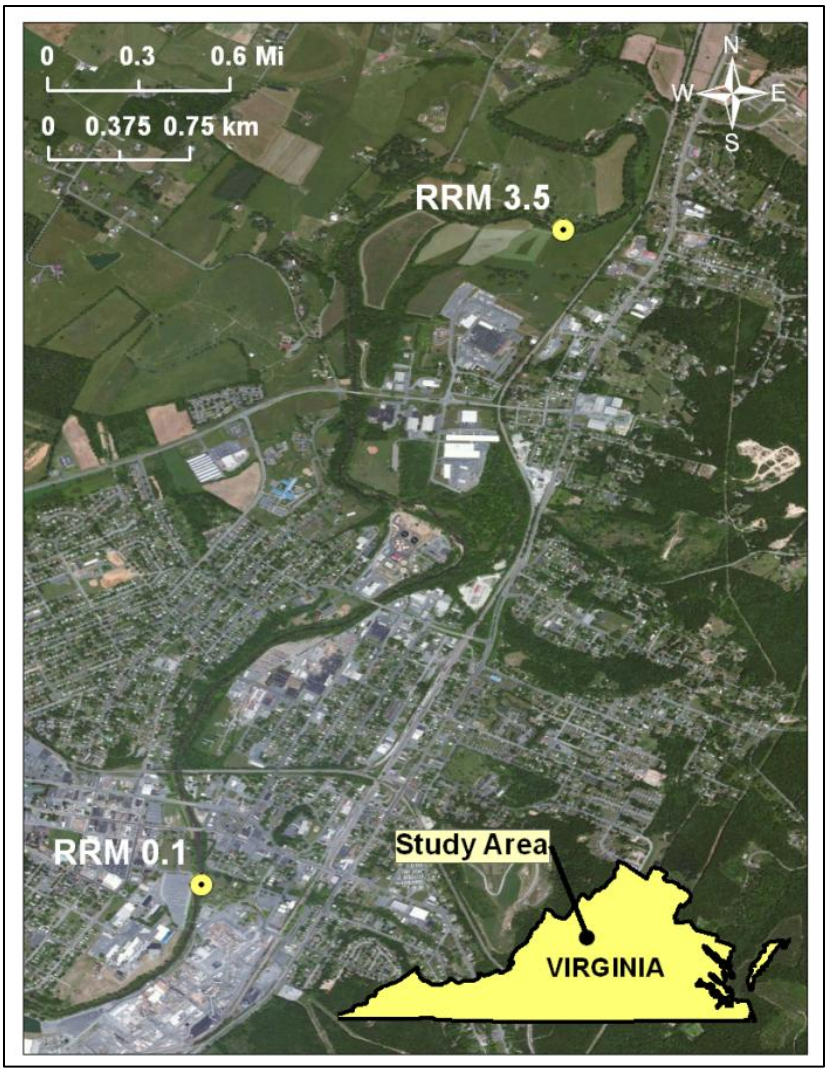


**Figure 1.1:** Study area near Waynesboro, Virginia

# **Chapter 2:** *Transformation of Hg-species in the hyporheic zone of the South River, Virginia*

## *2.1 Introduction*

The chemistry of mercury (Hg) in the natural environment is complex and difficult to predict under variable geochemical conditions and in the presence of organic matter. Sediments can act as both sources and sinks for Hg, depending on temporal changes in physical and geochemical conditions. Hyporheic zones are important for mediating exchange processes between surface water and groundwater, and are located beneath and immediately adjacent to the river channel. Metal-bearing sediment in the hyporheic zone of a river can be affected by physical and chemical changes, which may lead to the release of dissolved and colloidal Hg from sediments to the water phase. Under fluctuating hydraulic gradients, rivers can alternate from influent and effluent streams at differing locations along the flow path depending on seasonal effects. Therefore, contaminated sediment in the hyporheic zone can act as an ongoing, long-term source of bioavailable Hg to aquatic ecosystems (Ullrich et al., 2001). The storage and transport of Hg in hyporheic sediment is not well understood, and is complicated in river systems that are dominated by bank erosion and elevated hyporheic zone water flux (Heaven at al., 2000, Rhoades et al., 2009). To understand the complex (bio)geochemical cycling of Hg in river systems, a detailed understanding of Hg sorption, complexation and redox mechanisms contributing to the release of Hg from hyporheic sediments is needed.

The formation of methyl-Hg (MeHg) is a major concern due to its accumulation within the food chain, and can result in detrimental neurotoxic effects when consumed (Clarkson & Magos, 2006). The biological availability of Hg is largely dependent on the speciation and association of Hg with hydrophobic methyl compounds (Compeau & Bartha, 1985). The formation of organic MeHg is an anaerobic process which can occur in deep saturated soil, aquatic bottom sediment and anoxic waters (Morel et al., 1998, Benoit et al., 2002). River reaches with stagnant water and organic rich sediments are

potential sites for microbial methylation of Hg (Benoit et al., 1998); a process which primarily occurs in the presence of dissimilatory sulfate and iron reducing bacteria (Gilmour et al., 2012).

Seasonal flooding events can lead to the inundation of riverbanks and floodplain soils, and may generate favorable conditions for the formation of organic mercury compounds. Frequently flooded organic rich soil and sediment can result in fluctuating geochemical conditions and microbial populations within the sediment porewater. Depending on the mineralogy of the sediment, the alteration of redox conditions can also result in increased inorganic metal mobility and transport of soluble, colloidal or particulate Hg compounds into the adjacent river water. Geochemical characterization of contaminated riverbank sediments, and study of sediment leaching under resuspension and flushing conditions, can aid in the understanding of Hg-release from hyporheic sediments as an approach to managing the overall biological uptake of Hg down river.

The contribution of particulate (>0.45 µm) and dissolved (<0.45 µm) distribution of Hg within a river setting are thought to correlate with transport distance and bioavailability downstream (Slowey et al., 2005). Particulate-bound Hg has been identified as the primary mode of transport of Hg to aquatic environments (Choe et al., 2003). Through column transport experiment, Lowry et al. (2004) demonstrated that the majority of mobilized Hg from sediment consisted of sub-micrometer sized particles. The large surface area of colloidal particles can serve as Hg-sorption sites. However, colloidal-bound Hg can also be an important transport mechanism when sediment is eroded or resuspended, and can be deposited in methylating zones where transformations are ideal for biological uptake (Slowey et al., 2005, Babiarz et al., 2001).

### *2.1.1 Site description*

Experiments were conducted using sediment from the riverbank and water from the South River near Waynesboro, Virginia. The South River is a tributary to the headwater of the South Fork of the Shenandoah River which flows northeast within the Shenandoah Valley of Augusta County. The geologic

material in the study area consists of Cambrian carbonate rocks, sandstone, quartzite and shale. The South River is surrounded by forested (~60%) and agricultural (~25%) land, and small urban developments (~15%) (VADEQ, 2009). Near Waynesboro, VA, the South River has an average discharge of 4.2 +/- 1.8 $m^3$ $s^{-1}$ (USGS, National Water Information System, 2012). The mean monthly temperature ranges from 2.2-25.6 $^oC$, and the average annual precipitation is 9.9 cm (NOAA, 2012).

The historical point source of Hg is located in Waynesboro, Virginia, 39 km upstream of the confluence of the South River with the South Fork Shenandoah River. A textile manufacturing facility in Waynesboro utilized Hg-$SO_4$ as a catalyst in the manufacturing of Rayon$^{TM}$ fibers. Recovery of the catalyst was incomplete, with approximately 30% loss to the environment. As a result, thousands of kilograms of Hg were released into the soil, sewer system, groundwater and river water between 1929 and 1950 (Carter, 1977). Sediments and particulate matter were transported downstream and deposited in the banks and floodplain soils of the South River (Rhoades, O'Neal & Pizzuto, 2009). Historical sediment deposition rates in the South River were relatively high due to the presence of mill-dams and regional deforestation from agricultural land development. After 1957, many of the mill-dams along the river were breached resulting in increased rates of sediment erosion (Pizzuto & O'Neal, 2009). As a result, Hg-bearing sediment and soil was transported over time to distances up to 40 km downstream of the original point source. The concentrations of filtered inorganic Hg in the South River surface water ranged from <1 ng $L^{-1}$ up to 13 ng $L^{-1}$, with the greatest concentrations detected at 12-13 km downstream from the point source (Flanders et al., 2010). Surface water MeHg concentrations are consistently below 2 ng $L^{-1}$.

The storage and redistribution of Hg within the riverbank sediment is complex, and may be dominated by bank erosion processes and riverbed flux of particle-bound Hg (Flanders et al., 2010). In addition to sediment erosion inputs, the riverbanks are likely affected by advective transport processes (Rhodes et al., 2009), however exact pathways of contaminant transfer and transport are currently unknown. The accumulation of Hg-bearing, fine-grained sediment particles in near-bank areas, sand, gravel and cobble beds within the river channel, may be providing a sustained source of dissolved and

colloidal Hg that is available for uptake within the biological community. Frequent inundations of the riverbanks during flooding and storm events may be a contributing factor to the influx of dissolved and particulate Hg into the river system, resulting in sustained concentrations of Hg in the fish populations over the past 30 years.

### *2.1.2 Objectives*

The objectives of this study were to characterize the solid-phase composition and forms of Hg in bank sediments at two locations along the South River, Virginia using sediment digestion, chemical sequential extraction and X-ray absorption spectroscopy techniques. The potential for the release of Hg from riverbank sediments was assessed by simulating sediment resuspension events likely to occur as a result of riverbank erosion. Column transport experiments were used to assess the potential for Hg leaching under flow conditions representative of groundwater flow within the bank sediments. The flow rate through the columns was modified to simulate variations in hyporheic zone flow. Combined, this information will contribute to an improved understanding of the potential for Hg release under variable flow conditions to assist in development of remedial options for the South River, Virginia.

## *2.2 Methodology*

### *2.2.1 Sediment and water collection*

River bank sediment was collected along transects perpendicular to river flow at two locations on the river (Figure 2.1). Approximately 4-5 L of bank sediment was manually collected. Bank sediments were extracted horizontally from the edge of the bank surface towards the floodplain (SR2, SR3, SR4, SR5, SR6, SRC, SRD, SRE, SRF). River bottom samples were collected using vertical sediment cores (SR1, SRA, SRB). The riverbank samples were collected in May 2009 for samples extracted from the transect located approximately 0.1 relative river miles from the source zone (RRM 0.1), and the sediment collected at transect RRM 3.5 were extracted in Sept 2010. The sediment was shipped to the University of

Waterloo in Waterloo, ON Canada and was immediately refrigerated at 4 $^{o}$C. Dry sediment was considered oxic (RRM 0.1 SR4, SR5, SR6 and RRM3.5 SRD, SRF, SRE) and was individually homogenized by manual mixing under atmospheric conditions. Wet sediment was considered suboxic (RRM 0.1 SR1, SR2, SR3 and RRM3.5 SRA, SRB, SRC) and was homogenized within an anaerobic chamber (5% $H_2$ / 95% $N_2$). All storage containers were wrapped in aluminum foil and stored at 4 $^{o}$C.

The experiments were performed using water from the South River (SRW). The SRW was collected up-stream (approximately 0.2 miles) from the initial point source plant site. The containers of SRW were packed in ice and immediately shipped to the University of Waterloo, and were stored in dark conditions at 4 $^{o}$C. Concentrations of major and minor constituents were monitored frequently, including concentrations of Hg, to document any minor fluctuations in river water chemistry over time (Table 2.1).

### *2.2.2 Chemical and mineralogical analysis of sediments*

Total carbon and total sulfur were measured using an Eltra CS 2000 Carbon Sulfur Determinator at the University of Waterloo. A subset of each sediment sample was oven dried at 80 $^{o}$C and analysed in triplicate. The analyses were performed at 900 $^{o}$C using a CS-800 induction furnace. A subset of air-dried sediment samples was digested in aqua regia to determine the total elemental concentrations. The resultant digestate was determined by ICP-MS (EPA Method 3050b) by SGS Lakefield Laboratories, Lakefield, ON, Canada. Chemical sequential Hg extractions were performed following the procedure developed by Bloom et al. (2003) to selectively separate specific Hg compounds in the sediment. The following extraction steps were applied; F1) deionized water, F2) pH 2 HCl/$CH_3COOH$, F3) 1N KOH, F4) 12N $HNO_3$, and F5) aqua regia. Sediment digestate was analyzed using cold vapour atomic fluorescence spectroscopy (CVAFS) at Frontier Global Sciences, Seattle, WA. Particle-size distribution was determined by a combination of dry sieve and laser diffraction methods. Samples ranging from 100-130 g of air-dried sediment were processed by mechanical shaker for 30 minutes and passed through a

nested column of 7 sieve sizes. Sediment grains less than 2 mm in size were then analysed via laser diffraction by Analysette 22 NanoTec Plus (Fritsch, Germany) at the University of Waterloo.

Sediment samples were prepared as thin sections (30 μm) that were polished without water to prevent the dissolution of soluble phases in the sediment (Vancouver Petrographics, Langley, B.C.). Synchrotron-based techniques were performed at the Advanced Photon Source at the Argonne National Laboratory (Argonne, IL).The RRM 0.1 transect sediment was selected for synchrotron radiation micro X-ray absorption near edge structure (μXANES) and micro X-ray Fluorescence (μXRF) analyses. Samples and reference materials were analyzed on GSECARS beamline 13-BM-D using Si (111) monochromator and 16 element Ge fluorescence detector. A focussed beam of 10x30 mm was used for μXRF and μXANES measurements on sediment thin sections.

### *2.2.3 Experimental setup*

#### *2.2.3.1 Sediment resuspension experiments*

A modified elutriate test protocol described in the EPA Inland Testing Manual was employed (US EPA, 1996) to determine the potential for Hg leaching as sediment erodes from the riverbanks into the river. Batch vessels were sealed and gently agitated on a shaker table at approximately 115 rotations per minute for 30 minutes. The aqueous supernatant was decanted and centrifuged at 5000 rpm for 15 minutes, collected in a sterile luer-lock syringe, and passed through sterile filters arranged in series consisting of 1mm prefilter and 0.45 μm cellulose acetate membrane filters (Supor®, Acrodisc, Ann Arbor, MI). Each batch contained 160 g of SRW mixed with moist sediment added as 4, 8, 16 and 40 g equivalent dry weight, represented as SRW:sediment ratios of 40:1, 20:1, 10:1 and 4:1. Replicate experiments were conducted to account for variability in concentration and/or leaching of Hg from the sediment. Individual batches were conducted in duplicate for 33% and in triplicate for 11% of all batch

experiments. The redox potential and pH (unfiltered) and the alkalinity, concentrations of Hg, anions, and major and trace elements (filtered) of the supernatant were monitored as a function of time.

*2.2.3.2 Column leaching experiments*

Column transport experiments were conducted to assess Hg release from the sediment under water:sediment ratios typical of those that might occur at the bottom or in the banks of the river. The sediment was wet-packed into acrylic columns that were 15 cm in length and 5 cm in diameter (total internal volume 273 $cm^3$) (Figure 2.2). At both ends of the columns a coarse-mesh nylon screen was placed on the outside and a 120 ASTM mesh nytex screen was placed towards the inside of the column. Silica sand was placed in 2 cm layers at the bottom and top of each column to serve as a filter to prevent transport of fine particles. The sediment samples collected from the RRM 0.1 bank locations were packed into four identical columns. Sediment pore volumes were calculated based on the dry bulk density of the sediment, and were determined to be 100.6, 86, 98 and 72 $cm^3$ for the column experiments packed with SR1, SR3, SR5 and SR6 sediments, respectively. All acrylic columns were wrapped in aluminum foil to limit photochemical processes and microbial growth.

River water was pumped using a high-precision peristaltic pump (Ismatec, Switzerland) in an upward direction through the column. Column flow rates were initially set at one pore volume per week (0.2 cm $d^{-1}$) to simulate slow transport processes, and increased to 3 pore volumes per week (0.7 cm $d^{-1}$). The column velocity was occasionally interrupted by controlled periods of stagnation and variation in flow rates. The column effluent was collected in a sealed cell to control the interaction of the atmosphere with the column effluent. The column effluent was collected and analysed for unfiltered particulate (> 0.45 μm), colloidal (<0.45 μm), dissolved (<0.1 μm) and ultrafiltration (<5000 molecular weight cutoff (MWCO)) filter fractions of Hg. Membrane fiber filters with a diameter of 35 mm were used for 0.45 μm and 0.1 μm filtration (Supor). Ultrafiltration was performed using a $N_{2(g)}$ pressurized head and orbital shaker with a 5000 MWCO membrane (Vivacell 70, Sartorius Stedman Biotech, NY).

### *2.2.4 Analytical methods*

Redox potentials were measured on unfiltered aqueous samples using an Orion Pt redox electrode (model 96-78BN), checked with Zobell's solution (Nordstrom, 1977) and Light's solution (Light, 1972). Redox measurements were corrected to the standard hydrogen electrode, and were reported as Eh values. The pH was measured using an Orion Ross combination electrode (model 8156000) calibrated with standard buffer solutions of pH 7, 4 and checked against pH 10. Measurements of alkalinity were made on 0.45 μm filtered samples using a HACH digital titrator and bromocresol green/methyl red indicator and with 0.16 N $H_2SO_4$.

Aqueous samples were collected in a sterile Luer-lock syringe and passed through sterile 0.45 μm filters (Supor® membrane fiber filters, VWR) unless otherwise indicated. All samples were stored at 4$^{o}$C until analysis. Cation concentrations were determined by inductively coupled plasma – optical emission spectroscopy (ICP-OES; Thermo Scientific iCAP 6000), and trace elements were determined by inductively coupled plasma mass spectrometry (Thermo Scientific XSeries 2) on samples preserved to pH<2 with trace metal grade $HNO_3$. Concentrations of inorganic anions were determined by ion chromatography (IC-OH: Dionex DX600 ED50, Sunnyvale, CA) on unacidified samples. Organic acids were determined on an IC using a IonPac AS17-C hydroxide-selective ion exchange column and were separated with a hydroxide gradient. Samples for MeHg were collected in trace-clean amber glass vials and acidified with Omni trace ultra high purity HCl (Baker Instra Analyzed), and THg samples were acidified with Ultra pure $HNO_3$ (EMD Chemicals) to a pH of < 2. Concentrations of methyl and total Hg were determined by cold vapor atomic fluorescence spectrometry (CVAFS Model 2500, Tekran Instruments Corp., Canada) following EPA methods 1630 and 1631, respectively. Concentrations of DOC were measured by OI Analytical 1030W following EPA method 415.3 oxidation with persulfate. Calculation of saturation indices were made using the geochemical equilibrium/mass-transfer code MINTEQA2 (Allison et al., 1990). Thermodynamic constants in the database were modified to be consistent with WATEQ4F (Ball and Nordstrom, 1991).

## *2.3 Results and discussion*

### *2.3.1 Bulk physical and chemical composition*

The particle size distribution of sediment influences the hydraulic conductivity, residence time of the pore water, and chemical transport within the substrate. The sediment located at the top of the riverbanks at transects RRM 0.1 (SR6) and RRM 3.5 (SRF & SRE) consisted of > 70% sand (Figure A.1). Sediments collected mid-transect at the RRM 0.1 location (SR2, SR3, SR4, SR5) contained 40-70% sand and ~12% fine materials (silt and clay). Samples collected at RRM 0.1 and located at the base of the riverbank (SR1) had the greatest fraction of silt relative to all other sediments (~20%). RRM 3.5 sediment samples SRD, SRE & SRF also consisted of sand and contained silt fractions ranging from 12-16%. Sediment collected at locations SRB and SRC were coarse-grained gravels (> 50% gravel), and made up the cobble riverbed of the South River at 3.5 miles downstream from the point source.

The sediments collected at the RRM 3.5 location had slightly greater fractions of fine grained material. Fine grained sediments are often associated with greater porosity and grain surface area, and can influence sediment water interaction and colloid transport processes. Findings by Boszke et al. (2004) revealed a gradual decrease in Hg concentration with increasing grain size for riverbed sediments of the Odra River, Poland; however this trend was not observed for the South River bank sediments. A gradual decrease in % gravel was observed from the tops of the riverbank downward toward the riverbed for both riverbanks transects; however no correlation with total Hg concentrations was observed.

In addition to particle-size distribution, sulfur and carbon content are often associated with the release of Hg from sediment, and can influence the formation of mobile organic Hg. For the South River sediment samples analysed, the total sulfur concentrations were less than 0.7 mg $g^{-1}$ (Figure 2.3). Transitional hyporheic zones are potential locations for Hg methylation, and are dependent on porewater sulphur concentrations and available organic material. Elevated concentrations of sulfide can limit MeHg production (Compeau & Bartha, 1985) and can also result in the binding of Hg as insoluble Hg-sulfide.

Additionally, at both low and high concentrations of sulfate in the sediment, Hg methylation by sulfate reducers is inhibited, whereas methylation is maximized at intermediate sulfate concentrations (Gilmour et al., 1998).

The total carbon content of the river sediment decreased from 23 mg $g^{-1}$ at the top of the banks to 14 mg $g^{-1}$ at the riverbed in the RRM 0.1 sediment transect (Figure 2.3). Similarly in the RRM 3.5 sediment, total C concentrations ranged from 5.2 to 27 mg $g^{-1}$, and were lowest at the base of the riverbank (5.2 mg $g^{-1}$). Elevated concentrations of C were found in the cobblestone riverbed sample at RRM 3.5 (sample SRB, 27.2 mg $g^{-1}$). Organic carbon plays a role in Hg transport as $^{o}$C can retain Hg within the sediment. Soluble humic substances can also increase the mobility of Hg in aquatic sediments (Ravichandran et al., 2004).

Elevated concentrations of Hg were observed in the SR6 sample collected from the top of the RRM 0.1 riverbank transect (0.28 mg $g^{-1}$), and in the SRD sample (0.19 mg $g^{-1}$) collected near river flow elevation from the RRM 3.5 transect (Figure 2.3, Table A.1). Sediment collected at the base of the bank from the riverbed (SR1, SRB & SRC) contained low concentrations of Hg (1-13 μg $g^{-1}$), relative to all other bank sediments studied (22-75 μg $g^{-1}$). Strong positive correlations were observed for Hg and Cu for all sediment samples ($R^2$ 0.9, p value=$3E^{-5}$) was observed. The chalchophilic nature of both Hg and Cu suggests potential binding of Hg with sulfides in the sediment. An approximate 0.9:1 relationship (0.9+/- 0.3 Hg-Cu) was observed for RRM 0.1 sediment samples SR1, SR2, SR3, SR4, SR5, and RRM3.5 samples SRE, SRF, SRA. The Hg-Cu ratio for SR6 sediment was 2.3:1 and for SRD sediment was 1.2:1. The Hg-Cu ratios for sediments collected in the riverbed were < 0.5:1. Concentrations of Fe in sediment collected from both transects ranged from 12-30 mg $g^{-1}$, Mn ranged from 0.13-0.42 mg $g^{-1}$ and K ranged from 0.7-2 mg $g^{-1}$(Figure 2.3). Iron and manganese oxyhydroxides have a high capacity to adsorb Hg due to large surface area; however Hg can be released following mineral dissolution under anoxic conditions.

### *2.3.2 Selective extractions*

The toxicity and environmental mobility of inorganic Hg solid-phases are closely related to their relative solubility in aqueous media. Evaluation of Hg mobility and bioavailability in sediment systems requires knowledge of speciation and specific chemical and physical forms of solid-phase Hg. Chemical sequential extractions (CSE) provide operationally defined classes, or fractions of potentially toxic elements, with different potentials for human and ecological exposure. The CSE technique has many benefits and as well as limitations including small extractant volumes, re-distribution of analytes among phases, non-selectivity of reagents for target phases, incomplete extraction, and precipitation of new mineral phases during extraction (Bacon & Davidson, 2008, Kim et al., 2003, Nirel & Morel, 1990). The CSE results were used to develop a better understanding of the chemical forms of Hg and the potential for Hg leaching in the sediment samples.

The largest portion of Hg was observed in the less soluble F5 "residual" fraction; particularly in samples collected from the riverbank transect RRM 0.1 (40-80%) (Figure 2.4, Table A.2). With the exception of SRD (125 mg $kg^{-1}$), the masses of Hg in the F5 fraction were lower at RRM 3.5 than at RRM 0.1. The analyses suggest that after many decades of weathering under aerobic conditions, a portion of Hg remained in a relatively insoluble phase, particularly in the sediment collected near the industrial facility. The portion of Hg extracted by nitric acid in the F4 fraction was also large (5-58%), further suggesting that the Hg is present as a low-solubility phase. These findings are consistent with other sites where sediments and soils contain elevated concentrations of insoluble Hg, presumably Hg sulfides, under atmospheric conditions (Terzano et al., 2010, Flanders et al., 2010, Revis et al., 1989,).

Elevated masses of Hg were extracted in the F3 "organo-complexed" fraction for samples SR3, SR4 and SR6 at the RRM 3.5 location (3.42, 2.11 and 11.1 mg $kg^{-1}$ respectively). The F3 fraction is thought to be linked with sediment MeHg production, and may be a predictor for methylation potential (Bloom et al., 2003, Castelle et al. 2007, Flanders et al., 2010). Although CSE analyses suggest that the

Hg in the sediment was present primarily as less-soluble Hg sulfides such as cinnabar or metacinnabar, large masses of Hg were also extracted in the more soluble F1 and F2 fractions. These fractions include phases such as exchangeable or weakly complexed Hg, Hg chlorides, oxides and oxychlorides, which can be sufficiently available for release into infiltrating river or precipitation waters. The sum of water-soluble (F1) and stomach acid soluble (F2) fractions varied from 0.5 to 7 mg $kg^{-1}$ for all sediments analysed, with the exception of the SR6 sediment which had concentrations of ~ 44 mg $kg^{-1}$ of Hg in the F1 and F2 fractions. The sediment sample with the largest percentage of soluble (F1 and F2 fractions) Hg was observed in the SR3 sample, where 18% of the total solid-phase Hg was in a soluble phase.

### *2.3.3 X-ray adsorption spectroscopy*

Knowledge of the distribution and chemical form of the solid-phase Hg in sediment is useful to determine the potential bioavailability in the environment. X-ray absorption spectroscopy (XAS) is a tool that can provide detailed information on the chemical form of Hg-bearing compounds. Spectra were obtained for the SR6 sediment sample, which had a bulk Hg concentration of 280 mg $kg^{-1}$. The core level binding energy for Hg is found in the LIII electron, located in the 2p orbital of Hg, with an electron binding energy of 12284 eV. Normalized absorbance scans for Hg and their first derivative for the Hg $L_{III}$ absorption edges were obtained for the RRM 0.1 sediment samples (Figure 2.5). Data was also collected for Hg-bearing standards and included αHgS, βHgS, HgO, and $HgCl_2$.

Micro X-ray Flouresence (μ-XRF) maps were made for sediment samples collected from the RRM 0.1 riverbank transect. The μXRF maps indicate a large heterogeneity of Hg within the sediment. Strong positive correlations were observed for Hg and Cu for select spots located on SR6. However, other locations on the SR6 sediment μ-XRF maps, which were determined to contain elevated Hg concentrations, were observed to have little to no Cu. Because both Hg and Cu are highly chalcophilic, the positive correlation of Hg and Cu in some locations suggests the presence of sulfide phases. The results are consistent with sediment digestion and CSE analyses, suggesting that large portions of Hg

were associated with Hg-S minerals. However the occurrence of Hg in locations absent of Cu also suggests that Hg may occur in other phases.

XANES spectra collected from spots with elevated Hg were most similar to metacinnabar (β–HgS), suggesting that the dominant form of Hg was present as a low solubility HgS phase. The scans reveal that Hg was heterogeneously distributed in the sediment samples, where only two distinct zones of Hg could be detected in the SR6 thin section. The presence of HgS was consistent with the elevated masses of Hg determined by the F5 fraction for the SR6 sediment samples as determined by CSE.

The oxidative dissolution of HgS is generally favourable in the presence of dissolved oxygen (or ferric iron) and in the presence of water (equation 2.1):

$$HgS(s) + 2H_2O + 2O_2\,(aq) \leftrightarrow Hg(OH)_2 + {SO_4}^{2-} + 2H^+ \qquad K_{sp} = 10^{93} \tag{2.1}$$

However, the rate of HgS oxidation is relatively slow compared to other sulfide minerals which are more prone to oxidation (Holley et al., 2007, Blowes et al., 2003, Barnett et al., 2001). Resistance of oxidation of α or β–HgS has been reported for soils and sediments exposed to atmospheric oxygen (Wolfenden et al., 2005, Barnet et al., 1997). In addition to slow oxidation kinetics, the release of Hg through oxidative dissolution of Hg-S is also limited by the adsorption of Hg to Fe, Al and Mn oxyhydroxides, humic fractions and incomplete oxidation products on the Hg-S surface (i.e. $S_2O_3^{2-}$) (Holley et al., 2003). The presence of poorly crystalline metacinnabar is common in environmental samples, as the conversion of metacinnabar to the more stable cinnabar is often delayed by the presence of impurities that limit the conversion reaction (Kim et al., 2004).

Observation suggests that colloidal HgS can be released from sediment and transported in the presence of DOM (Ravichandran, 1998, Kim et al., 2004). The presence of colloidal cinnabar, as identified by EXAFS analyses on filtered samples collected from column experiments, suggests that HgS colloids can be transported through river bed sediments (Slowey et al., 2005, Lowry et al., 2004). At a site

where Hg-S tailings entered the Indrijca River, Slovenia, insoluble forms of Hg formed when the tailings were exposed to an oxygenated river system, or were mobilized as colloidal HgS bound to mineral surfaces. The presence of HgS solids in aerated riverbank sediments at the South River site is consistent with these studies showing persistence of HgS solids at industrial sites.

### *2.3.4 Batch resuspension experiments*

Sediment resuspension experiments were conducted to simulate the release of Hg during riverbank erosion events. Sediment from RRM 0.1 and RRM 3.5 locations were combined with river water at varying liquid to solid ratios of 40:1, 20:1, 10:1 and 4:1 SRW:sediment. Concentrations of Hg in the resuspension experiment supernatants generally increased with decreased liquid-solid ratios (Figure 2.6). Concentrations of Hg ranged from 0.2 to 80.2 µg $L^{-1}$ for experiments with sediment samples collected along the riverbank, and ranged from 6 to 30 ng $L^{-1}$ for cobblestone samples collected within the riverbed (refer to Fig. 2.1 for sample collection schematic). Elevated concentrations of Hg were released from the SR6 sediment relative to all other sediment resuspension experiments; Hg concentrations were 2.5 µg $L^{-1}$ for liquid-solid ratios of 40:1 and increased up to 80.2 µg $L^{-1}$ for liquid-solid ratios of 4:1 (Figure 2.6). The Hg concentrations of supernatant from experiments for the remaining sediment samples collected from the RRM 0.1 transect (in descending order from the top of the riverbank) were 0.4-6.7 µg $L^{-1}$ for SR5, 0.6-12.6 µg $L^{-1}$ for SR4, 1.6-10.6 µg $L^{-1}$ for SR3, 1.0-4.5 µg $L^{-1}$ for SR2 and 0.2-1.4 µg $L^{-1}$ for SR1. The resuspension experiments for sediments collected from the RRM 3.5 location had Hg concentrations of 0.2-1.0 µg $L^{-1}$ for SRE, 0.08-0.5 µg $L^{-1}$ for SRF, 2.0-7.9 µg $L^{-1}$ for SRD, and 0.3-3.2 µg $L^{-1}$ for SRA (in descending order from the top of the riverbank).

Randomly selected batch experiments for the South River sediment samples were repeated in duplicate for a third of the experiments, yielding an average variability of 30% from the mean. The highest variability was measured for batch experiments containing sediments with > 75 g $kg^{-1}$ of Hg, providing an additional indication of the heterogeneous distribution of Hg-bearing minerals in the

sediment. The concentrations of Hg were similar (<3.2 μg $L^{-1}$) for the experiments with samples collected at the base of the riverbank (SR1 and SRA) for both riverbank transect locations. The supernatant of experiments with sediment collected from the RRM 0.1 transect (SR2, SR3, SR4, SR5 and SR6) were generally elevated in concentrations of Hg compared to the RRM 3.5 riverbank transect sediments (SRF and SRE) when mixed with SRW, with the exception of the experiments conducted with the SRD sediment. The SRD sediment resuspension experiment supernatant for batches with SRW:sediment ratios of 4:1 had Hg concentrations of 8 μg $L^{-1}$. The SRD sediment sample was collected at an elevation subjected to fluctuating river base flow conditions.

The elevated concentrations of Hg observed in the water after contact with suspended sediment were consistent with the CSE results which indicated the presence of large masses of Hg in the F1 and F2 fractions. The concentrations of aqueous Hg observed in the resuspension experiments did not increase linearly with an increase in added sediment mass. This non-linear response suggests a possible solubility or rate limiting control for aqueous Hg released from the sediment. Field experiments have determined that soil resuspension can result in the rapid transfer of Hg and MeHg into the water column immediately following the event (Mucci et al., 1995). Acquavita et al. (2012) found that perturbations at the sediment water interface in simulated resuspension mesocosm studies resulted in a temporary spike in dissolved inorganic Hg concentrations and decreased with increased mixing time. Kim et al. (2004) determined that a spike in Hg concentration due to sediment resuspension is associated primarily with the Hg in the particulate phase.

The mass of Hg released into the river water in the resuspension experiments were poorly correlated with total solid-phase Hg concentrations. The results of the sediment resuspension experiments are consistent with similar leaching studies where < 1% of the total sediment Hg was released upon resuspension with seawater (Bloom & Lasorsa, 1999).

The F1 (water-soluble) Hg that was determined by CSE analysis was compared to the concentration of Hg released from sediments after resuspension with river water for all sediment samples (Table 2.3). The % of water-soluble Hg released from the sediments is described as (equation 2.2):

$$\%\ \text{of}\ H_2O\ \text{soluble Hg (F1)leached from the sediment} = \left( \frac{C_{RS}(\mu g_{Hg}\ L^{-1}{}_w) \times V_w(L)}{C_{F1}(\mu g_{Hg}\ g^{-1}{}_s) \times M_s(g)} \right) \times 100 \qquad (2.2)$$

where $C_{RS}$ represents the aqueous concentration of Hg in the supernatant after sediment resuspension; the $V_w$ term represents the volume of river water mixed with the sediment for each sediment resuspension experiment; the $C_{F1}$ term represents the solid-phase concentration of water-soluble Hg as determined by the F1 fraction of the CSE analysis; and the $M_s$ term represents the mass of sediment mixed with the river water for each sediment resuspension experiment.

The calculated % water-soluble Hg leached indicated that significantly less Hg was released from the sediment when resuspended with river water in comparison to Hg released when mixed with deionized water in the CSE analysis (<5.5% for all sediments and ratios studied). The differences in water-soluble Hg concentrations obtained from the CSE analyses and the resuspension experiments may be related to the low ionic strength of the deionized water. The CSE analyses was also conducted under longer mixing times (18 +/- 4 hours) at 100:1 DI:dry sediment ratios and with an end-over-end tumbler. The sediment resuspension experiments were conducted with river water, 30 minute mixing times and a horizontal shaker table rotation.

For the South River sediment resuspension experiments, less than 1% of water-soluble Hg (as determined by the F1 fraction) was leached from SR1, SRD, SRE & SRF sediments following the sediment resuspension experiments. The SR3 and SRA sediments contained the lowest total Hg concentrations (24 μg $g^{-1}$ and 22 μg $g^{-1}$, respectively) relative to all other riverbank sediment samples analysed, and released the greatest proportion of water-soluble Hg relative to all other sediment samples. The Hg in the SR3 sediment sample resuspension experiment supernatant had the greatest proportions of

water-soluble Hg (2.9-5.5%) relative to the other sediment samples, and was collected around the location of base river flow conditions on the RRM 0.1 bank transect. The SRA sediment sample was also collected at the base of the riverbank at location RRM 3.5, and the proportion of water-soluble (mass of F1) Hg released ranged from 2.4-3.6%. The SRB and SRC sediments released < 0.03% of the total sediment Hg available, and were comprised of large grained cobbles collected from the riverbed at location RRM 3.5.

The sediments with greater than 13% fines (SR1, D, E & F) released the lowest concentrations of Hg to the river water. The finer grained sediments may have a greater affinity for Hg, and therefore lower potential to release Hg in comparison to the coarser grained sediments such as SR3 and SRA. These results are consistent with similar studies that determined a strong relationship with sediment grain size and partitioning of Hg from aqueous to the solid-phase (Bloom & Lasorsa, 1999). The total Hg concentrations of the riverbed samples ranged from 1.1-11 $\mu g\ g^{-1}$, and pore water samples collected from the riverbed are reported to range from 15-1800 ng $L^{-1}$ (Flanders et al., 2010). Contrastingly, the cobble bed resuspension experiments (SRC and SRB) did not follow the trend versus grain size, the coarse-grained sediments released the lowest concentrations of Hg for all resuspension experiments.

The mass of solid-phase Hg in the F1 fraction of the sediment samples (as determined by CSE) was positively correlated with the total mass of Hg in the supernatant ($R^2$ 0.98, p value < 0.05) for all resuspension experiments with the exception of those performed with liquid-solid ratios of 40:1 for RRM 0.1, and 4:1 for RRM 3.5 experiments (Figure A.2). Statistically significant correlations were also determined between the Hg released in the resuspension experiments and the mass of Hg in the F2 fraction for each sediment sample (Table 2.3). These results suggest that both the F1 and F2 fractions can provide information regarding the Hg leaching potential from resuspended sediment containing similar Hg-bearing minerals. Poor correlations were determined for the remaining F3, F4 and F5 fractions with Hg concentrations in the sediment resuspension experiment supernatant.

The alkalinity of the river water increased as the water-sediment ratio decreased for all experiments, varying from 50 to 150 mg $L^{-1}$ (as $CaCO_3$) (Figure A.3). However, the alkalinity was generally lower relative to baseline SRW concentrations (87 mg $L^{-1}$), with the exception of the 4:1 (SRW:sediment) experiment for the SR1 sediment sample (150 mg $L^{-1}$). The pH was similar in range (7.5-8.1) for all experiments, and was similar to or slightly lower than the SRW (~8.1). The pH values were observed to decrease as the SRW:sediment ratio decreased in samples SR1, SR3, SR5 and SRE. The pH values for experiments including SR2, SR4, SR6, SRA, SRB, SRC, SRD and SRF sediment samples remained constant with increased sediment relative to SRW. The Eh values were elevated relative to SRW (~340 mV), and varied from 350 to 600 mV. The observed Eh values were consistent with well-oxygenated terrestrial soils and sediment (>350 mV) (Gabriel & Williamson, 2004).The supernatant from experiments with SR1, SR2, SR3 and SRD sediments increased in Eh by 30-130 mV as the SRW:sediment ratio increased. Values for Eh increased by 20-80 mV for SR4, SR5, SRA, SRB, SRC, SRE and SRF with decreasing SRW:sediment, whereas SR6 remained constant for all experiments.

Concentrations of major cations and anions were determined for the supernatants of batch experiments with SR1, SR3, SR5 and SR6 sediments of the RRM 0.1 riverbank transect, and generally increased when greater masses of sediment were added to the batch experiments (Figure A.3). Increased concentrations of $NO_3$, Mn and Fe were observed in the batch experiment supernatant with increased masses of sediment (lower SRW:sediment ratios). Concentrations of $NO_3$ were lowest in the SR1 supernatant (1.8-2 mg $L^{-1}$), and increased from 2.6 to 8.5 mg $L^{-1}$ for SR3, 3.2 to 11.4 mg $L^{-1}$ for SR5, and 3.2 to 7.2 mg $L^{-1}$ for SR6. The greatest Mn concentrations were observed for batch experiments containing the SR1 sediment, and increased from 190 to 640 μg $L^{-1}$. The concentrations of Mn in the supernatant of experiments containing SR3, SR5 and SR6 sediments increased from < 5 mg $L^{-1}$ up to 43 mg $L^{-1}$ with increased mass of sediment added to each batch experiment. Concentrations of Fe in the batch experiment supernatant were elevated for experiments containing SR6 (14-1414 μg $L^{-1}$) and increased from 21 to 252 μg $L^{-1}$ for SR1, 14 to 232 μg $L^{-1}$ for SR3 and 27 to 797 μg $L^{-1}$ for SR5. Concentrations of

$SO_4$ were similar for all batch experiments and ranged from 5.8-6.8 mg $L^{-1}$ (SRW concentrations ranged from 6-9 mg $L^{-1}$), suggesting $SO_4$ was reduced or adsorbed to the sediment surface.

### *2.3.5 Column studies*

Frequent inundations of riverbanks during flooding and storm events can lead to an influx of dissolved and particulate Hg into the river water. In this study, column transport experiments were conducted to assess the release of Hg at sediment:water ratios typical of those that might occur under saturated conditions at the bottom or near-edge deposits of the river margin. The flow rates were modified during the course of the experiments to simulate changes in flow which could potentially occur at the field site. The rate of flow of water through the columns was varied between 1 and 3 cm per day. Four columns were packed with bank sediment collected from RRM 0.1 transect from the base of the river to the top of the bank (SR1, SR3, SR5, and SR6). The sediment samples were selected to cover a range in total Hg concentrations (13-280 g $kg^{-1}$).

#### *2.3.5.1 Hg mobilization*

The column experiments were conducted in a manner to evaluate the potential influence of prolonged saturated conditions on the leaching of particulate and dissolved constituents from the bank sediment over time. Column experiments were conducted with bank sediment collected at the top of the riverbank (SR6), sediment collected at the upper middle and lower middle sections of the riverbank (SR5 and SR3, respectively) and at the base of the riverbank (SR1). Large fluctuations in Hg concentrations were observed in the column effluent over the course of the leaching experiments. Elevated concentrations of 0.45 μm filtered Hg were observed shortly after the flow velocity was increased and after periods of stagnation (Figure 2.7). Pronounced changes in Hg concentrations were observed for both the SR6 (68% increase) and SR3 (47% increase) column effluent following a flow increase from 1 pore volume per week to 3 pore volumes per week. Smaller changes in Hg concentrations were observed for

the SR5 (27% increase), and SR1 (14% increase) column effluent following the same increase in pore water velocity.

The initial Hg concentrations in the SR1 effluent were elevated (150 ng $L^{-1}$) and decreased to 30-50 ng $L^{-1}$ within the initial 15 pore volumes. Following the flow velocity increase at 18 pore volumes, SR1 effluent Hg concentrations increased to 70-80 ng $L^{-1}$ and gradually decreased to concentrations ranging from 30-40 ng $L^{-1}$ for the remainder of the experiment. The Hg concentrations of the SR3 effluent flowing at 1 pore volume per week resulted in initial concentrations of ~ 800 ng $L^{-1}$, peaked at 3800 ng $L^{-1}$ at 5 pore volumes, and decreased to 2500 ng$L^{-1}$ at 14 pore volumes. Following the increase in flow velocity to 3 pore volumes, Hg concentrations in the SR3 effluent increased gradually and peaked at 7100 ng $L^{-1}$ at 33 pore volumes. Concentrations gradually decreased over time to ~ 400 ng $L^{-1}$ after 200 pore volumes of flow.

Filtered Hg concentrations in the SR5 effluent were initially low (150-180 ng $L^{-1}$) and peaked at 830 ng $L^{-1}$ at 5 pore volumes before declining to ~350-400 ng $L^{-1}$ at 21 pore volumes. Upon the onset of the flow increase, the SR5 effluent Hg concentrations increased slightly by 15-30 ng $L^{-1}$ before gradually declining to ~ 30 ng $L^{-1}$ by 125 pore volumes. The 0.45 μm filtered Hg concentrations in the SR6 effluent were initially elevated relative to the other column experiments (3200 ng $L^{-1}$), and declined to ~ 1700 ng $L^{-1}$ by 22 pore volumes. The increase in flow velocity coincided with elevated Hg concentrations up to 5500 ng $L^{-1}$. An additional spike in Hg SR6 effluent concentrations was observed at 55 pore volumes and peaked at 7800 ng $L^{-1}$. After approximately 80 pore volumes of flow, the filtered Hg concentrations in the SR6 effluent ranged from 200-500 ng $L^{-1}$.

*2.3.5.1.1 Filter-passing mercury*

The concentrations of filter-passing Hg were determined for 0.45 μm. 0.2 μm, 0.1 μm and 5000 MWCO at various stages throughout the column experiments for SR1, 3, 5 and 6 effluents (Figure 2.8). Unfiltered concentrations on average ranged from 1.7-2.3 times greater than the concentration of 0.45 μm

filtered samples for the SR1, 3 and 5 columns. The concentrations of Hg in the unfiltered samples for the SR6 column effluent were on average 4.4 times greater in concentration than for the 0.45 μm filtered samples. The concentrations in the 5000 MWCO fraction averaged from approximately 40-48% of the filter-passing Hg (<0.45 mm) for all samples. Contrastingly, the concentrations of Hg in the 5000 MWCO ranged from 1.5-6.7% of the filter-passing Hg (<0.45 μm) in the river water following the simulated sediment resuspension experiments. The total Hg concentrations in the column effluent decreased for all sediment after prolonged periods of flow, while the contribution of dissolved and colloidal fractions remained constant over time.

These results suggest that micro-particle transport may be a significant factor during prolonged riverbank inundation events, where transport mechanisms contribute to the release of sustained and elevated concentrations of Hg into sediment pore water. Greater migration distances are possible when contaminants are associated with mobile colloids due to prolonged suspension in the water column relative to larger particles. Colloidal metal sulfides can form readily during flooding events in floodplain soil porewater, and can enhance transport to groundwater and exfiltration to rivers (Weber et al., 2009).The contribution of particle associated Hg due to the erosion and re-deposition of sediment may be a key factor in understanding Hg transport and distribution in the South River.

Fluctuating column flow rates and flow hiatus may influence the chemical composition of the pore water, as total Hg concentrations decreased and colloidal concentrations remained consistent throughout the course of the column experiments. The SR6 column was subjected to increased flow rates by a factor of three, from 1 to 3 to 9 pore volumes per week, as represented by the first three vertical bars in Figure 2.8. The % of filter-passing Hg did not substantially fluctuate in response to increased flow rates (~ 30% of unfiltered Hg). The final grey bar (Figure 2.8) represents a 2 week period of stagnant flow conditions, and later resumed flow at 1 pore volume per week. The concentration of total unfiltered Hg in the SR6 column effluent did not change following stagnant flow conditions, however the % filter-passing Hg increased by 40%. Filter fractions were not collected during the early stages of the SR6 column.

However, a replicate column experiment containing SR6 sediment indicated 93% of the total Hg concentration passed the 0.45 μm filter at 21 pore volumes of flow, and decreased to 77% at 65 pore volumes of flow. These results suggest that Hg concentrations in effluent from the SR6 sediment may have been influenced by transport of suspended particles during early stages of saturated flow.

*2.3.5.1.2 Release of water-soluble mercury*

The mass of Hg released from the column experiments were compared to the mass of water-soluble Hg available in the sediment (mass of Hg in the CSE F1 category). The cumulative water-soluble Hg leached from the sediments was calculated with the following equations:

$$Hg\ Available\ (ug) = (M_{sed}(g) \times \theta) \times Hg_{sed}(\mu g g^{-1}) \quad (2.3)$$

$$\%\ Hg\ Leached = \left(\frac{Hg_{pw}(ng\ L^{-1}) \times Vol_{samp}(L)}{Hg\ Available\ (\mu g)}\right) \times 100 \quad (2.4)$$

Where $M_{sed}$ represents the mass of the sediment contained within the column in grams, and $\theta$ represents the moisture content of the sediment sample. The $Hg_{sed}$ term represents the mass of Hg per gram of sediment as determined by the F1 (water-soluble) fraction of the CSE analyses. The % Hg leached was calculated based on the cumulative concentrations of Hg in the pore water. The $Hg_{pw}$ term represents the concentration of Hg observed in the column effluent at each point of sample collection. The $Vol_{samp}$ term represents the volume of column effluent corresponding to the Hg concentration. The % Hg leached were plotted in terms of cumulative % Hg leached over the course of the experiments (Figure 2.9).

Similar responses in cumulative Hg release after approximatley 80 pore flushes were observed for the different sediment samples (Figure 2.9). For each of the cumulative curves, a plateau in concentration was observed, indicating a decline in Hg output from most sediments. The SR1 column was the exception as the sediment continued to release sustained concencentrations of 30-50 ng of Hg $L^{-1}$. The mass of Hg

released over the course of the colum experiments represented only a small portion (< 12 %) of the mass of water-soluble Hg determined in the CSE extractions for the SR3 sediment, and even smaller portions (< 0.5%) for the SR1, SR5 and SR6 sediments. The release of soluble-Hg species may be limited by slow dissolution kinetics within the soil porewater. These results suggest that the F1 fraction may be a poor indicator of sediment leaching potential. Alternatively, the results may indicate that the orginal mass of water-soluble Hg was transformed to a less soluble form under the saturated conditions, shifting the more available soluble Hg to a less-soluble form. These results are consistent with other field studies in which the deposition of $Hg^0$ in placer tailings transformed to other Hg species including insoluble HgS (Slowey et al. 2005).

*2.3.5.2 Column effluent chemistry*

*2.3.5.2.1 Initial flow velocity (1 pore volume per week)*

Monitoring of the concentrations of dissolved constituents in the column effluent can provide insight into potential geochemical reactions governing the release of Hg from the bank sediments under saturated conditions. Over the course of the experiments, effluent pH values were near-neutral and ranged from 6.9 to 8.1 (Fig. A 2.4-Fig A. 2.7). The flow rate for all column experiments was ~ 1 pore volume per week for the initial 10-20 pore volumes of flow. The SRW influent solution pH ranged from 7.7-8.1, and was consistent with the initial pH values in the column effluent. A decline in effluent pH of approximately 0.5 units was observed within the initial 10-15 pore volumes for all column experiments. The pH of the SR1 effluent was slightly lower (7.5) than the effluent from the other columns throughout the course of the experiment. Initial elevated alkalinity concentrations in the column effluent may indicate the presence of carbonate minerals. The initial effluent alkalinity concentrations for columns containing SR3, SR5 and SR6 sediment ranged from 200-300 mg $L^{-1}$ (as $CaCO_3$), and stabilized at background SRW levels (70-100 mg $L^{-1}$) at approximately 15-20 pore volumes of flow. The effluent from the column containing SR1 sediment had alkalinity concentrations up to 600 mg $L^{-1}$ in the first pore

volume of flow. A decrease in effluent alkalinity concentrations for all columns was observed within the first 15 pore volumes of flow. The corresponding decline in pH may have been influenced by decreasing alkalinity throughout the course of the experiments.

Concentrations of exchangeable cations including Ca, Na, Mg and K were monitored in the column effluent relative to the influent solution. Elevated Ca concentrations were observed in all column effluent, and quickly declined within 5 pore volumes to 40-60 mg $L^{-1}$ in the effluent of all columns. A decline in effluent Ca concentrations was observed and coincided with decreased alkalinity, suggesting the initial influence of calcite dissolution. Concentrations of Ca in the SR1 column effluent were initially elevated (160 mg $L^{-1}$) relative to the other column experiments (<100 mg $L^{-1}$).

The SR6 effluent Na concentrations were initially lower (<2 mg $L^{-1}$) than the SRW influent (3 mg $L^{-1}$), and increased within the first 2-3 pore volumes up to 4 mg $L^{-1}$. The increase in Na concentrations coincided with a decrease in K concentrations from 2.1 to 1.4 mg $L^{-1}$, suggesting potential cation exchange reactions. Similar trends were observed in the SR3 effluent, where Na concentrations increased from below (2.3 mg $L^{-1}$) to slightly above (3.3 mg $L^{-1}$) the influent concentrations. The increasing Na concentrations coincided with K concentrations sharply decreasing from 13.6 to 3.5 mg $L^{-1}$ within the initial 17 pore volumes. Concentrations of both Ca and Mg decreased after the initial pore flushes in the SR3 and SR6 effluents.

Concentrations of K and Na in the SR5 column effluent were similar to the SRW influent solution, whereas concentrations of Ca declined from 73 to 40 mg $L^{-1}$ and Mg increased from 5.9 to 7.7 mg $L^{-1}$. Concentrations of all exchangeable cations in the SR1 column effluent decreased to SRW influent concentrations within the initial 20 pore flushes.

The Eh fluctuated between 300 and 600 mV throughout the course of the experiments. Concentrations of $NO_3$ were initially below analytical detection limits (<0.2 mg $L^{-1}$), and were less than SRW influent concentrations (~3 mg $L^{-1}$) for SR1, SR3 and SR5 effluents. Changes in redox conditions

can strongly influence Hg sorption, complexation, mineral precipitation or dissolution, and can therefore be a major control on Hg mobility in sediment pore water (Ullrich et al., 2001).

The SR6 effluent had initial $NO_3$ concentrations of 5 mg $L^{-1}$, and then rapidly decreased to <0.2 mg $L^{-1}$ (Figure 2.7). Concentrations of Mn were elevated (2-3 mg $L^{-1}$) relative to the SRW influent (<0.2 mg $L^{-1}$) for SR1 and SR3 effluents, whereas SR5 and SR6 effluents maintained concentrations similar to SRW. Concentrations of Fe were elevated in the initial pore volumes for SR1 (110 μg $L^{-1}$), SR5 (18 μg $L^{-1}$) and SR6 (42 μg $L^{-1}$) before decreasing to < 1 μg $L^{-1}$ within the initial 15 pore volumes of flow. The SR3 effluent Fe concentrations increased from ~ 1 μg $L^{-1}$ to 28 μg $L^{-1}$, peaking at 17 pore volumes just prior to an increase in flow velocity. Concentrations of $SO_4$ were relatively low in the SR1 effluent (~1 mg $L^{-1}$) and decreased to < 1 mg $L^{-1}$ within the initial 15 pore volumes. Similar trends were observed in the SR3 effluent that decreased from 16 mg $L^{-1}$ to < 1 mg $L^{-1}$. The $SO_4$ concentrations in the SR5 and SR6 effluent were initially 9.5 mg $L^{-1}$ and 19 mg $L^{-1}$ respectively, and stabilized at ~ 4 mg $L^{-1}$ within the initial 10 pore volumes of flow.

Facultative bacteria are capable of reducing organic carbon at the expense of a series of electron acceptors including $O_2$, $NO_3^-$, $Mn^{4+}$, $Fe^{3+}$ and $SO_4^{2-}$, listed in decreasing order of energetically favourable reactions (Stumm and Morgan, 1996). As oxidants are consumed, the reduction of the oxidized species increases in the specified order if the associated facultative bacteria and electron donors are present. Organic acids are labile sources of electrons that can be utilized by Mn, Fe and $SO_4$ reducers. Types of microbial metabolism that are feasible in anoxic sediment are dependent on the types of organic substrate and electron acceptors available, and include fermentative, nitrate reducing, sulfate reducing or methanogenic bacterium (Ehrlich, 2002, Compeau & Bartha, 1995). The fermentation of organic compounds in this environment results in the formation of organic acids including propionate, lactate and butyrate. Concentrations of acetate in the SRW influent ranged from 0.5 to 1 mg $L^{-1}$ and were consistent with the concentrations of the column effluent. All other organic acids in the column effluent were

measured at concentrations below analytical detection limits (0.1 mg $L^{-1}$) in the column effluent and SRW input solutions (Figure A.9).

*2.3.5.2.2 Increased flow velocity (≥3 pore volumes per week)*

After approximately 15-20 pore flushes, the flow velocity of the column experiments was increased from 1 pore volume per week to 3 pore volumes per week. Following the increase in velocity, the pH of all column effluent stabilized at values below SRW levels (<8) and the Eh values were elevated relative to SRW (> 340 mV). The SR5 effluent Eh increased to 760 mV followed by a decline to 300 mV, before stabilizing at ~ 500 mV for the remainder of the experiment. Alkalinity concentrations decreased to SRW levels (~ 90 mg $L^{-1}$ as $CaCO_3$) for all column effluent immediately following the increase in flow velocity.

Following the increase in flow velocity to 3 pore volumes per week, the concentrations of Ca declined to ~20 mg $L^{-1}$, and were similar to that of the influent. Concentrations of Na stabilized at ~2 mg $L^{-1}$ (below SRW influent levels), while concentrations of K stabilized at ~ 2-3 mg $L^{-1}$ (above input levels), suggesting potential cation exchange reactions. Concentrations of Si ions were initially elevated (8-20 mg $L^{-1}$) for the first 100 pore volumes of flow, and declined to 6-8 mg $L^{-1}$ in the effluent for all columns (2-4 mg $L^{-1}$ higher than the SRW influent). Elevated Si concentrations suggest dissolution of siliceous bearing materials, which can promote the mobilization of particulates in pore water (Slowey et al., 2005).

At the onset of the increase in velocity, a change in chemical composition of the column effluent was observed by slightly elevated concentrations of $NO_3$. The SR3 effluent $NO_3$ concentrations peaked at 5 mg $L^{-1}$ at pore volume 17, corresponding to the increase in flow velocity, and gradually decreased to < 1 mg $L^{-1}$ by 50 pore volumes. The effluent concentrations from columns containing SR1, SR5 and SR6 sediment were consistently below the concentrations of $NO_3$ in the SRW influent (<2 mg $L^{-1}$) (Figure 2.7). The SR5 effluent $NO_3$ concentrations increased from < 1 to 2 mg $L^{-1}$, and SR6 increased to 1.3 mg $L^{-1}$ following the increase in flow to 3 pore volumes per week. Little change was observed in $NO_3$

concentrations of the SR6 effluent following increased flow speed to 6 pore volumes per week, however a spike was observed (2.4 mg $L^{-1}$) following an increase in flow to 9 pore volumes per week at 154 pore volumes. The $NO_3$ concentration in the SR1 effluent were not affected by the increase in flow velocity, however elevated concentrations were observed up to 0.9 mg $L^{-1}$ between pore volumes 80-125. Ammonia concentrations were low (<1 mg $L^{-1}$) for all column effluent measured, with the exception of SR3 effluent at approximately 6 pore volumes (1.7 mg $L^{-1}$).

Concentrations of Mn in the SR1 and SR3 column effluent were initially elevated relative to SRW following the increase in flow velocity, ranging from 2-3 μg $L^{-1}$ and gradually declining to < 1 μg $L^{-1}$ after 30 pore volumes. In the SR3 column effluent, the Mn concentrations increased gradually following the increase in flow velocity, peaking at 14 mg $L^{-1}$ at 90 pore volumes. Relatively low concentrations of Mn in the SR5 effluent (< 2 μg $L^{-1}$) increased following the onset of the increase in velocity peaking at 45 pore volumes (0.5 mg $L^{-1}$), and declined shortly thereafter. Concentrations of Mn in the SR6 column effluent increased from 1 μg $L^{-1}$ at 22 pore volumes to 1.2 mg $L^{-1}$ by pore volume 26, and declined back to < 1 μg $L^{-1}$ by 100 pore volumes.

There was little to no change in Fe concentrations in effluent from columns containing SR1 and SR3 sediments. The Fe concentrations of SR1 effluent remained constant before and after the flow increase ranging from 6-10 μg $L^{-1}$. The Fe concentrations in the SR3 effluent ranged from 16-27 μg $L^{-1}$ from pore volumes 17-30, suggesting that Fe concentrations were not affected by the increased flow rate. However, a peak in Fe concentrations was observed in both the SR1 and SR3 (170 μg $L^{-1}$ and 500 μg $L^{-1}$) column effluents later in the experiments.

Fluctuations in Fe concentrations were observed to correlate with an increase in flow velocity for the column experiments containing sediment samples collected at the highest elevations on the riverbank (SR5 and SR6). The Fe concentrations in the SR5 column effluent increased from < 0.1 μg L-1 to 9 μg $L^{-1}$ following the increase in flow velocity, and increased to concentrations up to 190 μg $L^{-1}$ by 200 pore

volumes. A response in increased flow velocity from 1 to 3 pore volumes per week and 3 to 9 pore volumes per week corresponded with increased Fe concentrations in SR6 effluent.

Concentrations of $SO_4$ in SR1, SR3 and SR5 effluents remained constant during the period of flow increase. However SR3 $SO_4$ concentrations increased above background SRW levels up to 13 mg $L^{-1}$ after 100 pore volumes of flow. Similarly, $SO_4$ concentrations in the SR5 effluent gradually increased over the course of the experiment up to 13 mg $L^{-1}$. The $SO_4$ concentration in the SR6 effluent ranged from 4-6 mg $L^{-1}$ between pore volumes 8-80, suggesting that fluctuating flow conditions did not influence $SO_4$ production or consumption in the pore water. Following the two week period of stagnant flow conditions for the SR6 column experiment, flow resumed at a rate of 1 pore volume per week. Stagnant flow conditions corresponded with decreased $SO_4$ concentrations of 1 mg $L^{-1}$. Concentrations of $NO_3$, Fe and Mn were similar to concentrations observed during the initial stages of the column experiment with the same flow rate. The concentrations of all other constituents remained similar to levels observed during periods of flow perturbations, and did not return to pre-pertubation concentrations.

*2.3.5.3 Column studies discussion*

Concentrations of $NO_3$ and $SO_4$ were generally lower than those in the influent solution for all column effluent measured, suggesting possible reduction during transport through the column sediment. The SR3 column sulfate concentrations decreased to analytical detection limits of 0.01 mg $L^{-1}$ within 10 pore volumes of flow, corresponding with a rise in pore water $NO_3$, Mn and Hg concentrations. After 150 pore volumes of flow, complete removal of $NO_3$ and Mn was observed for the SR3 sediment column effluent, corresponding to increased concentrations of $SO_4$. Measurements of dissolved sulfide were below the analytical detection limit (5 mg $L^{-1}$), and may be due to removal of $HS^-$ through formation of secondary FeS, potential HgS phases, or incomplete reduction to sulphide.

With the exception of SR1 effluent, the concentrations of $SO_4$ in the column effluents gradually increased throughout the course of the experiments, and approached concentrations similar to the SRW

influent. The increase in $SO_4$ concentrations coincided with a decline in Hg concentrations that was observed over an extended period of saturated flow (>80 pore volumes). The trend suggests that $SO_4$ from the influent SRW was consumed (reduced) within the initial stages of the experiment. The available soluble $Hg^{2+}$ released into the sediment pore water may have bound to S in the initial stages of the column experiments. Following extended periods of saturated flow, significant concentrations of Hg continued to leach from the sediments stabilizing at 20-30 ng $L^{-1}$ for SR1 and SR5, and 300-500 ng $L^{-1}$ for SR3 and SR6 effluents.

As discussed in section 2.3.2, the sequential extractions suggest that Hg is present in both oxidized and reduced forms. Due to the low solubility of cinnabar and metacinnabar, fine grained colloids can contain HgS (Lowry et al., 2004). Although Hg-S solids are resistant to oxidising conditions, they can be weathered, transported and deposited downstream (Kim et al., 2004, Slowey et al., 2005, Lowry et al., 2004). The column effluent chemistry for SR3, SR5 and SR6 was modeled using MINTEQ2A, ignoring the presence of DOM interaction, and indicated that forms of HgS solids were thermodynamically favored in the column effluent (Figure A.8). These results suggest that filter-passing Hg concentrations may be in the form of dissolved HgS complexes.

Lowry et al., (2004) determined that colloidal HgS was the dominant form of Hg transported from column studies perturbed with high ionic strength solution for tailings with sulphide containing 50-100% HgS. Similar results were observed in column studies conducted by Slowey et al. (2005), where XAFS spectroscopic analysis identified colloidal HgS as the dominant mobile Hg-bearing phase of tailings consisting of > 75% soluble Hg species. As suggested, the solubility of HgS increases with decreasing particle size. Therefore mobilized HgS colloids are likely to contribute to the measured "soluble Hg" concentrations in column experiments.

The natural dissolution of HgS can occur in oxidizing environments, where the release of soluble Hg-compounds may occur simultaneously with the mobilization of less soluble forms such as βHgS. The

dissolution of HgS is described by equation 2.1. The elevated Hg concentrations observed in the resuspension experiments compared to the column experiements may be associated with the oxidation of these Hg-S minerals. The continuous mixing with oxygenated SRW may have provided conditions conducive to the oxidization of Hg-S minerals in the sediment during the sediment resuspension experiments relative to the column experiments. The elevated Hg concentrations observed from the sediment resuspension experiments suggest that aggressive mixing in atmospheric conditions may contribute to the release of Hg in comparison to the saturated-transport conditions of the column experiments.

Concentrations of MeHg in the column effluent ranged between <1 to 38 ng $L^{-1}$ for all experiments. The highest MeHg concentration was observed for the SR6 effluent at 61 pore volumes of flow (38 ng $L^{-1}$), followed by decreasing concentrations to < 1 ng $L^{-1}$ (Figure 2.10). The concentrations of MeHg peaked between 12-17 ng $L^{-1}$ in the SR1, SR3 and SR5 column effluents, and declined to < 1 after 150 pore volumes for all columns. Concentrations of MeHg in the column effluent generally corresponded to fluctuations in aqueous total Hg concentrations. Less than 1% of the total Hg concentrations in the SR3 and SR6 column effluent were in the form of MeHg. In contrast, up to 21% of the total Hg concentration in the SR1 column effluent was in the form of MeHg at 0.8 pore volumes, and decreased to 3% by 130 pore volumes. At 54 pore volumes, 11.5% of the total Hg concentration in the SR5 column effluent was in the form of MeHg, and decreased to 0.5% MeHg over the course of the experiments. Elevated fractions of MeHg in the SR1 column effluent suggests that sediment collected from the base of the riverbank may be affected by different biochemical conditions that can facilitate MeHg release under sustained saturated conditions.

The peak in Hg concentration in the SR6 effluent at approximately 55 pore volumes coincided with increased $NO_3$ concentrations and decreased concentrations of Fe and Mn, suggesting that an oxidizing front may have progressed through the column at this point in time. In general, molar ratios between Hg and $SO_4$ in the column effluent decreased within the first 10 pore volumes, and coincided

with an increase in molar ratios for Mn and Hg. Declining molar ratios for Mn and Hg coincided with increased molar ratios for $NO_3$ and Hg.

Observations from resuspension and column sediment leaching experiments revealed little to no additional sulfate was added to the river water after extensive interaction with the sediment. Further analysis of DOC and organic acid concentrations within the sediment leaching column effluent and SRW influent suggest that limited electron donors were available in the river water, indicating that sulfate reduction rates were likely limited. Sulfate reducing bacteria (SRB) can catalyze the oxidation of low molecular weight organic carbon coupled with sulfate reduction (equation 2.6). Additionally, the production of reduced sulfide in sediment pore water can promote the precipitation of low-solubility metal-sulfide minerals such as Hg-sulfide (equation 2.7), thereby decreasing aqueous concentrations of $Hg^{2+}$ in solution (Skyllberg and Drott, 2010).

$$SO_4{}^{2-} + 2CH_2O \leftrightarrow 2HC0_3{}^{-} + H_2S \quad (2.6)$$

$$HS^{-} + Hg^{2+} \leftrightarrow HgS + 2H^{+} \quad (2.7)$$

The presence of labile organic carbon can also increase the growth of certain heterotrophic SRB (i.e. *Desulfovibrio desulfuricans*) (Ehrlich, 2002). The addition of electron donors (such as low molecular weight dissolved organic carbon), and adequate electron acceptors (such as sulfate) to the South River bank sediments may incite geochemical reactions that would favor the immobilization of Hg.

### *2.4 Conclusions*

The geochemical characterization of the riverbank sediment of the South River was studied to assess the potential for Hg to become mobilized during riverbank inundation events and periods of high flow. The XAS analyses for sediment thin sections revealed localized Hg hot spots in all sediment samples analyzed. The sediment digestion analyses and μXRF maps indicated a strong positive correlation between Hg and Cu. XANES analyses of seven locations detected on the SR6 sediment thin

section closely resembled βHgS. Results were consistent with CSE analyses indicating the largest portion of Hg was present as insoluble species in the F5 fraction (HgS). Large quantities of soluble F1 and F2 extractable species were also detected (up to 7 mg $kg^{-1}$) in the collected riverbank sediment samples, with the greatest mass of water-soluble forms of Hg located in the SR6 sediment sample (44 mg $kg^{-1}$). The results are consistent with other field sites that suggest 1) the conversion of more-soluble Hg species to insoluble species can occur over time and 2) the oxidation kinetics of HgS are slow resulting in the existence of resistant Hg-bearing sulfide minerals in sediment that is frequently exposed to oxidising conditions.

Sediment resuspension experiments designed to simulate bank erosion events resulted in elevated concentrations of Hg in the river water for sediment collected from both riverbank locations (up to 80 μg $L^{-1}$). Significant variability in aqueous Hg concentrations was observed during replicate sediment resuspension experiments, likely reflecting variability in the distribution of Hg within the sediment. Less than 5.5% of the mass of water-soluble (F1) Hg was leached from the sediment during the 30 minute simulated sediment resuspension experiments. No trend was found for the % of F1 Hg released and the variation in the ratio of sediment to river water for each experiment. The SR3 sediment had relatively low Hg concentrations (24 mg $kg^{-1}$), yet leached the greatest proportions of water-soluble Hg. The results of the sediment resuspension experiments suggest that physical perturbations affecting the riverbank (such as storm and flooding events) may potentially increase Hg loading to the river water. Aggressive mixing of sediment and river water may result in the exposure of fresh mineral surface area to oxygenated waters.

The concentrations of Hg in the effluent from the column experiments were low relative to the concentrations in the resuspension supernatant; the differences in concentrations may be due to the enhanced oxidation of HgS minerals during the simulated sediment resuspension experiments or disaggreagation and enhanced dissolution due to a greater exposed surfaces. The column effluent chemistry varied for the different sediment samples, and Hg concentrations ranged from 0.03 to 8 mg $L^{-1}$ depending on the sediment sample. The concentration of Hg decreased following approximately 80 pore

flushes for most column experiments, with the exception of unchanged concentrations of 30-50 ng $L^{-1}$ in the SR1 effluent over time. Sustained saturated conditions in the column experiments may have decreased the Hg leaching potential of the sediments by converting soluble Hg to less-soluble forms under slightly reducing conditions. The unfiltered total Hg concentrations ranged from 1.7-2.3 times greater than the 0.45 μm filtered samples for SR1, SR3 and SR5 effluent, whereas the SR6 effluent had slightly larger contributions of particulate Hg. Approximately 40-48% of the 0.45 μm filtered Hg passed through the 5000 MWCO filter, indicating that colloidal Hg was being transported in the column porewater. The concentration of Hg passing the 0.45 μm filter increased for all column experiments in response to an increase in column flow rate, where the greatest effect was observed in column effluent of sediment containing the greatest solid concentrations of Hg (SR3 and SR6).

Concentrations of $NO_3$, Mn and Fe decreased throughout the duration of the experiments and were below SRW influent concentrations, whereas concentrations of $SO_4$ increased in most column effluent samples towards the end of the experiments. Elevated $SO_4$ concentrations relative to the influent and sustained presence of Hg in the effluent may indicate either sulfide oxidization or dissolution was occuring. Although the sediments studied have different portions of Hg as determined by the CSE analyses, the SR3, SR5 and SR6 exhbited similar Hg-leaching patterns over the course of the experiment.

**Table 2.1:** Chemical composition of South River water.

| Parameter | Input 1: SRW |
|---|---|
| Hg (ng $L^{-1}$) | 4.4 +/-1.1 |
| pH | 8.1 |
| Eh (mV) | 340 |
| Alkalinity (mg $L^{-1}$ as $CaCO_3$)) | 87 |
| Cl (mg $L^{-1}$) | 5.7 +/-1.6 |
| $NO_3$ (mg $L^{-1}$) | 3.3 +/-0.9 |
| $SO_4$ (mg $L^{-1}$) | 8.7 +/-2.8 |
| Ca (mg $L^{-1}$) | 18.6 +/-2.9 |
| K (mg $L^{-1}$) | 1.7 +/-0.7 |
| Mg (mg $L^{-1}$) | 7.0 +/-1.3 |
| Mn (µg $L^{-1}$) | 0.12 +/-0.1 |
| Na (mg $L^{-1}$) | 3.5 +/- 0.23 |
| Si ( mg $L^{-1}$) | 3.1 +/- 0.26 |
| Al (µg $L^{-1}$) | 31.7 +/-9.9 |
| Fe (µg $L^{-1}$) | 10.7 +/-9.7 |
| Lactate ( mg $L^{-1}$) | < 0.01 |

**Table 2.2:** Hg leaching as a result of sediment resuspension, represented as the % of soluble Hg (mass in F1) leached from the sediment at varying ratios of SRW:sediment.

| Sediment Sample | 40 : 1 | 20 : 1 | 10 : 1 | 4 : 1 |
|---|---|---|---|---|
| SR6 | 0.38 | 0.62 | 2.19 | 0.88 |
| SR5 | 0.49 | 0.49 | 1.93 | 0.60 |
| SR4 | 1.13 | 2.24 | 4.36 | 2.54 |
| SR3 | 5.50 | 4.66 | 2.94 | 3.70 |
| SR2 | 1.06 | 0.37 | 0.16 | 0.29 |
| SR1 | 0.25 | 0.25 | 0.19 | 0.17 |
| SRE | 1.04 | 1.05 | 0.69 | 0.46 |
| SRF | 0.79 | 0.95 | 1.04 | 0.52 |
| SRD | 1.08 | 0.68 | 0.88 | 0.42 |
| SRA | 3.19 | 3.07 | 2.43 | 3.63 |
| SRB | 0.03 | 0.01 | 0.01 | 0.01 |
| SRC | 0.003 | 0.002 | 0.001 | 0.001 |

**Table 2.3**: Calculated coefficient of determination ($R^2$) values for sediment resuspension experiments. Correlations were made between the mass of Hg leached into the aqueous phase as a function of total mass of Hg in the F1 and F2 fractions for a given mass of sediment.

| | RRM 0.1 | | RRM 3.5 | |
|---|---|---|---|---|
| **$H_2O$:Sed** | F1 | F2 | F1 | F2 |
| 40:1 | 0.71 | 0.71 | 0.99 | 0.99 |
| 20:1 | 0.89 | 0.98 | 0.98 | 1.00 |
| 10:1 | 0.95 | 0.95 | 0.99 | 0.99 |
| 4:1 | 0.93 | 0.97 | 0.96 | 0.96 |

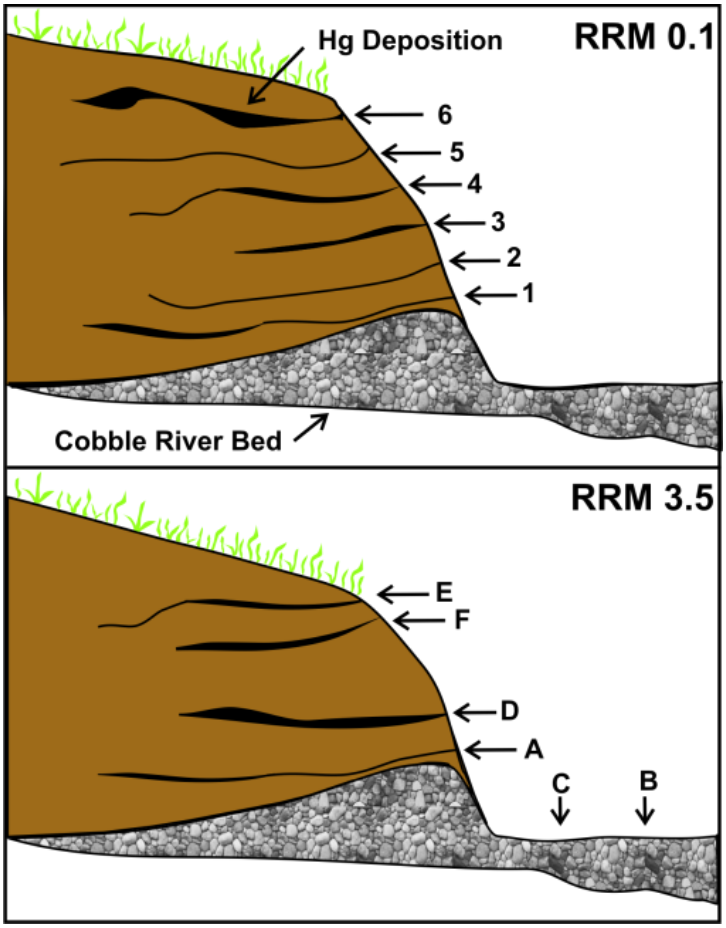


**Figure 2.1:** Schematic diagram of sediment sample locations for riverbank transect locations at 0.1 and 3.5 relative river miles (RRM) from the original point source.

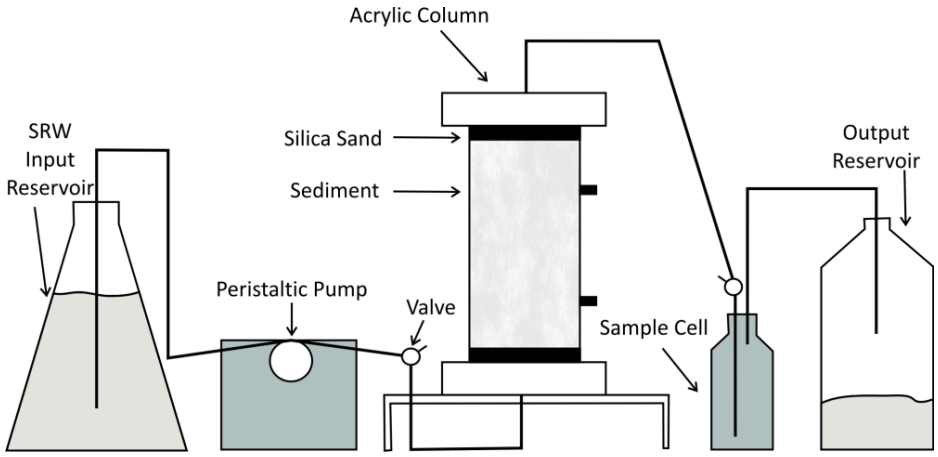


**Figure 2.2:** Schematic diagram of apparatus for column transport experiments.

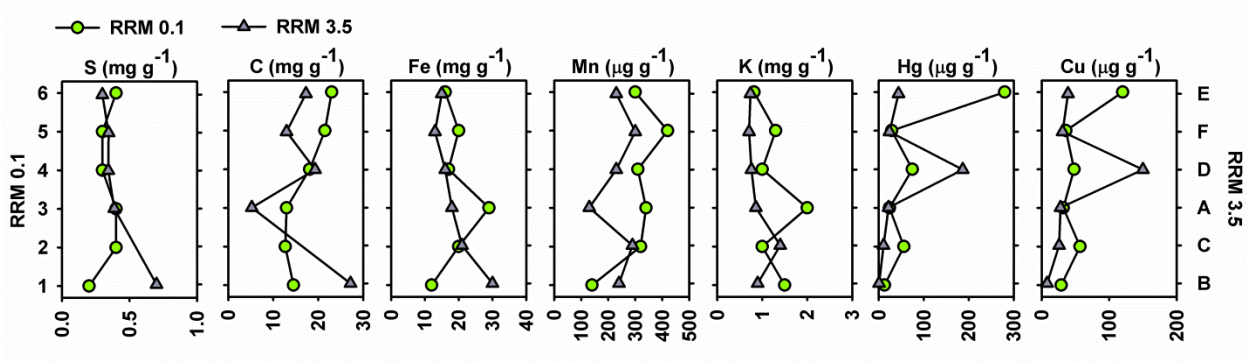


**Figure 2.3:** Depth profiles representing solid-phase concentrations of S, C, Fe, Mn, K, Hg, and Cu in the riverbank sediment for transects RRM 0.1 and RRM 3.5.

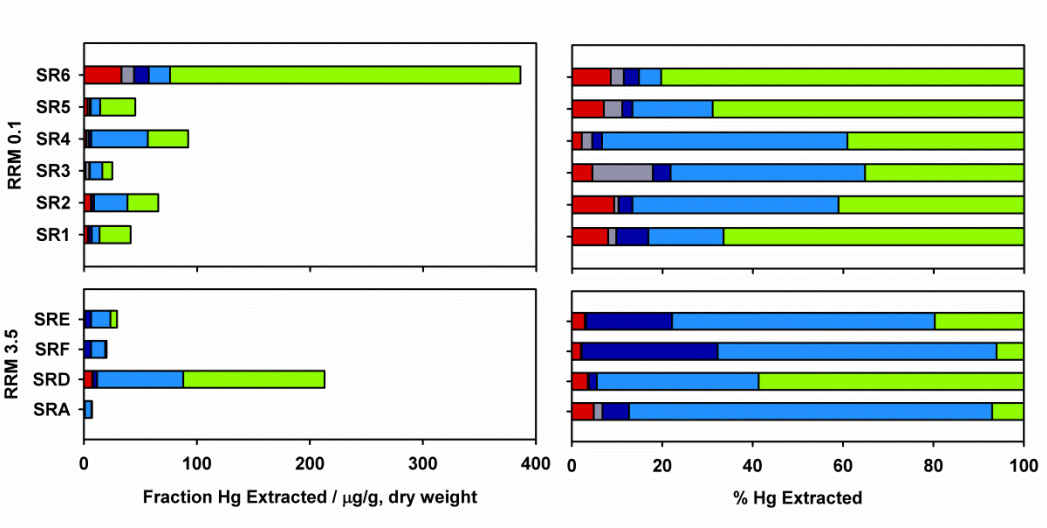


**Figure 2.4:** Operationally defined chemical fractions of Hg obtained by sequential chemical extraction methods developed by Bloom et al. (2003). Bank sediment profiles are represented by red ■ F1 green (deionized water) for water-soluble Hg species, grey ■F2 (HCl + acetate) for 'human stomach acid' soluble species, dark blue ■ F3 (KOH) for organo-chelated species, light blue ■ F4 ($HNO_3$) for elemental Hg, and green ■ F5 (aqua regia) for mercuric sulfide.

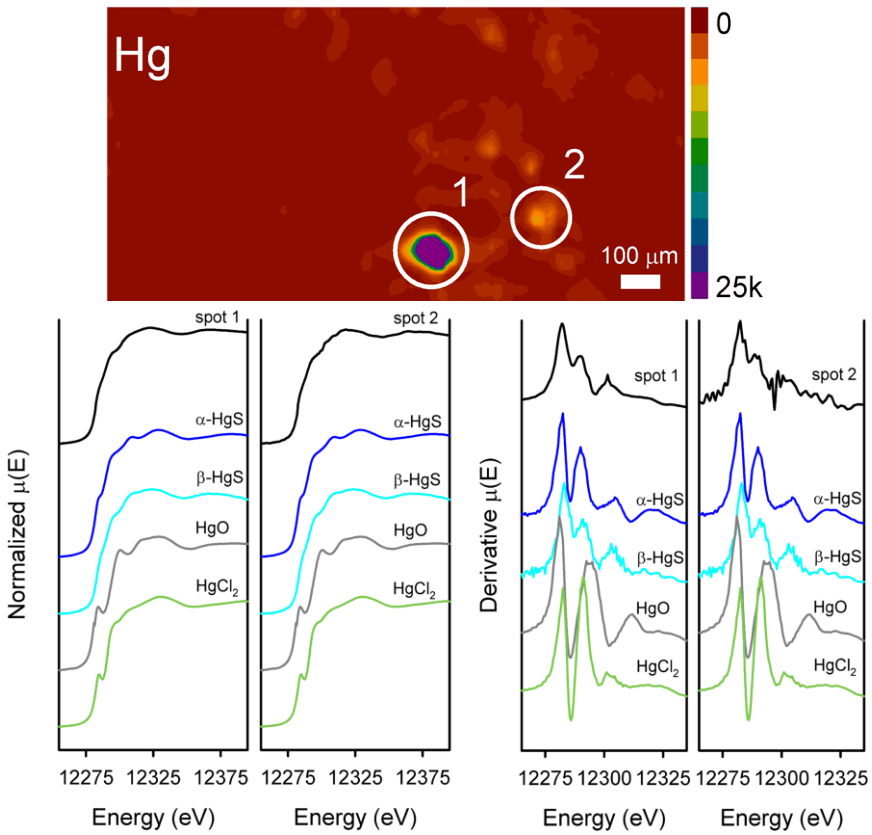


**Figure 2.5:** Micro-XRF map locations of Hg in SR6 sediment (a), comparisons of Hg L3 edge XANES spectra (b) and Hg L3-edge XANES fourier transform collected from representative standards (c).

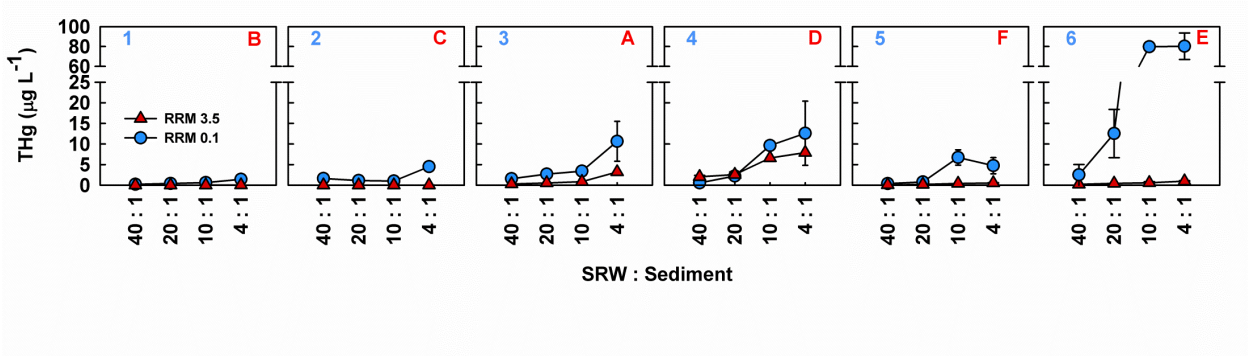


**Figure 2.6:** Concentrations of Hg in 0.45 µm filtered water samples released during sediment resuspension experiments reported as a function of the mass ratio of water and sediment. RRM 0.1 sediment is represented by ○, and RRM 3.5 sediment is represented by △.

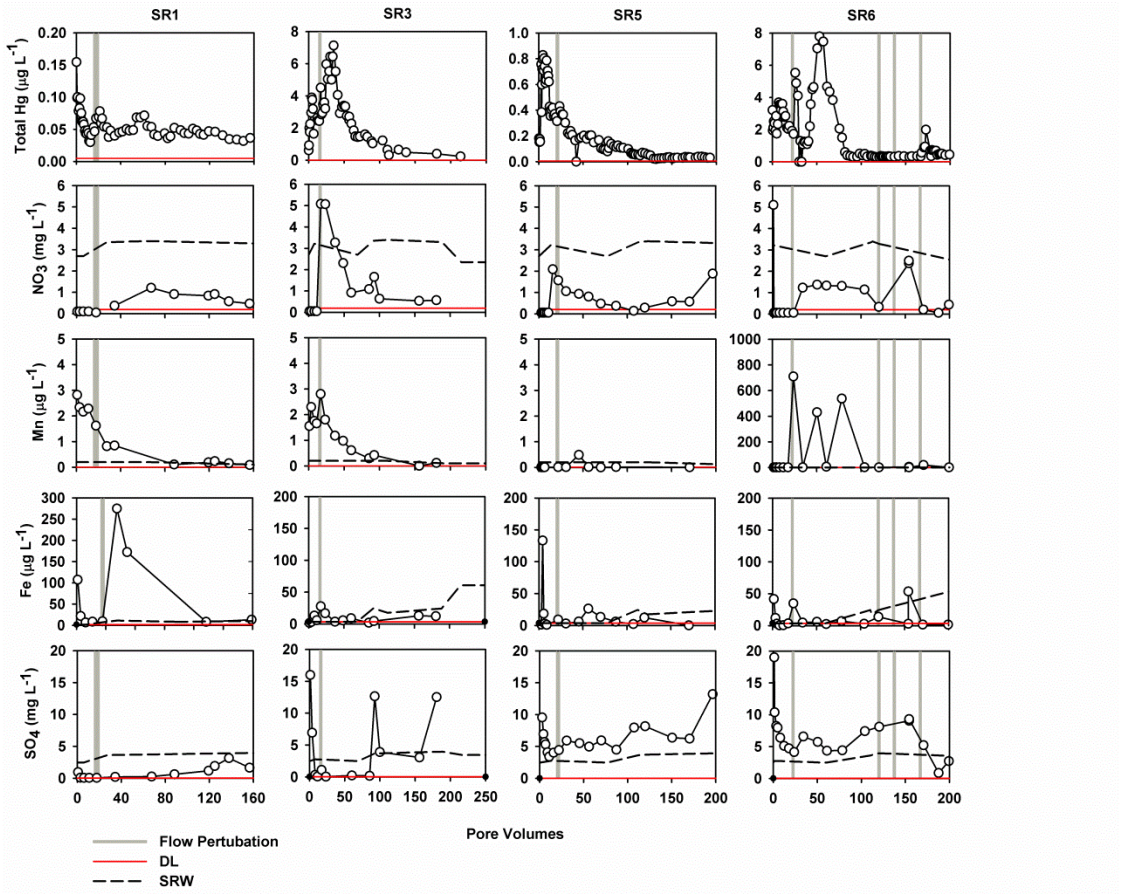


**Figure 2.7:** Aqueous concentrations of Hg and redox-associated species in the sediment column effluent. Gray bars signify a three times increase in flow velocity from one pore volume per week to three pore volumes per week. The second, third and fourth bars for the SR6 column represent 9 pore volumes per week, 12 pore volumes per week, and a two-week period of stagnant flow respectively. (DL=instrument detection limit)

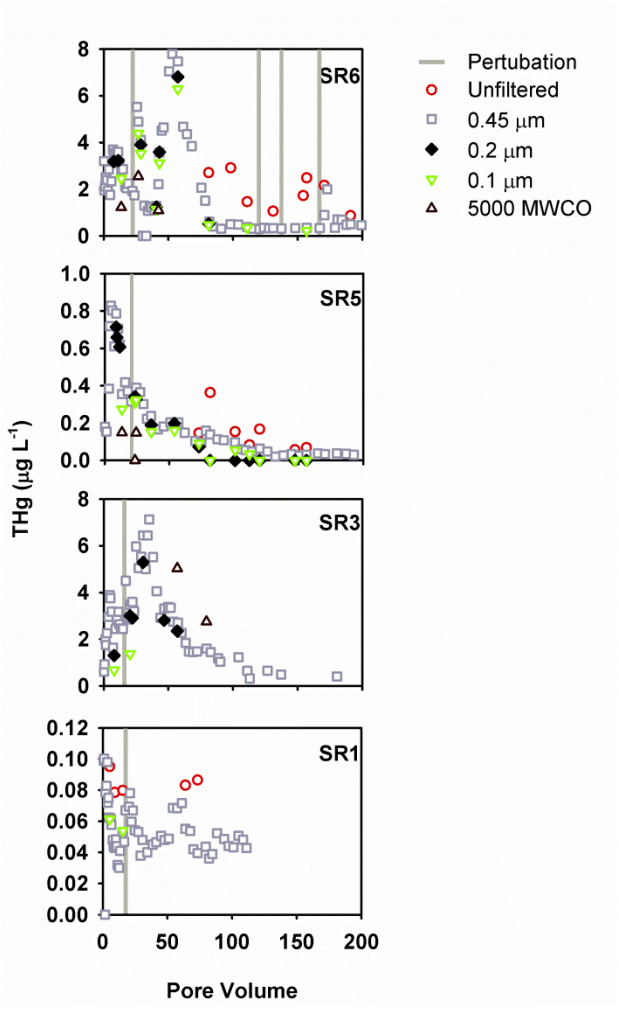


**Figure 2.8:** Concentrations of Hg in unfiltered and filtered effluent samples. Gray bars represent a three time increase in velocity, while the final bar for the SR6 plot represents a flow hiatus followed by flow resuming at one pore volume per week.

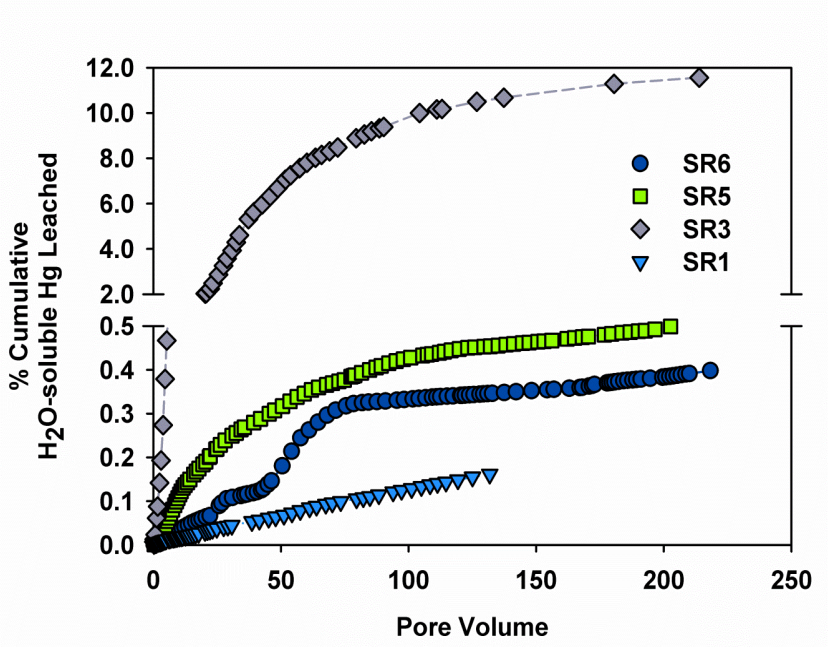


**Figure 2.9:** Cummulative % of the available water-soluble Hg leached from the sediment columns as a function of pore flushes.

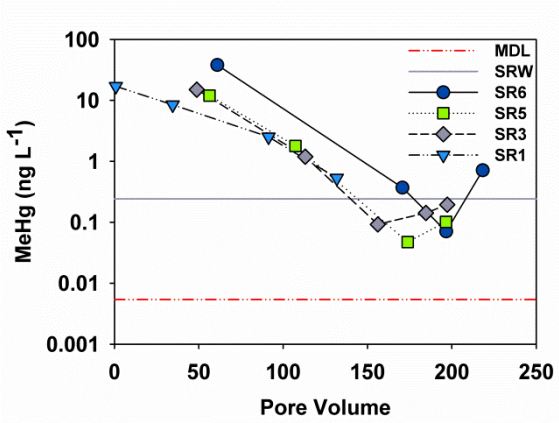


**Figure 2.10:** Methyl-Hg concentrations in column effluent over the course of the experiments.

# **Chapter 3:** *Treatment of Hg in the hyporheic zone pore water using reactive media*

## *3.1 Introduction*

Mercury (Hg) contamination in river systems by industrial and mining processes has been studied at numerous locations worldwide (i.e. Carson River (Nevada), Indrija, Slovenia and Soca Rivers (Italy), etc.). A lack of containment of industrial sources of Hg can result in the transport and dispersion of Hg throughout the floodplain, riverbank and riverbed soils over time. Soils and sediments have a large capacity to sequester Hg due to partitioning to mineral oxides and organic particles via adsorption, complexation (covalent and ionic bonding), and co-precipitation reactions (Suchanek et al., 2009). The interaction of surface water and groundwater in areas beneath and alongside streambeds (hyporheic zones) are important zones for exchange of dissolved constituents and nutrient cycling, where enhanced attenuation of Hg can occur.

During intense flow events, high velocity river water promotes increased erosion of riverbanks and can add to sediment loading into rivers (Pizzuto, 2012, Kocman et al., 2011). Mercury tends to sorb to particle surfaces, which when suspended, can be transported downstream. Additionally, Hg bound to colloidal and particulates can enter the water column via groundwater and surface water transport through the bank sediments and floodplain soils, and by advective-diffusive transport processes in the hyporheic zone (Figure 3.1a). Methyl-Hg (MeHg) has a high propensity to bioaccumulate, and can threaten wildlife and human health. The formation of MeHg is dependent on the biogeochemical conditions in sediments and soils, particularly the availability of aqueous $Hg^{2+}$, electron donors and acceptors, and the presence of methylating bacteria (Compeau and Bartha, 1985).

The solid-phase composition and forms of Hg in the sediment influence the solubility, mobility and toxicity; a detailed site characterization is often performed to evaluate site-specific remedial options.

River margins can bring about special remedial challenges as traditional management techniques are often complicated due to fluctuating river base-flow conditions. In general, common remedial approaches for river sediments include isolation (i.e. sediment capping), immobilization, stabilization or toxicity reduction (i.e. adsorption, ion exchange resin, chelating fibers, precipitating agents), and extraction (i.e. dredging, ex-situ treatment). In many cases, combinations of remedial approaches are used to limit the availability of Hg to aquatic organisms. Recent research has focused on the development of chemical additives to promote precipitation, coagulation, ion exchange or enhanced adsorption to limit mobilization of Hg (Cui et al., 2012, Zhang et al., 2012, Kwon et al., 2010). Ideally, the Hg retaining additive should be stable with respect to pH, redox, temperature, and microbial activity.

### *3.1.1 Site description*

Experiments were conducted using sediment from the riverbank and water of the South River near Waynesboro, Virginia. Mercury was introduced into the South River as a result of historical industrial operations between 1929 and 1950. Elevated concentrations of Hg are now observed in the riverbank sediments and floodplain soils up to 25 miles downstream from the point source, with the most elevated concentrations within approximately 8 km (5 miles) of the historical plant release site (Flanders et al., 2010). Solid-phase analysis using chemical sequential extractions and X-ray adsorption near edge structure (XANES) analyses indicated Hg is present in a form consistent with the structure of metacinnabar (HgS) (Chapter 2). However, significant masses of Hg are also present in more-soluble phases.

Results of characterization studies for bank sediments collected from the South River, as described in Chapter 2, was in agreement with further studies at the same location (Flanders at al., 2010, Rhoades et al., 2009), suggesting that frequent inundations of the riverbanks and regular erosion events are a potential source of Hg and Hg-bound particulates to the river water. Monitoring of Hg concentrations in river water and fish have resulted in fish advisories which have been in place since the

1970's (USGS, 2006). Concentrations of Hg in water, sediment and fish increase with increasing distance from the original point source in Waynesboro (Flanders et al., 2010), suggesting complicated Hg storage and transport mechanisms.

Natural attenuation is sometimes effective in dynamic fluvial environments, as natural sedimentation processes eventually limit advection/diffusion of the Hg-bearing sediment to the overlying water column. Due to elevated concentrations of Hg in the riverbank and floodplain soils, natural sedimentation processes may result in the transport and deposition of Hg. Dredging and capping techniques are often successful in decreasing the Hg available to aquatic organisms. Due to the extent and area of riverbank and floodplain soils in the South River containing elevated concentrations of Hg, dredging and capping alone may not adequately address the release, transport and deposition of Hg-bearing sediment. The most effective method is likely the combination of multiple techniques targeting specific Hg release zones.

Reactive treatment zones provide an alternative approach to stabilizing Hg-contaminated riverbanks, and can target biosorption, chemical precipitation, filtration, and ion exchange processes. Permeable reactive barriers are often used for the removal of contaminants in groundwater, where the reactive material is placed in the path of water flow to immobilize the contaminant within the reactive material (Blowes et al., 2000). Similarly, the placement of layers of reactive media along the riverbanks would promote the removal of Hg from water flowing through the media during ground water-surface water exchange, and overbank flooding events (Figure 3.1b). Similar techniques have been used for the remediation of organic and inorganic contaminants in river and lake bottoms (Knox et al., 2012, Ghosh et al., 2012, McDonough et al., 2007, Berg et al., 2004). However, few in situ treatment zones have been implemented in the environment for the specific immobilization of Hg in riverbank sediments.

### *3.1.2 Objectives*

The objectives of this study were to investigate the removal of aqueous Hg generated by the interaction of river water with the bank sediments of the South River, VA. Reactive materials were applied to South River sediment samples to assess the extent of removal of Hg from river water at environmentally relevant Hg concentrations. Riverbank sediments were amended with various types of reactive material including complexing agents, reductants and charcoals. The Hg-immobilization potential, longevity, and sorption capacity of the reactive amendments was assessed. Column studies were used simulate the flow of river water containing elevated concentrations of Hg through reactive media containing charred hardwood material. The temporal limitations and treatment effectiveness under continuous Hg loading were investigated. The objective of the experiments was to evaluate the potential effectiveness of reactive materials as amendments to the bank sediment to limit the release of Hg.

## *3.2 Materials and methodology*

### *3.2.1 Materials and reagents*

Sediment was collected from the banks of the South River at 0.1 relative river miles (0.16 km) downstream from the original Hg point source in Waynesboro, VA. Sediments were manually collected along a vertical transect extending from the base to the top of the bank by extracting 4-5 L of sediment in a horizontal direction inward from the bank surface. The sediment samples were immediately refrigerated until shipped to the University of Waterloo, where they were stored at $4^{o}$C and in dark conditions.

Three different riverbank sediment samples were used in conjunction with the reactive materials. Sediment sample SR6 was collected at the top of the riverbank and had a total Hg concentration of approximately 280 μg/g (Figure 3.1a). Sediment sample SR4 was collected beneath the SR6 sediment, and had Hg concentrations of approximately 90 μg/g. Sediment sample SR3 was collected at the halfway point between the base of the river and the top of the bank, and was collected directly beneath the SR4

sediment. The SR3 sediment has an approximately Hg concentration of 24 μg/g .The sediment samples extracted from each respective elevation along the riverbank were homogenized prior to experimental analysis.

Water was collected from the South River for use in both batch and column experiments. The water was collected at a location upstream from the point source, and was sealed in polypropylene containers, shipped to the University of Waterloo, and stored at 4$^{o}$C in dark conditions. Concentrations of Hg in the South River water were consistently below 5 ng $L^{-1}$. The chemical composition of the initial river water is reported in Table 3.1.

Seven different reactive materials were amended with the SR4 bank sediment (Table 3.2). Two clay materials were applied, including a hydrated magnesium aluminum silicate Attapulgite (a.k.a. palygorskite) clay (ATP), and commercially available organically modified bentonite clay (MRM). Chemical reductants were obtained, including granular zero valent iron (ZVI) (56 grade, $H_2$Omet TM 45 – 600 μm) shavings and granular elemental sulphur ($S_o$) pellets. The S pellets were crushed with a mortar and pestle to < 2 mm before use. A thiol-based compound 2,5-dimercapto$^{-1}$,2,4-thiadiazole (Thiol II) (a.k.a bismuthiol I) complexing agent was also obtained. The Thiol II compound was first dissolved in ethanol, air dried in a clean-hood, and sealed in a polypropylene container. A pure lump charcoal (CL2) was produced from maple and oak hardwood and kiln-dried at >500$^{o}$C in low oxygen conditions. The charcoal was crushed and sieved to < 2 mm and stored in sealed containers to avoid reaction with atmospheric water and contaminants. Granular activated carbon (GAC) (8-20 mesh) was used as a reference material.

Mixtures of the reactive materials were used in the sediment batch experiments. Batch experiments containing more than one type of reactive materials were blended together in equal volumes, with the exception of the ATP+Thiol II compound. The ATP+Thiol II compound was prepared by

dissolving 10 g of Thiol II in a solution containing 100 mL of ethanol and 100 g of ATP clay for 10 hours, followed by rinsing several times with deionized water (Gibson et al., 2011).

### *3.2.2 Hg immobilization batch experiments*

Sediment batch experiments were conducted to evaluate the change in Hg release from sediments in the presence of solid-phase reactive media additives. Approximately 80 +/- 1 mL of South River water (SRW) was mixed with 20 +/-0.1 g of wet SR4 sediment sample and 2 +/-0.05 g of dry reactive material. The batch experiments were conducted with a mass ratio of 40:10:1 SRW:sediment:media. Batch mixture controls were conducted using Milli-Q deionized water, SRW and SRW-sediment mixtures of the same ratio as the treatment batch experiments. Each batch experiment was performed in acid-washed 500 mL wide-mouth Nalgene amber bottles capped with Teflon lids. The mixtures were shaken for 30 seconds by hand and allowed to equilibrate for 14 days. The batch experiments were hand-shaken once more prior to decanting and collecting the supernatant for analysis. The de-watered sediment-media mixtures were then allowed to aerate for 33 days. Following the 33 day aeration period, an additional aliquot of 80 mL of SRW was added to each bottle, shaken for 30 seconds and allowed to equilibrate for 14 days.

The reactive media were blended with the sediment individually as well as in combinations (Table 3.2). The ATP clay was applied to the sediment individually and mixed at 1:1 ratios with ZVI, S and Thiol II. The MRM organically modified clay was applied to sediment batch experiments independently and co-blended at 1:1 ratio with S. ZVI was applied independently as well as blended with S at a 1:1 ratio. The crushed S was applied individually as well as mixed at 1:1 ratios as described above. The Thiol II compound was co-blended with the iron-silicate ATP clay as well as applied individually to the sediments.

A separate set of experiments was conducted with a subset of reactive materials (ATP, MRM, CL2, ZVI+S), and co-blended with sediment sample SR4 and with sediment sample SR6 to evaluate the effect of varying the mass of reactive media on the concentration of Hg in the river water supernatant.

The reactive materials were amended with SR4 sediment at dry weight proportions equal to 0.5, 1, 2 and 5%, and reactive materials were amended with the SR6 sediment at 1, 2, 5 and 8% (Table 3.2). The batch reactors were vigorously agitated for 30 seconds and allowed to equilibrate for 14 days.

All batch experiments were gently hand-shaken after the 14 day reaction, and were decanted into acid washed polypropylene centrifuge tubes. The samples were then centrifuged at 5000 rpm for 15 minutes. The sample was decanted from the remaining sediment in the centrifuge tube and transferred into a sterile *luer-lock* syringe, and passed through sterile filters arranged in series consisting of 1mm prefilter and 0.45 μm cellulose acetate membrane filters (Supor®, Acrodisc, Ann Arbor, MI).

### *3.2.3 Column experiments*

Two sets of column transport experiments were conducted, each of which consisted of two columns in series: a sediment leaching column, which contained sediment collected from the South River field site, and a treatment column which contained reactive media (Figure 3.2). The acrylic columns were approximately 340 $cm^3$ (15cm X 5 cm). At either end of the columns a coarse-mesh nylon screen was placed on the outside and a 120 ASTM mesh nytex screen was placed towards the inside of the column. A 2 cm layer of silica sand was placed at the bottom and top of each column to prevent fine particle transport. Two sediment samples that were collected from the South River bank were packed into separate columns. Column 1 contained sediment sample SR3 (24 mg $kg^{-1}$ of Hg) and column 2 contained sediment sample SR6 (280 mg $kg^{-1}$ of Hg). The columns containing sediment were packed in a fume hood under saturated and flowing conditions. South River water was pumped through the columns using a peristaltic pump (Ismatec, Switzerland) from the bottom upwards at approximately 3 pore volumes per week.

After an initial period of flow through the SR3 column (78 pore volumes), and the SR6 column (29 pore volumes) the columns were connected in series to a column of equal volume containing 1:1 (v/v) CL2 hardwood charcoal (< 2 mm) and granular silica sand. The treatment columns were packed under dry

conditions, and were purged with $CO_2$ gas for 2 hours before saturated. The initial pore flushes of the treatment columns were performed with SRW. After the treatment column was saturated the effluent from the sediment leaching column was directed into the sediment treatment column. The influent solutions and columns were wrapped in aluminum foil to limit photochemical reduction and microbial growth.

The column effluent was collected in a sealed cell to limit the interaction of the atmosphere with the column effluent (Figure 3.2). Aqueous samples were collected on a daily basis for the first month, and on a weekly basis thereafter. The treated column effluent was siphoned from the sample collection apparatus using a sterile Luer-*lock* syringe. The column effluent was analyzed for unfiltered particulate (> 0.45 μm), and colloidal (<0.45 μm) filter fractions of Hg using sterile filters (Supor® membrane fiber filters, VWR).

### *3.2.4 Analytical techniques*

Redox potentials were immediately measured on unfiltered aqueous samples using an Orion Pt redox electrode (model 96-78BN), after checking with Zobell's (Nordstrom, 1977) and Light's solution (Light, 1972). Redox measurements were corrected by the standard hydrogen electrode, and were reported as Eh values. The pH was measured using an Orion Ross combination electrode (model 8156000) calibrated with standard buffer solutions at pH 7, 4 and checked at a pH of 10. Measurements of alkalinity were made on 0.45 μm filtered samples using a HACH digital titrator and bromocresol green/methyl red indicator and with 0.16 N $H_2SO_4$.

Samples for Hg analysis were passed through sterile 0.45 μm filters, acidified with trace metal grade $HNO_3$ to a pH of less than 2, and stored in trace-clean amber glass vials. Total Hg concentrations were determined by cold vapour atomic fluorescence spectrometry (CVAFS Model 2500, Tekran Instruments Corp., Canada) following EPA method 1631. Samples for MeHg were acidified with trace ultra high purity HCl (Baker Instra Analyzed). Methyl-Hg concentrations were determined by CVAFS (Western University, ON) following EPA method 1630. A filtered aliquot of water was acidified with 12

N trace metal grade $HNO_3$ to a pH of <2, and total cations were determined by inductively coupled plasma – optical emission spectroscopy (ICP-OES; Thermo Scientific iCAP 6000), and trace elements were determined by inductively coupled plasma mass spectrometry (Thermo Scientific XSeries 2). An unacidified aliquot was used for analysis of anions ($SO_4$, $NO_3$, $NO_2$, Cl) (IC: Dionex ED50). Organic acids were determined on an IC using a IonPac AS17-C hydroxide-selective ion exchange column and were separated with a hydroxide gradient. SRW influent was periodically sampled for all aforementioned parameters, and was utilized to monitor variations in river water chemistry. Samples for MeHg were immediately frozen until time of analysis, and samples for all other analyses were immediately refrigerated at 4$^{o}$C and kept in darkness until time of analysis.

### *3.2.5 Solid-phase characterization*

Characterization of the sediment, reactive material, and sediment amendment mixtures were conducted by scanning electron microscopy (SEM) and fourier transform infrared spectroscopy (FTIR). Sediment amendment mixtures containing 5% reactive material were retrieved following the decanting of the supernatant. The de-watered amended sediments were extracted from the batch experiments containing 5% reactive material, oven dried at 35$^{o}$C, and kept at < 0$^{o}$C until time of analysis.

Mineralogical examination was performed on a LEO 1530 field-emission SEM (FE-SEM) fitted with an EDAX Pegasus 1200 energy-dispersion spectroscopy (EDS) system (Waterloo, ON). Samples were mounted on carbon adhesive, and coated with Au prior to analysis. A Robinson backscatter detector (RBSD) was used to collect the distribution of different elements in the samples. FTIR was performed at the University of Waterloo (Bruker Tensor 27). Samples for FTIR were mixed with KBr at an approximate ratio of 1v:300v and compressed into pellets. The spectra were recorded between the wavelengths of 4000 to 400 $cm^{-1}$.

## *3.3 Results and discussion*

### *3.3.1 Reactive amendment batch experiments*

Mercury removal was evaluated in the presence of seven reactive materials and combinations of these materials. The sorption or complexation of inorganic Hg for each of the reactive materials was assessed by amending with SR4 sediment and mixing with river water. The treatment effectiveness was determined by comparing the Hg concentration in the batch supernatant relative to un-amended sediment and water batches. The chemical composition of the supernatant was monitored to assess the release of constituents into the river water after interaction with the reactive amendments. The reactivity of the amendment mixtures was then tested by aerating the de-watered mixtures for 33 days prior to re-saturation. Re-saturation of the amended materials was used as an initial indicator of the extent to which the reactive materials retained the complexed/adsorbed Hg under variable saturation conditions. Control experiments were conducted with deionized water and SRW to assess the presence of background concentrations of Hg. The concentrations of Hg in the control experiments were consistently below 15 ng $L^{-1}$.

#### *3.3.1.1 Hg immobilization*

The selected reactive materials were mixed with SR4 sediment to evaluate the extent of removal of Hg from river water. The total Hg concentration of the SR4 sediment is approximately 75 mg/kg, of which 92% is likely present as less-soluble forms (HgS, HgSe, HgAu, $Hg_2Cl_2$, $Hg^0$) (Chapter 2). Six control experiments were performed where SR4 sediment was mixed with SRW in the absence of a reactive material. The average Hg concentration in the SR4 control experiments was 1900 ng $L^{-1}$ +/-580 with a 95% confidence interval of 722.

Concentrations of Hg in river water were generally lower than the control experiments for all reactive materials tested (Figure 3.3). The Hg concentrations of the reactive amendment supernatants

ranged from 75-99% less than the control experiments with SR4 sediment only. Concentrations of Hg in the treated supernatant ranged from 34-492 ng $L^{-1}$, with the exception of supernatant from the Thiol II batch experiments which were consistently below the analytical method detection limit (<2 ng $L^{-1}$). The lowest concentrations of Hg in the sediment-amendment supernatant was in the order of Thiol II (1 ng $L^{-1}$), GAC (34 ng $L^{-1}$) and S+MRM (111 ng $L^{-1}$) following the 2 week reaction period (Figure 3.3).

The observed Hg concentrations in supernatant from sediment amendments containing ATP (ATP, ZVI+ATP, S+ATP) ranged from 226-243 ng $L^{-1}$, with the exception of Thiol II +ATP (141 ng $L^{-1}$). The Hg concentration of the supernatant from the MRM amendment (169 ng $L^{-1}$) was somewhat elevated relative to MRM amendment blended with elemental S. The supernatant from the experiment with just elemental S amendment had Hg concentrations of 494 ng $L^{-1}$, and the supernatant from the experiment with ZVI had concentrations of 307 ng $L^{-1}$. The sediment amendment containing both ZVI+S had Hg concentrations of 226 ng $L^{-1}$, suggesting that the addition of both S and Fe together are more effective at decreasing Hg in water then when added individually.

Each sediment amendment batch experiment was de-watered and exposed to atmospheric conditions for 33 days before a second aliquot of SRW was added. The null hypothesis for the re-wetting experiments was that no significant change in Hg concentration in the supernatant would result following a period of aeration. The aeration and rewetting of the SR4 sediment control experiment resulted in lower concentrations of Hg in the river water supernatant (271 ng $L^{-1}$) relative to the Hg concentrations from initial saturation (1900 ng $L^{-1}$).

The re-saturation of most sediment-amendments failed to reject the null hypothesis; no significant change of Hg concentration in the river water was observed relative to the control experiment following a drying period of 33 days for each of the sediment-batch amendment experiments. Rewetting of the amended materials resulted in similar removal of Hg relative to the initial wetting experiments (Figure 3.4). Concentrations of the Hg in the supernatant of the re-wetted sediment amendment mixtures ranged

from 12-294 ng $L^{-1}$. On average, the Hg concentration of the sediment-amendment supernatants decreased by 95 ng $L^{-1}$ relative to Hg concentrations in the supernatant of the initial wetting experiments.

The decrease in Hg concentrations in the river water relative to the control experiment were greater than 80% for ATP+Thiol II, Thiol II, GAC and ZVI+Fe. The supernatant from the ATP, MRM, GAC, ZVI+ATP, S, and S+ATP amendments resulted in 18-59% difference in Hg concentrations relative to the rewet SR4 control. The supernatant for the S+MRM sediment amendment resulted in slightly elevated Hg concentrations (~300 ng $L^{-1}$) relative to both the SR4 control and initial wetting experiments. Similarly, the Hg concentration of the initial MRM supernatant was 22 ng $L^{-1}$ lower than the concentration of the rewetted amendment supernatant. The observed increase in Hg concentrations after the 33 day period of aeration suggests that the stabilization of Hg in the MRM amended SR4 sediment under variable saturated conditions was less consistent relative to the other amendments studied.

*3.3.1.2 Aqueous geochemistry*

Analysis of total cations and anions in the batch experiment supernatant were made to aid in determining the reaction mechanisms associated with the release or retention of Hg from the sediment. The release of trace metals and nutrients due to the addition of reactive materials was monitored in comparison to un-amended sediment batch experiments to determine the effects of different media to the composition of SRW (Figure 3.3, Table B.1).

The ATP clay amended with the SR4 sediment resulted in similar nutrient concentrations as the South River water and SR4 sediment control experiment (SRW+SR4). Concentrations of $NO_3$ (30 mg $L^{-1}$) were similar to the SRW+SR4 concentrations, and were elevated relative to the other amendment systems. Concentrations of $SO_4$ were slightly elevated (13 mg $L^{-1}$) relative to the sediment control (7-10 mg $L^{-1}$). The redox potential for ATP was approximately 400 mV, and was similar in range to all other amendments (280-460 mV). The negatively charged surface sorption sites of clays are due to the characteristic tetrahedral layers of clay materials, resulting in cationic exchange processes on the surface

layers. ATP is a hydrated magnesium aluminum silicate clay that has been used for the sorption of cations including organic compounds and heavy metals (Zhao et al., 2009, Fan et al., 2009). ATP clay has been studied for contaminant treatment due to a moderate affinity for cation exchange, abundant surface hydroxyl groups, high surface area, and relatively high abundance and low cost compared to other types of reactive materials (Chen and Wang, 2007).

MRM adsorption media is a commercial product formulated to target the treatment of dissolved organic compounds, arsenic, and Hg. Organo-clays incorporate covalent or iono-covalent bonding to strongly bind the organic material to the clay particle to stabilize the organo-functional groups (Tonle et al., 2003). Final concentration of $NO_3$ (3 mg $L^{-1}$) in the supernatant following the co-blending of MRM with SR4 sediment and SRW was lower than that of the SRW+SR4 control (30 mg $L^{-1}$). The final concentration of $SO_4$ in the river water was elevated to approximately 130 mg $L^{-1}$ after interaction with the MRM amendment, which was similar to final $SO_4$ concentrations of the sediment amended with elemental S (162-293 mg $L^{-1}$). The final Cl concentration for the MRM amended experiment was 412 mg $L^{-1}$, and was 1.8 times greater than the average Cl concentration for all other amendments. The MRM batch experiment supernatant also had elevated concentrations of Ca (110 mg $L^{-1}$) relative to the control (45 mg $L^{-1}$).

Periodic overbank flooding and fluctuating water tables can temporarily limit $O_2$ diffusion into the soil and cause microbial communities to respire terminal electron acceptors, such as iron oxy hydroxides and sulfate. Elevated concentrations of Fe (26 μg $L^{-1}$) were observed in the blended ZVI supernatant relative to supernatant from the control and from all other sediment amendments, with the exception of Thiol II (1050 mg $L^{-1}$). The elevated concentrations of Fe in the blended ZVI treatment supernatant were likely associated with the dissolution of (oxy)hydroxide coatings on the surface of the ZVI filings. Concentrations of $SO_4$ (9.4 mg $L^{-1}$) were similar to the SRW+SR4 control, as were concentrations of total S (4 mg $L^{-1}$).

The oxidation of ZVI can occur from interacting with river water either via the reduction of $H_2O$ or $SO_4$ governed by the following reactions:

$$Fe^0{}_{(s)} + 2H^+ \rightarrow Fe^{2+}{}_{(aq)} + H_{2(g)} \quad (3.1)$$

$$4Fe^0{}_{(s)} + SO_4{}^{2-}{}_{(aq)} + 8H^+ \rightarrow S^{2-}{}_{(aq)} + 4Fe^{2+}{}_{(aq)} + 4H_2O_{(l)} \quad (3.2)$$

The redox potential of the ZVI supernatant (275 mV) was less than that of the control (417 mV), however was not in the typical range of sulfate reduction (Stumm and Morgan, 1996). The alkalinity was 30 mg $L^{-1}$ (as $CaCO_3$) and was less than that that of the control, suggesting that alkalinity may have been consumed.

The pH of the amended MRM batch experiment supernatant was 7.7 and was similar to the SRW+SR4 control (pH ~ 7.9). The concentration of Mn was ~ 4 μg $L^{-1}$, and the SRW+SR4 control was <0.6 μg $L^{-1}$. The elevated Mn concentration in the supernatant following the interaction with the MRM amendment suggests that $MnO_2$ may have been reduced and $Mn^{2+}$ was mobilized. Manganese may have been reduced by $Fe^{2+}$ according to the following reaction:

$$2Mn^{4+} + 2Fe^{2+} + H^+ \rightarrow 2Mn^{2+} + 2Fe^{3+} \quad (3.3)$$

The concentration of $NO_3$ in the S-amended batch experiment supernatant was ~ 0.2 mg $L^{-1}$, and decreased relative to the control SRW+SR4 supernatant by 30 mg $L^{-1}$. However concentrations of $NH_3$-N were similar to the control (0.07 mg $L^{-1}$). The concentration of Mn was elevated at 49 μg $L^{-1}$, and Fe increased by 5.5 μg $L^{-1}$ from the control to a concentration of 15 μg $L^{-1}$. The concentrations of $SO_4$ and total S were 163 mg $L^{-1}$ and 52 mg $L^{-1}$, respectively. The overall S concentration varied from the control experiment by 1300-1600%. Dissolved elemental S is expected to oxidize to $SO_4$ upon interaction with well oxygenated river water. The oxidation of elemental sulfur by the reduction of $O_2$, Mn (IV) or Fe (III) may have occurred, resulting in elevated concentrations of sulfate. The pH of the supernatant (7.1) was 0.9 units lower than the control, and the alkalinity was 62 mg $L^{-1}$ (as $CaCO_3$), suggesting the production

of acid and the consumption of alkalinity in the batch experiment water. Svensson et al. (2006) observed that the oxidation of elemental S with HgO results in the production of HgS and a decrease in pH.

$$4S^0{}_{(s)} + 2HgO + H_2O \rightarrow 3HgS + SO_4{}^{2-} + 2H^+ \qquad (3.4)$$

The redox potential of the S-amended supernatant was elevated (444 mV) relative to the other amendment batch experiments, with the exception of ZVI+S. Sulfur and/or sulfide minerals are effective at binding up $Hg^{2+}$ in the environment (Barnett et al., 2001). The majority of compounds used for the treatment of Hg-contaminated water contain sulfur due to the strong covalent bonds created by the Hg-S complex (200 KJ $mol^{-1}$). The decline in alkalinity observed for batch experiments containing Thiol II, S, ZVI+S, S+MRM was likely due to consumption of alkalinity through reaction with acid generated from sulfide mineral oxidation (Evangelou and Zhang, 1995, Benner et al., 1999). However, Hg concentrations in the elemental S experiment were elevated relative to other experiments (494 ng $L^{-1}$). The formation of excess $SO_4$ in the river water may have resulted in the production of mobile $HgS_2{}^{2-}$. The sorption of $Hg^{2+}$ in soils and sediments is pH dependent and can decrease with decreasing pH.

The supernatant of the Thiol-based compound experiment had the highest concentrations of Mn (60 mg $L^{-1}$) and Fe (1053 mg $L^{-1}$) relative to the other amendment experiments. Concentrations of $NO_3$ were similar to the control (26 mg $L^{-1}$). Sulfate concentrations were low (19 mg $L^{-1}$) relative to other S containing batch amendments (163-293 mg $L^{-1}$). The total S concentration for the Thiol II batch experiment was much higher than all other compounds tested (512 mg $L^{-1}$). A yellow precipitate/flocculent was observed in the supernatant from the Thiol II experiments, and may indicate super saturation with respect to elemental sulfur. The pH of the Thiol II supernatant was 4.8 and the redox potential was 300 mV. Alkalinity decreased by 87 mg $L^{-1}$ (as $CaCO_3$) relative to the control with concentrations of 53 mg $L^{-1}$. The greatest aqueous concentrations were observed for Ca, Mg, Si, Ni, Se, Zn, Al and As in the supernatant of the Thiol II amended with SR4 sediment. Thiol compounds have a

high affinity for Hg, and can result in a polymerized Hg–thiolate compounds and thermally stable metal-sulfide covalent bonds (Blue et al., 2010).

The ATP+Thiol II supernatant had less elevated concentrations of $NO_3$, Mn, Fe, S, Ca, Si, Ni, Se, Zn, Al and As relative to the supernatant from the batch experiment containing the Thiol II compound alone. Elevated pH (8) and alkalinity (205 mg $L^{-1}$ as $CaCO_3$) in the Thiol II & ATP supernantant compared to the Thiol II supernatant suggests that the Thiol II & ATP mixture provided additional sorption and pH buffering. Dissimilar from the independent experiments for both the Thiol II and the ATP batch experiments, the ATP+Thiol II supernatant had depleted concentrations of $NO_3$ (0.25 mg $L^{-1}$) and elevated concentrations of $SO_4$ (310 mg $L^{-1}$). The redox potential was similar to the Thiol II supernatant (300 mV) and may indicate the potential reduction of $NO_3$ by reduced $S^{2-}$.

The water quality guidelines for Virginia State (adjusted for alkalinity) were exceeded for Ni (106 μg $L^{-1}$), Zn (2.4 μg $L^{-1}$), Cu (245 μg $L^{-1}$), and exceeded the drinking water quality guidelines for Fe (0.7 mg $L^{-1}$) for the Thiol II amendment supernatant. Additional research is required to identify the release of chemical constituents under constant flushing conditions and long term experimental analysis to determine if the guidelines can be met according to the total method detection limit (TMDL). Sulfate concentrations exceeded the limits for drinking water quality guidelines (>250 mg $L^{-1}$) for all of the reactive materials containing S compounds (S+ATP, ATP+Thiol II, S+MRM, ZVI+S), with the exception of Thiol II. The critical drinking water guidelines for Cl (230 mg $L^{-1}$) were exceeded for MRM, and were only slightly below for the S+MRM amendment. The measured concentrations of Cu in the river water approached the limit when the sediment was mixed with amendments containing Fe. Virginia water quality guidelines for chronic freshwater concentrations for arsenic are 150 μg $L^{-1}$, and were not exceeded for any reactive compounds tested.

The potential mechanism leading to the removal of Hg in river water following the application of reducing agents (ZVI and S) is dependent on the redox potential, oxidation of Fe, and reduction of $SO_4$.

Sulfate reducing bacteria (SRB) can utilize $H_{2(g)}$ as an electron donor to produce hydrogen sulfide via the following reactions:

$$Fe^{0}{}_{(s)} + 2H^{+} \rightarrow Fe^{2+}{}_{(aq)} + H_{2(g)} \quad (3.5)$$

$$SO_4{}^{2-}{}_{(aq)} + 4H_{2(g)} + H^{+} \rightarrow HS^{-}{}_{(aq)} + 4H_2O_{(l)} \quad (3.6)$$

The reduction of sulfate may result in the formation of less-soluble sulfides with divalent metals, and precipitate out of solution.

$$Hg^{2+}{}_{(aq)} + S^{2-}{}_{(aq)} \rightarrow HgS_{(s)} \quad (3.7)$$

A similar reaction mechanism is observed in column experiments demonstrating the use of ZVI to treat Hg in groundwater (Weisener et al., 2005). The reduction of $SO_4$ by ZVI resulted in decreased concentrations of Hg, and the precipitation of an identified Hg-S mineral in the column material. A similar mechanism may have been responsible for the removal of Hg in the ZVI and ZVI+S batch experiments. The experiments were performed in an aerobic environment with approximately 5-6 cm of headspace in the sample bottle, and the concentrations of dissolved sulfide were not measured. In addition to redox mechanisms, the available $Hg^{2+}$ may have adsorbed to Fe-hydroxide minerals on the surface of the ZVI fillings.

### *3.3.2 Hg treatment capacity*

A subset of reactive materials was selected to determine the optimal Hg adsorption capacity for each reactive material. The treatment experiments were performed using adjusted doses of reactive material to determine the removal of Hg from river water per mass of media applied. The Hg treatment capacity experiments were performed using variable doses of ATP, MRM, ZVI+S and a hardwood charcoal material (CL2). The reactive materials were blended with two different sediment samples (SR4 and SR6) that vary in terms of total Hg concentration, chemical association of Hg, and Hg leaching potential.

The SR6 bank sediment (THg ~ 280 g $kg^{-1}$) was selected due to the relatively elevated Hg concentrations that were leached from the sediment during simulated resuspension and column leaching experiments (Chapter 2). The SR4 bank sediment (THg ~ 75 g $kg^{-1}$) was chosen due to the relatively smaller amount of soluble-Hg species and high portion of insoluble Hg complexes in comparison to SR6 sediment. The mass of reactive material added was determined based on the Hg-leaching potential of the SR4 and SR6 sediments, where 0.5, 1, 2 and 5 % and 1, 2, 5 and 8 % (dry weight) of reactive material were applied, respectively. The SR4 control experiments supernatant had Hg concentrations of 1900 ng $L^{-1}$ +/-580, and the SR6 control experiments had Hg concentrations 13330 ng $L^{-1}$ +/-2600 (95% confidence interval of 4140).

The concentration of Hg in supernatant of experiments containing SR4 sediment amended with ATP ranged from 222-443 ng $L^{-1}$, with the lowest Hg concentration occurring in the experiment containing 5% ATP material (Figure 3.5). Concentrations of Hg in the supernatant experiments containing SR6 sediment amended with ATP ranged from 2300-3600 ng $L^{-1}$, with the lowest Hg concentration in the experiment containing 8% ATP. Concentration of Hg in supernatant of experiments containing MRM ranged from 107-502 ngL-1 when amended with SR4 sediment, and ranged from 1200-2700 ngL-1 when amended with SR6 sediment. When amended with SR4 and SR6 sediment, the supernatant for experiments containing MRM material had the lowest Hg concentrations when amended at 5% and 2% respectively. Concentration of Hg in supernatant of experiments containing ZVI+S ranged from 240-150 ngL-1 when amended with SR4 sediment, and ranged from 980-11000 ng $L^{-1}$ when amended with SR6 sediment. When amended with SR4 and SR6 sediment, the supernatant for experiments containing ZVI+S had the lowest Hg concentrations when amended at 2% and 8% respectively. Concentration of Hg in supernatant of experiments containing CL2 ranged from 380-750 ng $L^{-1}$ when amended with SR4 sediment, and ranged from 1500-7800 ng $L^{-1}$ when amended with SR6 sediment. When amended with SR4 and SR6 sediment, the supernatant for experiments containing CL2 had the lowest Hg concentrations when amended at 5% and 8% respectively.

The maximum treatment effectiveness was determined as the mass of Hg removed from solution per unit mass of reactive material. The metal uptake capacities of each reactive material were calculated for the SR4 and SR6 sediment samples to determine the optimal ratio for application to the riverbank sediment (Table 3.3). Mercury uptake capacity was calculated using the following equation:

$$Q = \frac{C_i V_i - C_f V_f}{m} \quad (3.8)$$

Where Q is the uptake capacity (ng $g^{-1}$), $C_i$ is the initial concentration without treatment, $V_i$ is the initial volume of the batch, $C_f$ is the final aqueous concentration after the addition of reactive material, $V_f$ is the volume of the treated sample, and m is the mass of reactive material. Uptake capacity was calculated based on an average initial Hg concentration obtained by independent quadruplicate batch experiments to determine $C_i$. The SR6 $C_i$ was determined to be 13330 ng $L^{-1}$, and the SR4 $C_i$ was used 1900 ng $L^{-1}$.

The estimated mass of Hg removed per unit mass of reactive material was greatest for the SR6 sediment (209 +/- 122 ng $g^{-1}$) in comparison to experiments with the SR4 sediment (115 ng $g^{-1}$ +/- 81) (Table 3.3). Some variability in Hg removal capacity is likely attributed to the non-uniform distribution of Hg within the sediment, resulting in inconsistent Hg leaching from the sediment for each batch experiment. In general, Hg uptake capacity decreased with increased dosage of reactive material. The sorption efficiency may be limited due to reaction kinetics (Zhao et al., 2009), adsorption site availability or surface area (Dzombak et al, 1987). The lowest uptake capacity was observed when SR6 sediment was amended with low doses of ZVI+S.

The Hg uptake capacities varied for each reactive material depending on the sediment and ratio of reactive material added to each batch. The Hg uptake capacity for the ATP and MRM experiments averaged 180 ng $g^{-1}$ +/- 120, and 190 +/- 150 ng $g^{-1}$, respectively. The maximum adsorption capacity of $Hg^{2+}$ onto ATP was found to be 388 ng $g^{-1}$ for the amendment of 2% ATP with SR6 sediment. Zhao et al. (2009) found that a polyacrylamide/ATP blend resulted in primarily chemisorption of $Hg^{2+}$ up to 193 mg $g^{-1}$, and that adsorption decreased with increased dosage for both ATP and the ATP blended material.

Similarly, Hg adsorption up to 800 mg $g^{-1}$ was observed for a polyaniline-ATP composite material (Cui et al., 2012). Although, the literature referenced sorption of these materials were conducted with artificially spiked Hg solutions at concentrations unlikely to be found in the environment.

The average Hg removal of the ZVI+S amendment was less variable (130 ng $g^{-1}$ +/- 90) than the ATP and MRM amendments. The CL2 hardwood charcoal was the most consistent of all the amendments studied with an average uptake capacity of 125 ng $g^{-1}$ +/-67 for both the SR4 and SR6 sediment for all dry weight additions. The maximum calculated uptake capacity for CL2 charcoal was approximately 200 ng $g^{-1}$ for both SR4 sediment (0.5%) and SR6 sediment (2%).

The overall adsorption of mercury to mineral and organic particles can be dependent on surface area, organic content, cation exchange capacity, and grain size. The ATP and MRM amendments had the greatest calculated metal uptake capacities for all experiments, with the exception of the experiments using 5% amendment to the SR6 sediment. Clay and organic-rich soils generally have high capacity for adsorption and retention of contaminants (Gabriel & Williamson, 2004, Zhao et al., 2009). The MRM clay was observed to have slightly better Hg uptake capacities for most experiments relative to the ATP clay. Clays that have been modified by the addition of organic amino or thiol based compounds generally have higher cation exchange capacities and metal chelating functionality (Vieira et al., 1997). Charred organic material has a high propensity for cation exchange, and is particularly effective due to high surface area. Functional groups on the surface of the charred particles may allow for the removal of Hg, particularly in the forms of $Hg(OH)_2$, $HgCl_2$, $Hg(NO_3)_2$), and HgO (Kim et al., 2005). Zhu et al., (2009) concluded that enhanced removal of Hg by modified activated carbon amendment was greatest when S and N ligands were present. With consistent removal of Hg for both sediment samples, in addition to low variability in Hg uptake capacity for varied masses of reagent added, the CL2 harwood charcoal material was selected to assess the treatment effectiveness under continuous Hg loading conditions.

### *3.3.3 Amendment characterization*

The surface structure of the reactive materials was characterized using SEM-EDX analysis. The elemental compositions of the reactive materials were verified by EDAX scans accompanying the SEM imagery (Figure 3.6). The image of ATP shows that the clay is generally comprised of uniform, well-rounded particles that are homogenous throughout the material. The brightened image of ZVI indicates the presence of heavy metals with a crystalline surface structure. The ZVI+S image depicts a crushed elemental S pellet among smooth silicate clay particles. The image of MRM reveals a heterogeneous mixture of materials, with some S, Si, and Al mixed throughout. The Thiol II image depicts clumps of small crystalline structures composed of S. The CL2 image depicts porous and distorted layered structures of various sizes and shapes, as well as visible micro and macropores in woody debris. The CL2 charcoal is composed of C (84%) and O (12%). The ATP clay was comprised of Si (31%), O (40%), Al (8%), Mg (6%) and Fe (5%). MRM consisted of mainly S (87%), O (10%), Si (2%) and Al (1%), and Thiol II was composed of S (75%) and O (20%) (Table B.2).

The surface organic-inorganic ligands were characterized by FTIR to determine the presence of major functional groups on the material before and after interaction with Hg contaminated sediment (Figure 3.7). In general, the spectra for the sediment amendment samples resembled the spectra signatures of the SR4 and SR6 sediment, likely due to the amendment ratio of 20 parts sediment and one part reactive material. The peaks at 3620 $cm^{-1}$ correspond to the stretching vibrations of Al-OH and were present in both the SR4 and SR6 sediments in addition to all the sediment amendments studied, with the exception of ATP. Both the SR4 and SR6 sediments contained double peaks between 2800-3000 $cm^{-1}$, indicating the stretching vibrations of $CH_3$ and $CH_2$. The SR4 and SR6 sediment samples also revealed a broad peak at approximately 3600 $cm^{-1}$, which is indicative of hydroxyl groups (Tonle et al., 2003). Peaks were observed at 2600-3200 $cm^{-1}$ in all sediment amendments and indicated O-H stretching vibrations. Small but broad peaks were observed at ~ 1640 $cm^{-1}$, and suggested the presence of

carboxylate groups. The asymmetry towards 2600 $cm^{-1}$ is indicative of strong hydrogen bonding (Biniak et al., 2009).

The spectra for the ATP control had similar spectra to the sediment controls. Peaks at 1650 $cm^{-1}$ in the sediment, sediment amendments and ATP reference material suggest absorbed water (Li and Wu, 2011). Similar findings were determined by the EDAX scan which suggested that a large proportion of oxygen may also be indicative of water being retained in the clay material. The spectra signature of the ATP material was similar to the sediment samples from 3500-4000 $cm^{-1}$; a signal which was not observed in other reactive materials. A stretching at 3450 $cm^{-1}$ in the ATP reference material and sediment samples may also indicate stretching of $-NH_2$ groups (Wang & Wang, 2010). Characterization of treatment media by XAFS of aqueous $HgCl_2$ mixed with ATP and with Thiol II (2,5 dimercapto-1,3,4-thiadiazole) revealed Hg-S bonding (Gibson et al., 2011). In addition, Gibson et al., (2011) suggested Hg-O bonding on activated carbon and granular iron fillings.

The MRM material is dissimilar to the sediment and other reactive materials at wavelengths less than 1500 $cm^{-1}$. The MRM media has peaks at 2926 $cm^{-1}$ which are associated with C-H stretching. An additional peak was observed at 1475 $cm^{-1}$ indicating the presence of carboxyl-carbonate groups, and 2904 $cm^{-1}$ illustrates the presence of a C-H aromatic stretching vibration. The peak at 1509 $cm^{-1}$ represents the presence of C=C alkenes, in addition to peaks from 1450-1600 $cm^{-1}$. An N-H vibration may also be present at 1651 $cm^{-1}$. The Thiol based compound has peaks as 3056, 3020 and 2857 $cm^{-1}$, however signals at these wavelengths were not observed in the sediment amendment. Additional alkene peaks for the Thiol control were detected at 1504 $cm^{-1}$ and indicate the occurrence of double bond vibrations and aromatic rings. A peak was observed at approximately 2500 $cm^{-1}$ for the Thiol II control, and is indicative of –SH stretching. The C-S stretching was also observed for the Thiol II media at 710 $cm^{-1}$.

### *3.3.4 Column experiments*

A series of sediment columns were designed to emulate the slow advective diffusive processes due to flow of water through the riverbanks under saturated conditions, and were connected in series to columns containing charred hardwood material. The column series evaluated treatment effectiveness under continuous Hg loading, and were used to assess the temporal limitations of the reactive material under flow rates typical of field conditions.

#### *3.3.4.1 Hg immobilization*

The total Hg concentrations released from both the SR3 and SR6 leaching columns gradually declined over time (Figure 3.8 and Figure 3.9, respectively). The 0.45 μm filtered SR3 column effluent declined from 1.8 to 0.3 μg $L^{-1}$ over a period of 14 months, and the SR6 effluent Hg concentration declined from 13 to 2.5 μg $L^{-1}$ over a period of 7 months. The unfiltered effluent from the SR3 column did not appear to fluctuate over the course of the experiment, and suggests a large particulate contribution to the total Hg concentrations released from this sediment sample. Towards the end of the experiments, the filter-passing Hg ranged from ~22-25% of the total Hg in the effluent for both columns. Approximately 87-89% of the filtered passing Hg passed through the 0.1 μm filter, suggesting that ~20% of the total Hg in the column effluent is in the colloidal or dissolved phase.

After approximately 165 pore volumes of the SR3 column effluent passed through the CL2 treatment column, the concentration of filter-passing Hg in the water decreased to < 20 ng $L^{-1}$, with a treatment effectiveness of 98%. The diversion of the SR6 column effluent through the CL2 treatment column resulted in a gradual increase in Hg concentration within the initial 40 pore volumes, with a maximum Hg concentration of 146 ng $L^{-1}$. The filtered Hg concentration of the SR6 treated effluent stabilized at approximately 100-120 ng $L^{-1}$, resulting in 98% removal after 122 pore volume of flow. A slight decrease in Hg concentrations (from the treated pore water was observed after the treatment column

was stagnant for ~3 days to allow for sediment column sampling. These decreases indicates that flow rate may have influenced Hg removal and that an increase in pore water residence time improved the Hg removal. Similar results were reported as breakthrough curves for $Hg^{2+}$ ions and granular activated carbon experiments conducted by Goyal et al. (2009). Increased hydraulic loading rates resulted in faster breakthrough times, suggesting that increase residence time in the pore water increased Hg sorption capacity.

The Hg concentrations of the unfiltered and untreated effluent from both the SR3 and SR6 columns were much greater than the filtered Hg concentrations. On average, 23% of the total unfiltered Hg passed through the 0.45 μm filter, suggesting that the majority of Hg from the untreated column effluent is in the particulate form. Conversely, the unfiltered effluent from the treatment columns did not significantly deviate from the 0.45 μm filtered Hg concentrations, suggesting that the particulate Hg was retained within the treatment columns. However, one sample collected at ~ 50 pore volumes for the SR3 treatment column experiment had unfiltered concentrations of 19 ng $L^{-1}$ and filtered Hg concentrations of 4.6 ng $L^{-1}$ (Figure 3.10), and may be attributed to sampling error. The analysis of different filter fractions of the treatment column effluent suggests that the CL2 char is equally effective at removing the dissolved, colloidal and particulate concentrations from the influent.

After the initial saturation of the sediment material, MeHg concentrations of 15 ng $L^{-1}$ were observed in the SR3 column effluent, and decreased to less than 1 ng $L^{-1}$ after 150 pore flushes (Figure 3.11). When the SR3 column effluent was diverted into the CL2 column, MeHg concentrations decreased to < 0.1 ng $L^{-1}$. The initial MeHg concentration in the SR6 column effluent was 9 ng $L^{-1}$, and decreased to < 1.4 ng $L^{-1}$ after 20 pore flushes. The SR6 effluent MeHg concentration averaged to 2.5 ng $L^{-1}$ between pore volumes 50-110. As the SR6 effluent was diverted into the CL2 treatment column, the MeHg concentration decreased to < 1.5 ng $L^{-1}$. The % MeHg for the SR6 treated effluent was ~1.5% of the total Hg concentration for the treated effluent, whereas the % MeHg in the SR3 treated effluent was < 0.3% of

the total Hg. These results suggest that conditions conducive for Hg methylation were not present in the treatment column.

Normalized Hg concentration curves indicate a lack of Hg breakthrough in both treatment column effluents (Figure 3.12). The ratio of the treated concentration to the untreated concentration remained below 0.04 for both columns over time, indicating that the Hg removal capacity had not been reached at the time of experiment termination. Assuming no sorption to the silica sand and uniform interaction of the water with the reactive material throughout the column length, the calculated uptake of $Hg^{2+}$ in the CL2 char was 0.24 μg $g^{-1}$ for the SR3 treatment and ~1 μg $g^{-1}$ for the SR6 treatment. Assuming that the majority of removal occurred within the initial 2-3 cm, the calculated uptake of $Hg^{2+}$ was 1.2 μg $g^{-1}$ and 7.7 μg $g^{-1}$ for the SR3 and SR6 treatment, respectively. As no breakthrough was observed in both CL2 column experiments, the optimal Hg uptake capacity of this material was not calculated for these experiments. Similar experiments have reported greater $Hg^{2+}$ adsorption capacity (Goyal et al., 2009) ranging from 16 mg $g^{-1}$ to 59 mg $g^{-1}$.

The metal uptake capacity for the CL2 column connected in series with the SR6 sediment was six times greater than the average uptake capacity of the CL2 batch amendment experiments with the same sediment (160 ng $g^{-1}$). The comparison of the metal uptake capacity of the column and batch experiments indicates that the CL2 char has considerably variable Hg uptake potential. Variability in the calculated Hg uptake capacity may be due to contact area, reaction kinetics and transport mechanisms (Goyal et al., 2009). Optimal Hg removal per mass of CL2 reactive material uptake may vary under natural flow conditions and is dependent on the interaction of Hg in the sediment pore water and river water with the reactive material. The experimental sediment and treatment columns were continuously saturated, and may represent conditions uncharacteristic of the natural environment. The evaluation of treatment effectiveness under variable geochemical conditions would provide further insight into the Hg treatment capacity expected in the field.

*3.3.4.2 Aqueous geochemistry*

Measurements of effluent pH from the SR3 column effluent stabilized around 7-7.5, and were consistent with the pH of the CL2 column effluent (Figure 3.8). Initial alkalinity concentrations were elevated in the CL2 effluent (890 mg $L^{-1}$ (as $CaCO_3$) and rapidly declined within the initial 7 pore volumes. The alkalinity of the treatment column stabilized at approximately 70-100 mg $L^{-1}$, and was similar to the SR3 column effluent.

An abrupt decrease in Ca concentrations from 75 to 31 mg $L^{-1}$ coincided with decreasing K concentrations from 25 to 8 mg $L^{-1}$ in the treated SR3 effluent within the initial 10 pore volumes. The decline in alkalinity, Ca and K may indicate the dissolution or mobilization of carbonate minerals on the surface of the CL2 material. The concentrations of Mn, Fe, $SO_4$, acetate and Cl remained at concentrations similar to the influent solution. The Si concentrations were initially low in the treated effluent relative to the untreated effluent from the SR3 column. Concentrations of Si increased in the treated column effluent to approximately 5 mg L-1 at 160 pore volumes, and were similar to Si concentrations in the untreated SR3 column effluent.

The initial pH of the treated SR6 effluent (~8) was elevated relative to the untreated SR6 column effluent (~7.5) (Figure 3.9). Following the onset of the SR6 column influent into the CL2 treatment column, the pH decreased from 8.2 to 7.7 within the initial 5 pore volumes, and stabilized at values similar to the untreated SR6 column effluent. The alkalinity of the treatment column effluent was similar to the SR6 column effluent (100-130 mg $L^{-1}$ as $CaCO_3$), as were concentrations of Ca. Concentrations of Si were low in the CL2 column effluent prior to connecting the columns in series, and increase to similar concentrations as the untreated SR6 effluent (~7 mg $L^{-1}$) within the initial 7 pore volumes after connection.

The redox potential of the treated effluent was slightly elevated (200-300 mV) in comparison to the untreated SR6 effluent (150-230 mV). The concentrations of Mn were elevated (180-245 mg $L^{-1}$)

relative to the influent within the initial 10 pore volumes following the onset of the SR6 influent, and decreased to concentrations similar to the influent (0.2-0.5 mg $L^{-1}$) after 30 pore volumes. The initial elevated Mn concentrations may indicate that Mn reduction occurred due to the oxidation of organic material, as suggested by the following half reaction:

$$MnO_{2_{(s)}} + 2e^- + 4H^+ \rightarrow Mn^{2+}{}_{(aq)} + 2H_2O_{(aq)} \quad (3.9)$$

The elevated Mn concentrations coincided with elevated K concentrations in the treatment column effluent relative to the influent. The elevated pH and subdued alkalinity within the initial pore volumes suggests that the reduction of Mn may have occurred, contributing to the elevated redox potential relative to the influent Eh. A corresponding spike in effluent Fe concentrations may indicate Fe oxidation by Mn.

### *3.4 Conclusions*

Mercury removal was evaluated in the presence of different reactive materials amended with Hg-bearing sediment from the riverbanks of the South River. The results from the stabilization batch experiments indicate that the mass of Hg released from the sediment could be lessened with the addition of reactive media. The lowest concentrations of aqueous Hg were observed for amendments with Thiol II (< 5 ng $L^{-1}$), GAC (34 ng $L^{-1}$), and S+MRM (112 ng $L^{-1}$). The Thiol II compound was the most successful at decreasing Hg concentrations in the river water. Further information is needed to understand any potential undesirable effects of the Thiol II on river water chemistry. The thiol-based amendment would likely be suited for use under controlled terrestrial sites. Concentrations of Hg in the batch experiment supernatant were much lower after a period of aeration and re-wetting (~85%). In general, aerating and re-wetting the sediment amendments resulted in equal or greater removal of Hg from the water for all reactive materials tested.

A subset of reactive materials (ATP, MRM, ZVI+S, CL2) was selected to determine the optimal Hg adsorption capacity, and was applied to two different sediment samples. The greatest decrease in Hg

concentration relative to the control was observed at 5% dry weight amendments for the SR4 sediment, and 8% for the SR6 sediment. The greatest Hg uptake capacity (Hg captured per mass of material) was observed for the lowest doses of reactive media at 0.5% for SR4 sediment (194-265 ng $g^{-1}$) and 2% for SR6 sediment (203-499 ng $g^{-1}$), and may be attributed to reaction kinetics and surface area (Zhao et al., 2009). The change in aqueous Hg concentrations in the river water at large doses of reactive material generally had lower Hg uptake capacities (~34 ng $g^{-1}$ for SR4 at 5%, and ~160 ng $g^{-1}$ for SR6 at 8%). The uptake capacity for all treatment media was greatest for treatment of water with elevated concentrations of Hg. The Hg uptake capacities were low relative to Hg uptake capacities of similar reactive materials in the literature (100-800 mg $g^{-1}$ (Zhao et al., 2009, Cui et al., 2012)). The low Hg uptake capacities observed relative to the literature is likely due to the low concentrations of Hg in the untreated water, and the chemical complexity of the supernatant relative to pure system experiments. Even so, the % of Hg removed from the supernatants was >78% when applied at 5% d.w. to SR4 sediment and 8% d.w. to SR6 sediment.

Sediment column experiments were designed to emulate the leaching of Hg under slow flow typical of groundwater movement through the riverbanks, which were connected in series to columns containing charred hardwood material. The concentration of Hg in the sediment pore water was measured before and after the leached Hg was passed through a column containing CL2 reactive material. The concentration of filtered Hg was < 20 ng $L^{-1}$ and < 120 ng $L^{-1}$ for treated effluent from columns containing SR3 and SR6 sediment, respectively. The filter fractionation of the treatment column effluent indicated that the CL2 char is equally effective at removing the dissolved, colloidal and particulate concentrations from the influent. Both column experiments exhibited > 98% removal of Hg from the water. Concentrations of MeHg in the treated column effluent were < 1 ng $L^{-1}$.

Assuming that the majority of removal occurred within the initial 2-3 cm of the treatment column, the calculated uptake of $Hg^{2+}$ was 1.2 μg $g^{-1}$ and 7.7 μg $g^{-1}$ for the SR3 and SR6 treatment, respectively. As no breakthrough was observed in both CL2 column experiments, the optimal Hg uptake capacity of

this material has not been adequately characterized. The uptake capacity for the CL2 material was much greater for the column experiments relative to the batch experiments, suggesting that the uptake capacity is limited by Hg loading. The chemical composition of the treated column effluent was similar to the South River water, suggesting that the material did not add or remove significant constituents during the duration of these experiments. The experiments suggest that CL2 hardwood material may be an effective amendment to be used in remedial efforts on the banks of the South River.

**Table 3.1:** Chemical composition of South River water.

| Parameter | Value |
|---|---|
| Hg $ngL^{-1}$ | 4.4 +/-1.1 |
| pH | 8.1 |
| Eh (mV) | 340 |
| Alkalinity $mgL^{-1}$ as $CaCO_3$ | 87 |
| F mg $L^{-1}$ | 0.08 +/-0.2 |
| Cl mg $L^{-1}$ | 5.7 +/-1.6 |
| $NO_3$ mg $L^{-1}$ | 3.3 +/-0.9 |
| $SO_4$ mg $L^{-1}$ | 8.7 +/-2.8 |
| Ca mg $L^{-1}$ | 18.6 +/-2.9 |
| K mg $L^{-1}$ | 1.7 +/-0.7 |
| Mg mg $L^{-1}$ | 7.0 +/-1.3 |
| Mn µg $L^{-1}$ | 0.12 +/-0.1 |
| Na mg $L^{-1}$ | 3.5 +/- 0.23 |
| Si mg $L^{-1}$ | 3.1 +/- 0.26 |
| Al µg $L^{-1}$ | 31.7 +/-9.9 |
| Fe µg $L^{-1}$ | 10.7 +/-9.7 |

**Table 3.2:** Reactive material abbreviations and amendment additions

| Reagent | Abbrev | Source | Amendment (% D.W.) SR4 | SR6 |
|---|---|---|---|---|
| (1) 2,5-dimercapto,2,4-thiadiazole | Thiol II | CANMET (Doug Gould) | 5 | - |
| (2) Granular Activated Carbon | GAC | Sigma Aldrich, Canada | 5 | - |
| (3) Zero-valent Iron | ZVI | Quebec Metal Powders Ltd. Sorel-Tracey, QC | 5 | - |
| (4) Elemental Sulfur | S | Georgia Gulf Sulphur, Valdosta, GA. | 5 | - |
| (5) Attapulgite Clay | ATP | Zemex Industrial Minerals | 0.5, 1, 2, 5 | 2, 5, 8 |
| (6) Organically-modified Clay | MRM | Cetco, Hoffman Estates, IL | 0.5, 1, 2, 5 | 2, 5, 8 |
| (7) Hardwood Charcoal | CL2 | Cowboy Charcoal, Co., Alabany, KY | 0.5, 1, 2, 5 | 2, 5, 8 |
| (1) and (5) | Thiol II +ATP | - | 5 | - |
| (3) and (4) | ZVI+S | - | 0.5, 1, 2, 5 | 2, 5, 8 |
| (3) and (5) | ZVI+ATP | - | 5 | - |
| (4) and (5) | S+ATP | - | 5 | - |
| (4) and (6) | S+MRM | - | 5 | - |

**Table 3.3:** Metal uptake capacity representing the mass of Hg removed from solution per unit mass of reactive material

| | | % Dry Weight | ATP | MRM | ZVI+S | CL2 |
|---|---|---|---|---|---|---|
| Q (ng Hg $g^{-1}$ media) | SR4 | 0.5 | 246 | 235 | 265 | 194 |
| | | 1 | 135 | 137 | 122 | 121 |
| | | 2 | 71.2 | 73.8 | 70.4 | 47.8 |
| | | 5 | 35.7 | 36.9 | 32.6 | 32.1 |
| | SR6 | 2 | 388 | 499 | 38.2 | 203 |
| | | 5 | 220 | 215 | 202 | 117 |
| | | 8 | 150 | 149 | 170 | 161 |

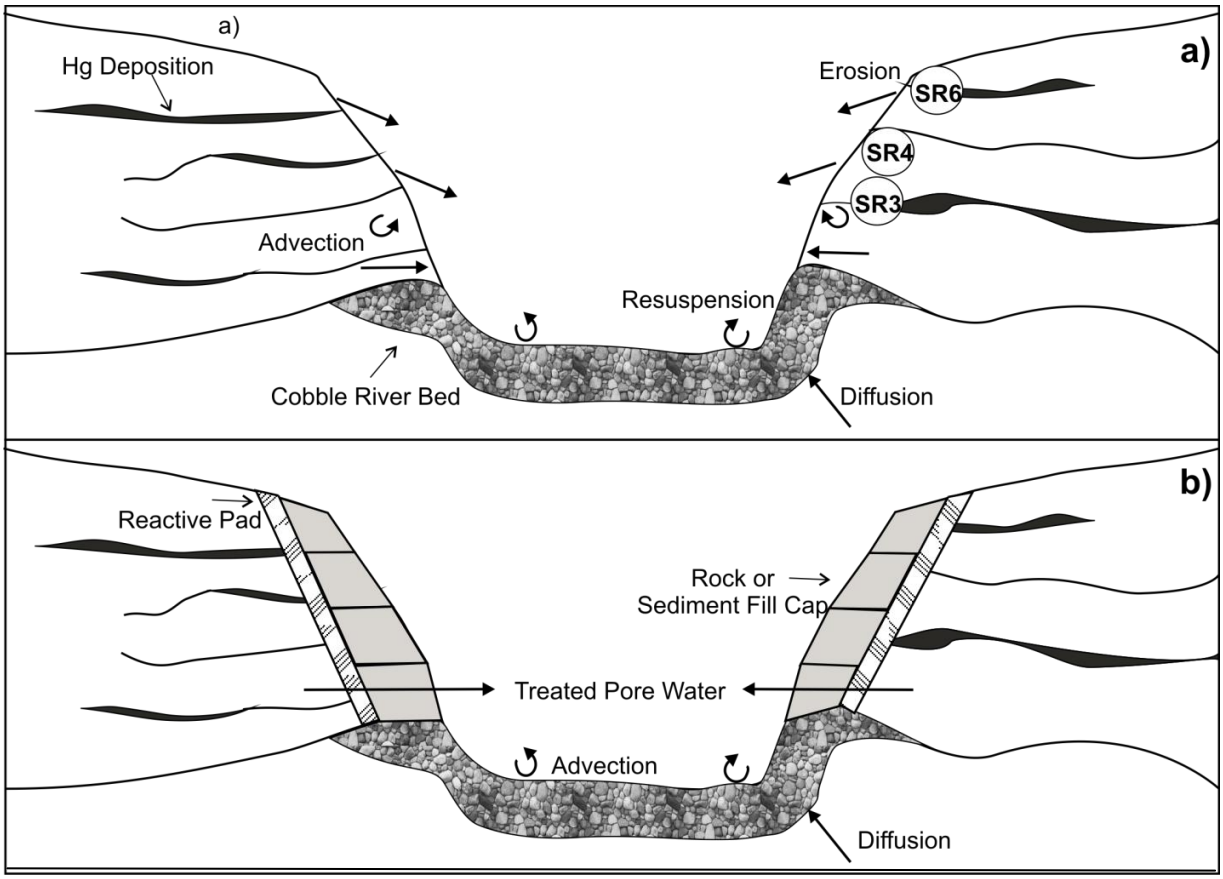


**Figure 3.1:** Schematic diagram of Hg-contaminated river margin (a) and remedial application of reactive riverbank under armor (b).

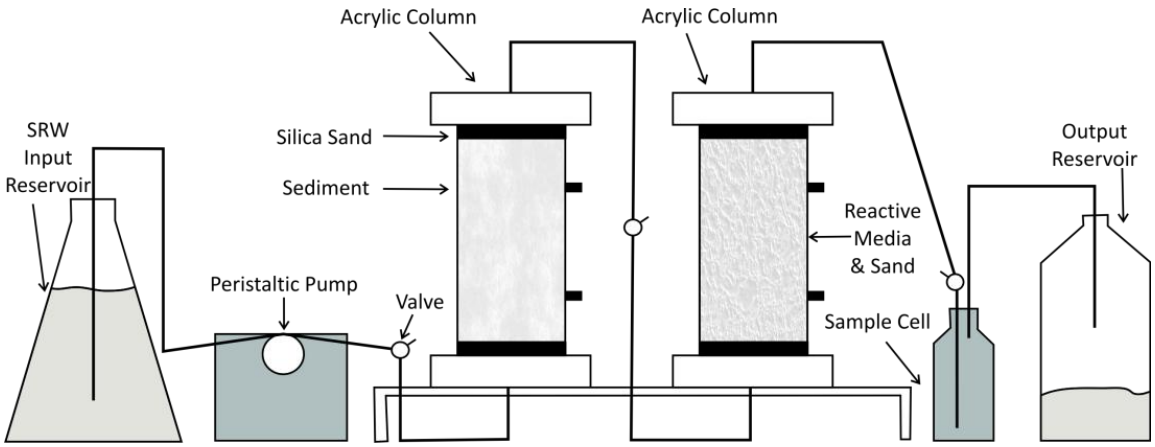


**Figure 3.2:** Schematic diagram of sediment flow column and reactive treatment column apparatus.

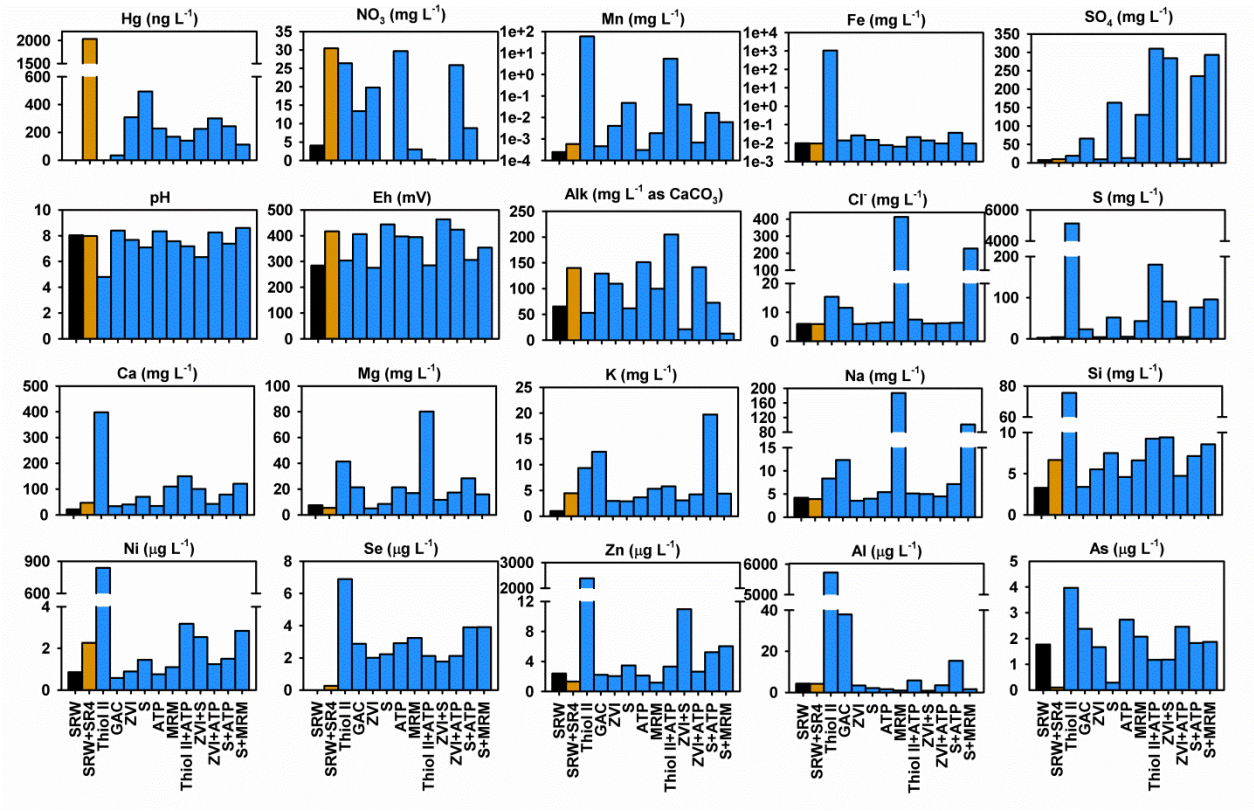


**Figure 3.3:** Water chemistry for initial wetting of reactive sediment amendments. Note log scales for Mn and Fe.

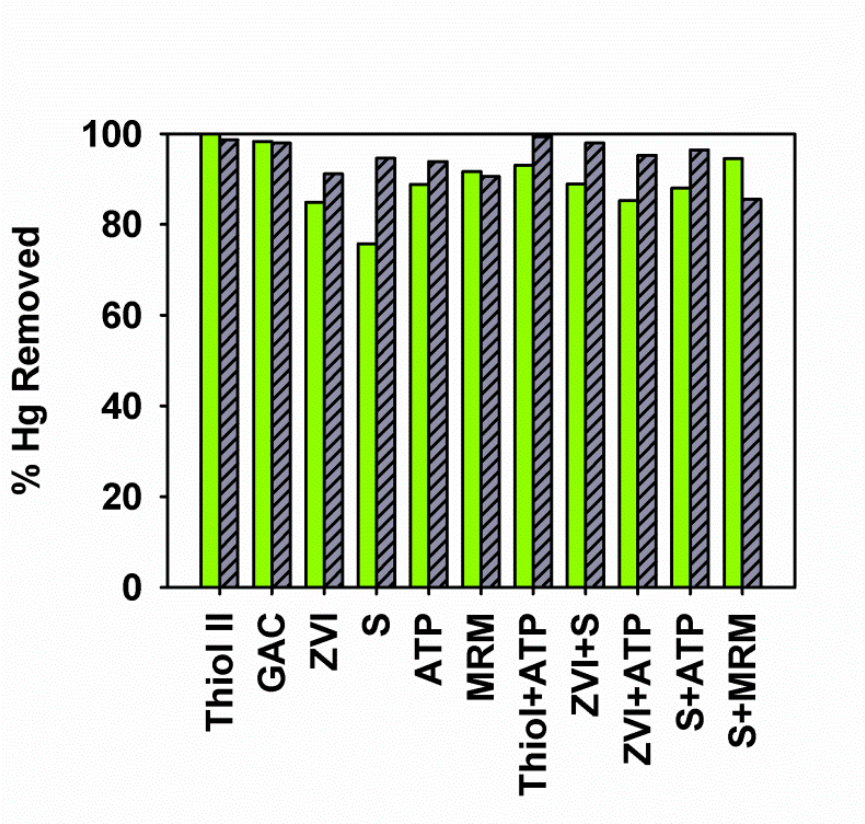


**Figure 3.4:** Reductions in aqueous Hg concentrations (<0.45 μm) following the addition of reactive amendments. Solid bars represent the % Hg reduction after the inital wetting of the sediment amendment, and stripped bars represent the % Hg reduction after 33 days of aeration and re-saturation of the sediment-amendment material.

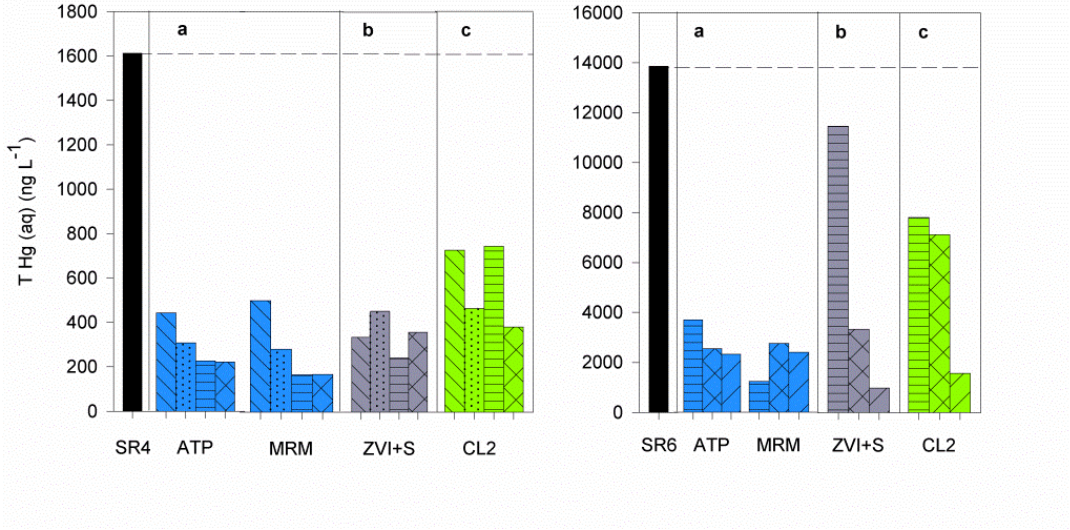


**Figure 3.5:** Hg concentrations after variable masses of reactive material were added to SR4 (a) and SR6 (b) sediment. Black bars indicate the initial Hg concentration without the addition of a reactive-amendment. Diagonal stripes from left-top to right-bottom represent 0.5%, d.w., dots represent 1% d.w., horizontal lines represent 2% d.w., criss-cross represents 5% d.w., and diagnonal stripes from right-top to left-bottom represent 8% d.w.

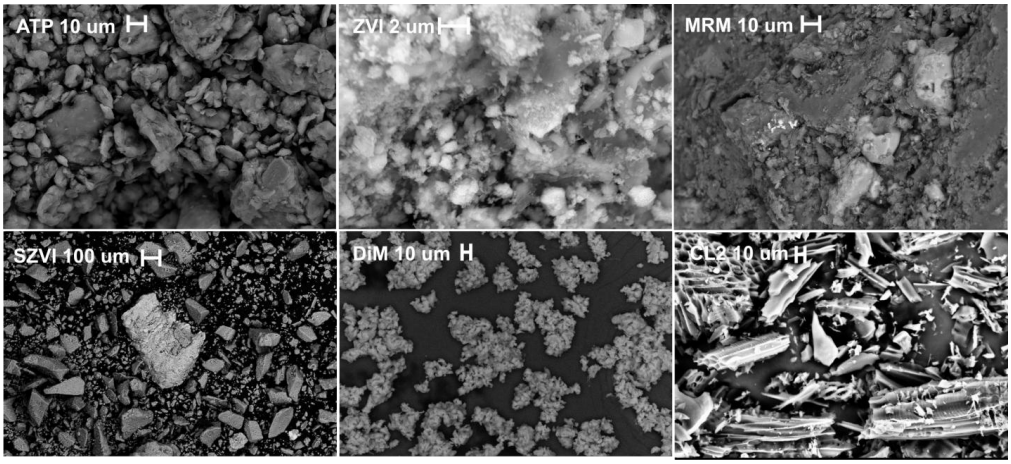


**Figure 3.6:** SEM images of reactive media ATP, ZVI, MRM, ZVI+S, Thiol II and CL2.

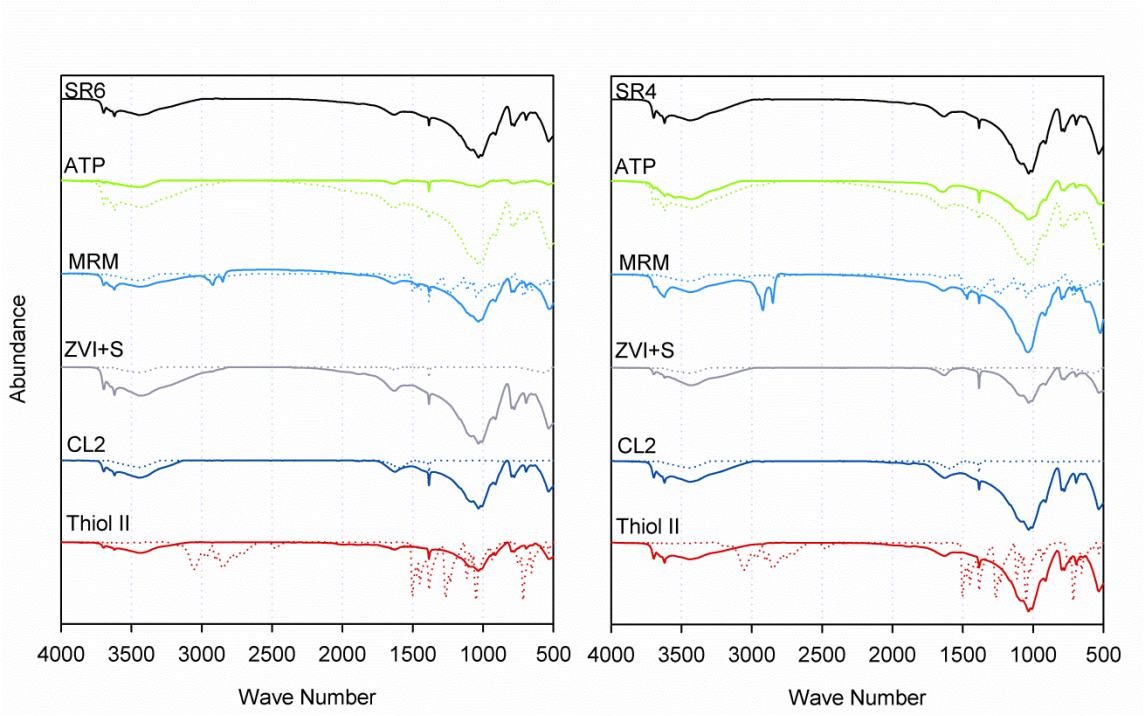


**Figure 3.7:** FTIR spectra for SR6 and SR4 sediments, and the sediment-amendment material. Dotted lines represent the reactive material, solid lines represent the sediment-reactive media mixtures.

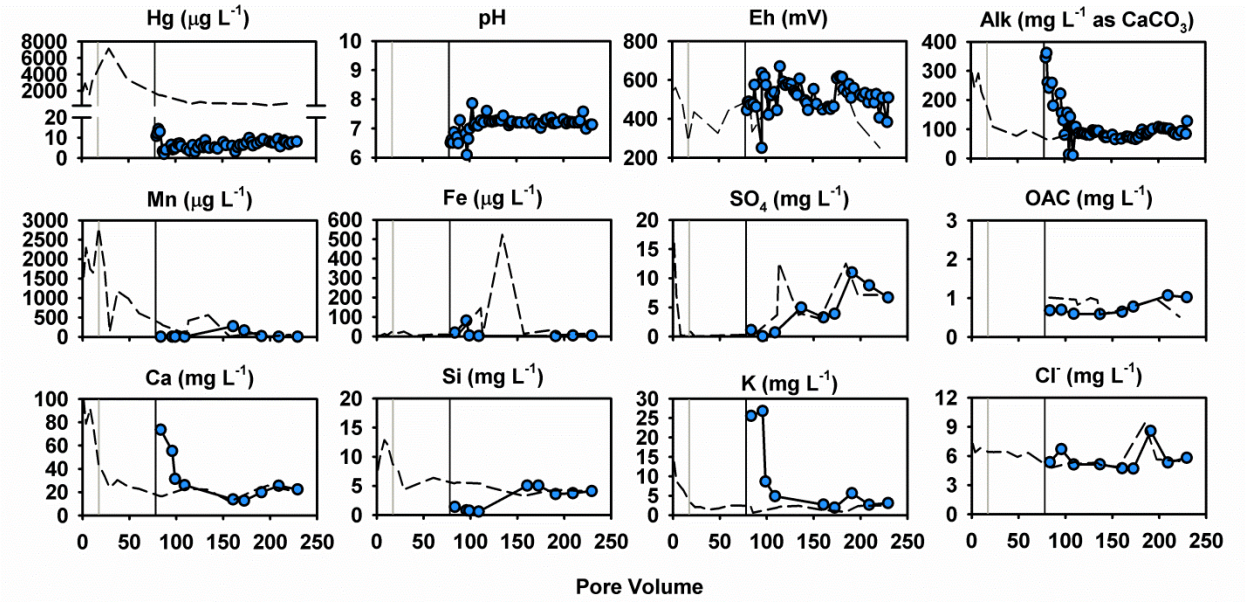


**Figure 3.8:** Monitoring of major cations and anions of the SR3 sediment leaching column, represented by a short dashed line. The SR3 column was connected in series to a hardwood char treatment column, and is represented by ○. The grey bar represents an increase in SR3 column flow rate from 1 pore volume to 3 pore volumes per week at 17 pore volumes of flow. The black bar represents the SR3 column effluent diverted into the treatment column at 78 pore volumes of flow.

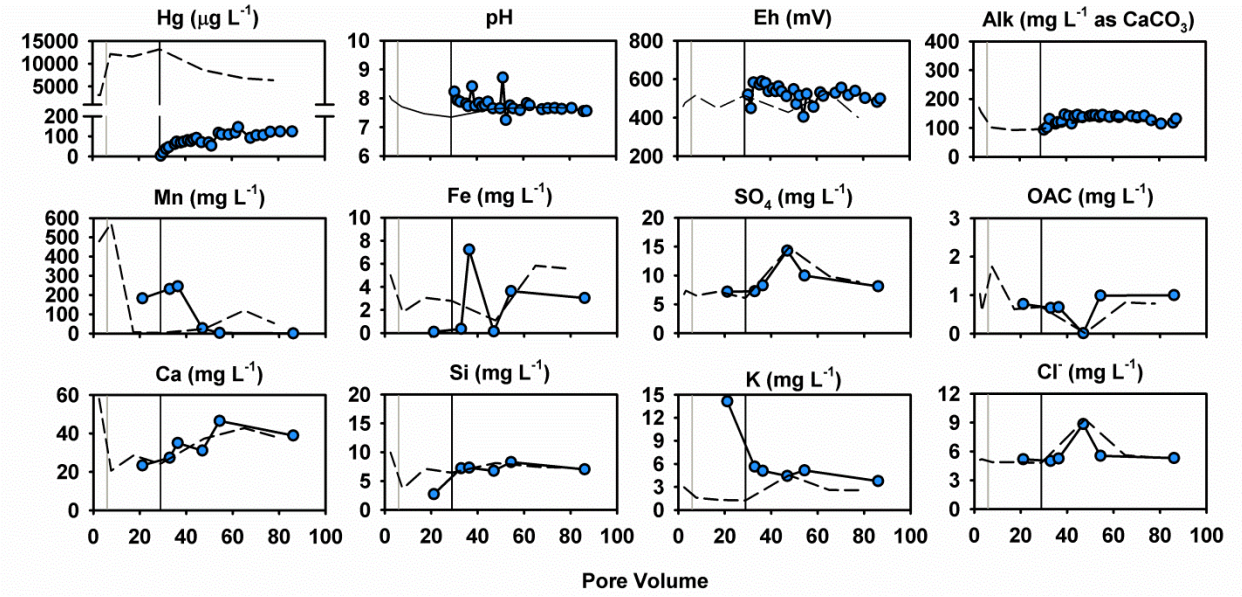


**Figure 3.9:** Column effluent major cations and anions from the SR6 sediment leaching and treatment columns. SR6 column effluent is represented by a short dashed line, and the treatment column effluent is represented by ○. The grey bar represents an increase in SR6 column flow rate from 1 pore volume to 3 pore volumes per week at 6 pore volumes of flow, and the black bar represents the SR3 column effluent diverted into the treatment column at 29 pore volumes of flow.

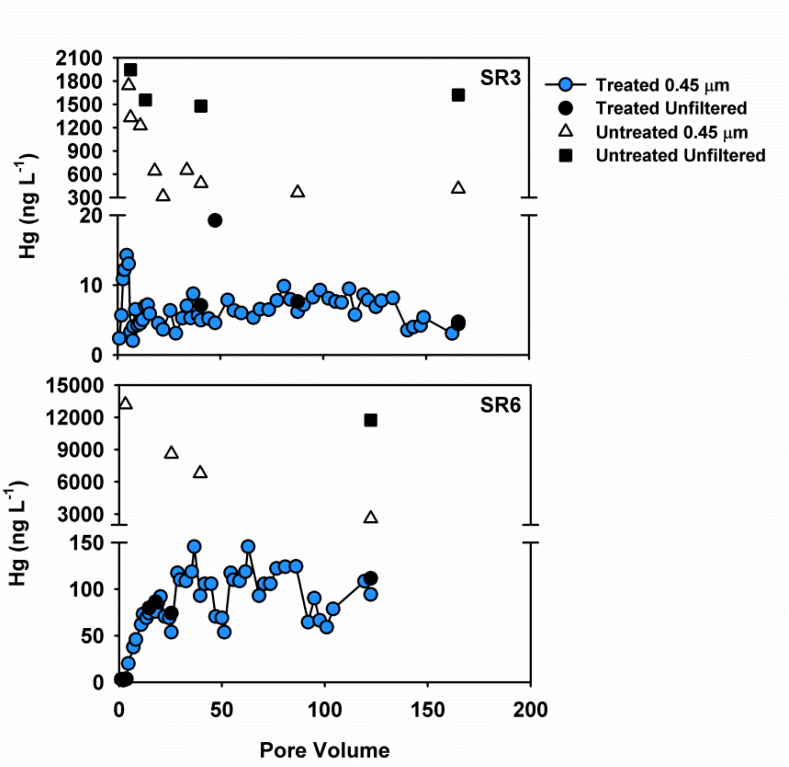


**Figure 3.10:** Comparison of concentrations of Hg in the treated and untreated column effluent for SR3 and SR6 sediments for 0.45 μm and unfiltered samples over time.

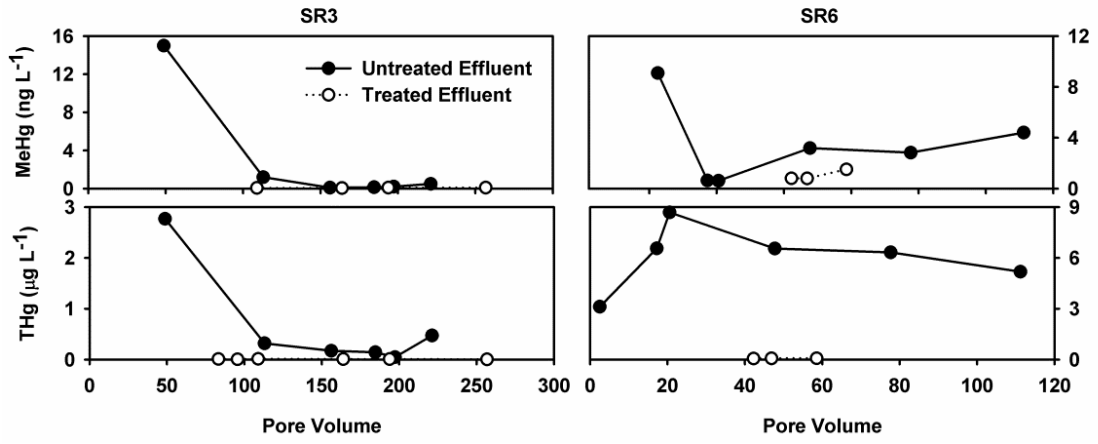


**Figure 3.11:** MeHg and THg concentrations in the untreated and treated column effluent.

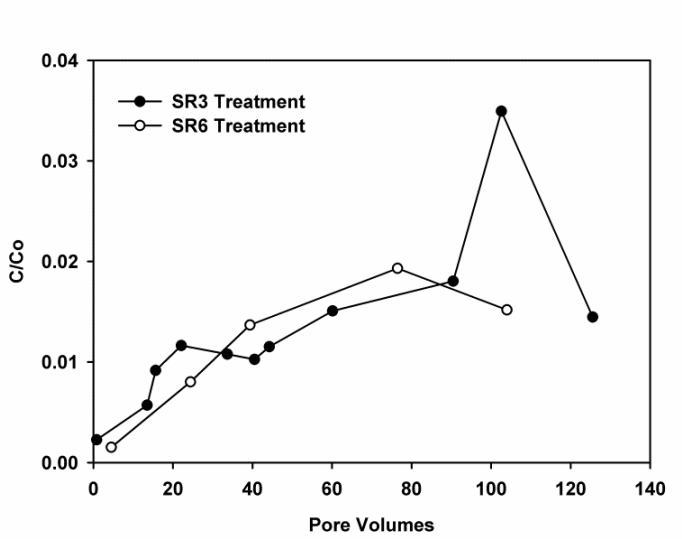


**Figure 3.12:** Normalized $Hg^{2+}$ removal onto CL2 as a function of pore volumes.

# WORKS CITED


Acquavita, A., Emili, A., Covelli, S., Faganeli, J., Predonzani, S., Koron, N., et al. (2012). The effects of resuspension on the fate of hg in contaminated sediments (Marano and Grado Lagoon, Italy): Short-term simulation experiments. Estuarine, Coastal and Shelf Science, 113, 32-40.

Allison, J.D., Brown, D.S., Novo-Gradac, K.L. (1990). MINTEQA2/PRODEFA2, A Geochemical Assessment Model for Environmental Systems, Version 3.0 User's Manual. Environmental Research Laboratory, Office of Research and Development, US EPA, Athens, GA.

Babiarz, C., Hoffmann, S., Wieben, A., Hurley, J., Andren, A., Shafer, M., et al. (2012). Watershed and discharge influences on the phase distribution and tributary loading of total mercury and methylmercury into lake superior. Environmental Pollution, 161(0), 299-310.

Bacon, J. R., & Davidson, C. M. (2008). Is there a future for sequential chemical extraction? Analyst, 133(1), 25-46.

Ball, J.W., Nordstrom, D.K. (1991). User's manual for WATEQ4F with revised thermodynamic database and test cases for calculating speciation of major, trace and redox elements in natural waters, U.S. Geological Survey, Open-File Rep. 91-183.

Barnett, M. O., Turner, R. R., & Singer, P. C. (2001). Oxidative dissolution of metacinnabar (β-HgS) by dissolved oxygen. Applied Geochemistry, 16(13), 1499-1512.

Barnett, M.O., Harris, L.A., Turner, R.R., Stevenson, R.J., Henson, T.J., Melton, R.C., Hoffman, D.P. (1997). Formation of mercuric sulfide in soil. Environmental Science and Technology 31(11), 3037-3043

Benner, S.G., Blowes, D.W., Gould, W.D., Herbert Jr., R.B., Ptacek, C.J. (1999). Geochemistry of a permeable reactive barrier for metals and acid mine drainage. Environmental Science and Technology 33, 2793-2799.

Benoit, J. M., Gilmour, C. C., Heyes, A., Mason, R. P., & Miller, C. L. (2002). Geochemical and biological controls over methylmercury production and degradation in aquatic ecosystems. ACS Symposium Series, 835, 262-297

Benoit, J. M., Mason, R. P., Gilmour, C. C., & Aiken, G. R. (2001). Constants for mercury binding by organic matter isolates from the florida everglades. Geochimica Et Cosmochimica Acta, 65(24), 4445-4451.

Benoit, J. M., Gilmour, C. C., Mason, R. P., & Heyes, A. (1999). Sulfide controls on mercury speciation and bioavailability to methylating bacteria in sediment pore waters. Environmental Science and Technology, 33(6), 951-957.

Berg, U., Neumann, T., Donnert, D., Nuesch, R., Stuben, D. (2004). Applied Geochemistry, 19, 1759-1771.

Biester, H., Müller, G., & Schöler, H. F. (2002). Binding and mobility of mercury in soils contaminated by emissions from chlor-alkali plants. Science of the Total Environment, 284(1-3), 191-203.

Biniak, S., Szymański, G., Siedlewski, J., & Światkoski, A. (1997). The characterization of activated carbons with oxygen and nitrogen surface groups. Carbon, 35(12), 1799-1810.

Bloom, N. S., Preus, E., Katon, J., & Hiltner, M. (2003). Selective extractions to assess the biogeochemically relevant fractionation of inorganic mercury in sediments and soils. Analytica Chimica Acta, 479(2), 233-248.

Bloom, N. S., & Lasorsa, B. K. (1999). Changes in mercury speciation and the release of methyl mercury as a result of marine sediment dredging activities. Science of the Total Environment, 237-238, 379-385.

Blowes, D.W., Ptacek, C.J., Jambor, J.L., Weisener, C.G. (2003). The geochemistry of acid mine drainage. Treatise on Geochem. Volume 9. Editor: Barbara Sherwood Lollar. Executive Editors: Heinrich D. Holland and Karl K. Turekian. pp. 612. ISBN 0-08-043751-6. Elsevier, 149-204

Blowes, D.W., Ptacek, C.J., Benner, S.G., McRae, C.W.T., Bennet, T.A., Puls, R.W. (2000). Treatment of inorganic contaminants using permeable reactive barriers. Journal of Contaminant Hydrology, 45, 123-137.

Blue, L.Y., Jana, P., Atwood, D.A. (2010). Aqueous mercury precipitation with the synthetic dithiolate, BDTH2. Fuel, 89, 1326-1330.

Borch, T., Kretzschmar, R., Skappler, A., Van Cappellen, P., Ginder-Vogel, M., Voegelin, A., et al. (2010). Biogeochemical redox processes and their impact on contaminant dynamics. Environmental Science and Technology, 44(1), 15-23.

Boszke, L., Głosińska, G., & Siepak, J. (2002). Some aspects of speciation of mercury in a water environment. Polish Journal of Environmental Studies, 11(4), 285-298.

Carter, L.J. (1977). Chemical Plants Leave Unexpected Legacy for Two Virginia Rivers. Science, New Series (198) No. 4321, 1015-1020.

Castelle, S., Schäfer, J., Blanc, G., Audry, S., Etcheber, H., & Lissalde, J. (2007). 50-year record and solid state speciation of mercury in natural and contaminated reservoir sediment. Applied Geochemistry, 22(7), 1359-1370.

Choe, K. -., Gill, G. A., & Lehman, R. (2003). Distribution of particulate, colloidal, and dissolved mercury in San Francisco Bay estuary. 1. Total Mercury. Limnology and Oceanography, 48(4), 1535-1546.

Choe, K. -., & Gill, G. A. (2003). Distribution of particulate, colloidal, and dissolved mercury in san francisco bay estuary. 2. Monomethyl mercury. Limnology and Oceanography, 48(4), 1547-1556.

Clarkson, T. W., & Magos, L. (2006). The toxicology of mercury and its chemical compounds. CRC Critical Reviews in Toxicology, 36(8), 609-662.

Compeau, G.C. and Bartha, R. (1985). Sulfate-reducing bacteria: principal methylators of mercury in anoxic estuarine sediment. Applied Environmental Microbiology, 50, 498-502.

Cui, H., Qian, Y. Li, Qin, Zhang, Qiu, Zhai, Jianping (2012). Adosprtion of aqueous Hg(II) by polyaniline/attapulgite composite. Chemical Engineering Journal, 211-212, 216-233

Drott, A., Lambertsson, L., Bjorn, E., Skyllberg, U., 2007. Importance of dissolved neutral mercury sulfides for methyl mercury production in contaminated sediments. Environmental Science and Technology, 2270-2276.

Ehrlich, H. L. (2002). How microbes mobilize metals in ores: A review of current understandings and proposals for further research. Minerals and Metallurgical Processing, 19(4), 220-224.

Evangelou, V.P., Zhang, Y.L. (1995). A Review: Pyrite oxidation mechanisms and acid mine drainage prevention. Crit. Rev. Environmental Science and Technology 25(2), 141-199

Fan, Q. H., Tan, X. L., Li, J. X., Wang, X. K., Wu, W. S., & Montavon, G. (2009). Sorption of eu(III) on attapulgite studied by batch, XPS, and EXAFS techniques. Environmental Science and Technology, 43(15), 5776-5782.

Flanders, J. R., Turner, R. R., Morrison, T., Jensen, R., Pizzuto, J., Skalak, K., et al. (2010). Distribution, behavior, and transport of inorganic and methylmercury in a high gradient stream. Applied Geochemistry, 25(11), 1756-1769.

Fitzgerald, W.F. and. Lamborg, C.H., 2003. Geochemistry of mercury in the environment. In: Treatise on Geochemistry, Vol. 9, (B.S. Lollar, Ed). Eds. H.D. Holland and K.K. Turekian, Elsevier Science, Pergamon Press, Amsterdam. Ch. 4 pp. 107-148.

Gabriel, M. C., & Williamson, D. G. (2004). Principal biogeochemical factors affecting the speciation and transport of mercury through the terrestrial environment. Environmental Geochemistry and Health, 26(3-4), 421-434.

Gagnon, C., Pelletier, E., & Mucci, A. (1997). Behaviour of anthropogenic mercury in coastal marine sediments. Marine Chemistry, 59(1-2), 159-176.

Ghosh, U., Luthy, R., Cornelissen, G., Werner, D., Menzie, C. (2011). In-situ Sorbent Amendments: A New Direction in Contaminated Sediment Management. Environmental Science and Techology, 45, 1163-1168.

Gibson, B. D., Ptacek, C. J., Lindsay, M. B. J., & Blowes, D. W. (2011). Examining mechanisms of groundwater Hg(II) treatment by reactive materials: An EXAFS study. Environmental Science and Technology, 45(24), 10415-10421.

Gilmour, C.C., Henry, E.A., Mitchell, R. (1992). Sulfate stimulation of mercury methylation in freshwater sediments. Environmental Science and Technology 26, 2281-2287.

Goyal, M., Bhagat, M., & Dhawan, R. (2009). Removal of mercury from water by fixed bed activated carbon columns. Journal of Hazardous Materials, 171(1-3), 1009-1015.

Graham, A.M., Aiken, G.R., Gilmour, C.C. (2012). Dissolved organic matter enhances microbial mercury methylation under sulfidic conditions. Environmental Science and Technology, 46, 2715-2723.

Chen, H. , Wang, A.Q. (2007). Kinetic and isothermal studies of lead ion adsorption onto palygorskite clay, J. Colloid Interface Science, 307 309–316.

Heaven, S., Ilyushchenko, M.A., Kamberov, I.I., Politkov, M.I.., Tanton, T.W., Ullrich, S.M., Yanin, E.P. (2000). Mercury in the River Nura and its floodplain, Central Kazakhstan: II. Floodplain soils and riverbank silt deposits. The Science of the Total Environment 260, 45-55.

Holley, E. A., James McQuillan, A., Craw, D., Kim, J. P., & Sander, S. G. (2007). Mercury mobilization by oxidative dissolution of cinnabar (α-HgS) and metacinnabar (β-HgS). Chemical Geology, 240(3-4), 313-325.

Kim, C. S., Bloom, N. S., Rytuba, J. J., & Brown Jr., G. E. (2003). Mercury speciation by X-ray absorption fine structure spectroscopy and sequential chemical extractions: A comparison of speciation methods. Environmental Science and Technology, 37(22), 5102-5108.

Kim, C. S., Rytuba, J. J., & Brown Jr., G. E. (2004). Geological and anthropogenic factors influencing mercury speciation in mine wastes: An EXAFS spectroscopy study. Applied Geochemistry, 19(3), 379-393.

Kim, C.S., Rytuba, J.J., Brown Jr., G.E. (2004). EXAFS study of mercury (II) sorption to Fe and Al-(hydr)oxides I. Effects of pH. J. Colloid Interface Science, 270, 9-20.

Knox, A., Paller, M., Roberts, J. (2012). Active Capping Technology – new approaches for In Situ remediation of contaminated sediments. Remediation, 22(2), 93-117.

Kocman, D., Kanduč, T., Ogrinc, N., & Horvat, M. (2011). Distribution and partitioning of mercury in a river catchment impacted by former mercury mining activity. Biogeochemistry, 104(1-3), 183-201.

Kwon, S.; Thomas, J. W.; Reed, B. E.; Levine, L.; Magar, V. S.; Ghosh, U. (2010). Evaluation of sorbent amendments for in situ remediation of metal contaminated sediments. Environmental Toxicology and Chemistry, 29, 1883–1892.

Light, T.S. (1972). Standard solution for redox potential measurements. Analytical Chemistry, 44, 1038-1039

Lovley, D. R. (1991). Dissimilatory Fe(III) and Mn(IV) reduction. Microbiological Reviews, 55(2), 259-287.

Lowry, G. V., Shaw, S., Kim, C. S., Rytuba, J. J., & Brown, G. E. (2004). Macroscopic and microscopic observations of particle-facilitated mercury transport from New Idria and Sulphur Bank mercury mine tailings. Environmental Science & Technology, 38(19), 5101-5111.

Li, M., Wu, Z.S., Kao, H.T. (2011). Study on preparation, structure and thermal energy storage property of capric–palmitic acid/attapulgite composite phase change materials. Applied Energy, 88, 3125–3132.

McDonough, K., Murphy, P., Olsta, J., Zhu, Y., Reible, D., Lowry, G. (2007). Development and Placement of a Sorbent-Amended Thin Layer Sediment Cap in the Anacostia River. Soil and Sediment Contamination, 16, 313-322.

Morel, F. M. M., Kraepiel, A. M. L., & Amyot, M. (1998). The chemical cycle and bioaccumulation of mercury. Annual Review of Ecology and Systematics, 29, 543-566.

Mucci, A., Lucotte, M., Montgomery, S., Plourde, Y., Pichet, P., & Hua Van Tra. (1995). Mercury remobilization from flooded soils in a hydroelectric reservoir of northern Quebec, La Grande-2: Results of a soil resuspension experiment. Canadian Journal of Fisheries and Aquatic Sciences, 52(11), 2507-2517.

National Oceanic and Atmospheric Administration (2012). National Weather Information System. http://www.noaa.gov/

Nordstrom, D.K. (1977). Thermochemical redox equilibria of ZoBell's solution. Geochim. Cosmochim. Acta 41, 1835-1841.

O'Neal, M. A., & Pizzuto, J. E. (2011). The rates and spatial patterns of annual riverbank erosion revealed through terrestrial laser-scanner surveys of the South River, Virginia. Earth Surface Processes and Landforms, 36(5), 695-701.

Oyekola, O. O., Harrison, S. T. L., & van Hille, R. P. (2012). Effect of culture conditions on the competitive interaction between lactate oxidizers and fermenters in a biological sulfate reduction system. Bioresource Technology, 104, 616-621.

Oyekola, O. O., van Hille, R. P., & Harrison, S. T. L. (2010). Kinetic analysis of biological sulphate reduction using lactate as carbon source and electron donor: Effect of sulphate concentration. Chemical Engineering Science, 65(16), 4771-4781.

Paquette, K., Helz, G. (1995). Solubility of cinnabar (red HgS) and implications for mercury speciation in sulfidic waters. Water Air Soil Pollut. 80, 1053-1056.

Pizzuto, J. (2012). Predicting the accumulation of mercury-contaminated sediment on riverbanks-an analytical approach. Water Resources Research, 48(7), art. no. W07518

Pizzuto, J., & O'Neal, M. (2009). Increased mid-twentieth century riverbank erosion rates related to the demise of mill dams, South River, Virginia. Geology, 37(1), 19-22.

Pizzuto, J. (2005). A conceptual geomorphic model for mid-atlantic streams. Proceedings of the 2005 Watershed Management Conference - Managing Watersheds for Human and Natural Impacts: Engineering, Ecological, and Economic Challenges, pp. 1397-1405.

Ravichandran, M. (2004). Interactions between mercury and dissolved organic matter—a review. Chemosphere, 55(3), 319-331.

Revis, N. W., Osborne, T. R., Holdsworth, G., & Hadden, C. (1989). Distribution of mercury species in soil from a mercury-contaminated site. Water, Air, and Soil Pollution, 45(1-2), 105-113.

Rhoades, E. L., O'Neal, M. A., & Pizzuto, J. E. (2009). Quantifying bank erosion on the south river from 1937 to 2005, and its importance in assessing hg contamination. Applied Geography, 29(1), 125-134.

Schuster, E. (1991). The behavior of mercury in the soil with special emphasis on complexation and adsorption processes – a review of the literature. Water Air and Soil Pollution. 56, 667-680.

Skyllberg, U., & Drott, A. (2010). Competition between disordered iron sulfide and natural organic matter associated thiols for mercury(II) - an EXAFS study. Environmental Science and Technology, 44(4), 1254-1259.

Slowey, A. J. (2010). Rate of formation and dissolution of mercury sulfide nanoparticles: The dual role of natural organic matter. Geochimica Et Cosmochimica Acta, 74(16), 4693-4708.

Slowey, A.J., Brown Jr., G.E. (2007). Transformations of mercury, iron, and sulfur during the reductive dissolution of iron oxyhydroxide by sulfide. Geochim. Cosmochim. Acta 71, 877-894.

Slowey, A. J., Rytuba, J. J., & Brown, G. E. (2005). Speciation of mercury and mode of transport from placer gold mine tailings. Environmental Science & Technology, 39(6), 1547-1554.

Slowey, A. J., Rytuba, J. J., & Brown, G. E. (2005). Speciation of mercury and mode of transport from placer gold mine tailings. Environmental Science & Technology, 39(6), 1547-1554.

Stumm, W. and Morgan, J.J.(1996): Aquatic Chemistry, Chemical Equilibria and Rates in Natural Waters, 3rd ed. John Wiley & Sons, Inc., New York, 1022p.

Suchanek, T.H., Cooke, J., Keller, K., Jorgensen, S., Richerson, P.J., Eagles-Smith, C.A., Harner, E.J., Adam, D.P. (2009). A mass balance mercury budget for a mine-dominated lake: Clear Lake, California. Water Air Soil Pollution, 196, 51-73.

Svensson, M., Allard, B., and Düker, A. (2006). Formation of HgS—mixing HgO or elemental Hg with S, FeS, or $FeS_2$. Science of the Total Environment 368, 418-423.

Terzano, R., Santoro, A., Spagnuolo, M., Vekemans, B., Medici, L., Janssens, K., et al. (2010). Solving mercury (Hg) speciation in soil samples by synchrotron X-ray microspectroscopic techniques. Environmental Pollution, 158(8), 2702-2709.

Tonle, I. K., Ngameni, E., Njopwouo, D., Carteret, C., & Walcarius, A. (2003). Functionalization of natural smectite-type clays by grafting with organosilanes: Physico-chemical characterization and application to mercury(II) uptake. Physical Chemistry Chemical Physics, 5(21), 4951-4961.

U.S. EPA (2002). Method 1631, Revision E: Mercury in Water by Oxidation, Purge and Trap, and Cold Vapor Atomic Flourescence Spectrometry. Report No. EPA-821-R-02-019.

U.S. EPA. (1983). Method 160.3. Methods for chemical analysis of water and wastes. EPA 600-4-79-020.

U.S. EPA (1996). Evaluation of dredged material proposed for discharge in waters of the U.S. – Testing Manual. EPA 823-B-98-004.

Ullrich, S.M., Tanton, T.W., Abdrashitova, S.A. (2001). Mercury in the aquatic environment: a review of factors affecting methylation. Crit. Rev. Environmental Science and Technology 31, 241-293.

United States Geological Survey (2012). National Water Information System. http://maps.waterdata.usgs.gov/mapper/

USGS. (2006). South River Mercury TMDL. Water Resources of Virginia. USGS

Vieria, E.F.S, Sumoni, J.D., Airoldi, C. (1997). Interaction of cations with SH-modified silica gel: thermochemical study through calorimetric titration and direct extent of reaction determination. Journal of Materials Chemistry, 7, 2249-2252.

Virgina Department of Environmental Quality (2009). http://www.deq.state.va.us/

Wallschläger, D., Desai, M. V. M., Spengler, M., & Wilken, R. -. (1998). Mercury speciation in floodplain soils and sediments along a contaminated river transect. Journal of Environmental Quality, 27(5), 1034-1044.

Wang, Q., Kim, D., Dionysiou, D.D., Sorial, G.A., Timberlake, D. (2004). Sources and remediation for mercury contamination in aquatic systems – a literature review. Environmental Pollution 131, 323-336.

Waples, J. S., Nagy, K. L., Aiken, G. R., & Ryan, J. N. (2005). Dissolution of cinnabar (HgS) in the presence of natural organic matter. Geochimica Et Cosmochimica Acta, 69(6), 1575-1588.

Waybrant, K.R., Ptacek, C.J., Blowes, D.W. (2002). Treatment of mine drainage using permeable reactive barriers: column experiments. Envrion. Sci. Technol. 36, 1349-1356.

Weber, F. -., Voegelin, A., & Kretzschmar, R. (2009). Multi-metal contaminant dynamics in temporarily flooded soil under sulfate limitation. Geochimica et Cosmochimica Acta, 73(19), 5513-5527.

Weisener, C.G., Sale, K.S., Smyth, D.J.A., Blowes, D.W. (2005). Field column study using zero valent iron for mercury removal from contaminated groundwater. Environmental Science and Technology 39, 6306-6312.

Wolfenden, S., Charnock, J. M., Hilton, J., Livens, F. R., & Vaughan, D. J. (2005). Sulfide species as a sink for mercury in lake sediments. Environmental Science and Technology, 39(17), 6644-6648.

Yu, R. -., Flanders, J. R., MacK, E. E., Turner, R., Mirza, M. B., & Barkay, T. (2012). Contribution of coexisting sulfate and iron reducing bacteria to methylmercury production in freshwater river sediments. Environmental Science and Technology, 46(5), 2684-2691.

Zhang, C., Sui, J., Li, J., Tang, Y., & Cai, W. (2012). Efficient removal of heavy metal ions by thiol-functionalized superparamagnetic carbon nanotubes. Chemical Engineering Journal, 210, 45-52.

Zhang, H., & Lindberg, S. E. (1999). Processes influencing the emission of mercury from soils: A conceptual model. Journal of Geophysical Research D: Atmospheres, 104(D17), 21889-21896.

Zhang, H., Feng, X., Larssen, T., Shang, L., & Li, P. (2010). Bioaccumulation of methylmercury versus inorganic mercury in rice (oryza sativa L.) grain. Environmental Science and Technology, 44(12), 4499-4504.

Zhao, Y., Chen, Y., Li, M., Zhou, S., Xue, A., & Xing, W. (2009). Adsorption of Hg2+ from aqueous solution onto polyacrylamide/attapulgite. Journal of Hazardous Materials, 171(1-3), 640-646.

Zhu, J., Yang, J., & Deng, B. (2009). Enhanced mercury ion adsorption by amine-modified activated carbon. Journal of Hazardous Materials, 166(2-3), 866-872.

# **Appendix A:** *Supplementary Information for Chapter 2*

Table A.1: Table of bulk sediment elemental analysis

| **Transect** | Sample | Hg | Mn | Fe | Cu | K | Mg | C | S |
|---|---|---|---|---|---|---|---|---|---|
| | | | | μg $g^{-1}$, dry | | | | mg $g^{-1}$, dry | |
| **RRM 0.1** | 6 | 280 | 300 | 16000 | 120 | 820 | 930 | 23.0 | 0.4 |
| | 5 | 29 | 420 | 20000 | 36 | 1300 | 1100 | 21.5 | 0.3 |
| | 4 | 75 | 310 | 17000 | 48 | 1000 | 910 | 18.1 | 0.3 |
| | 3 | 24 | 340 | 29000 | 32 | 2000 | 1200 | 13.0 | 0.4 |
| | 2 | 56 | 320 | 20000 | 57 | 1000 | 870 | 12.7 | 0.4 |
| | 1 | 13 | 140 | 12000 | 29 | 1500 | 710 | 14.5 | 0.2 |
| **RRM 3.5** | E | 44 | 230 | 15000 | 39 | 740 | 810 | 17.3 | 0.3 |
| | F | 24 | 300 | 13000 | 31 | 710 | 1100 | 13.0 | 0.3 |
| | D | 187 | 230 | 16000 | 150 | 760 | 1200 | 19.3 | 0.3 |
| | A | 22 | 130 | 18000 | 28 | 860 | 1500 | 5.23 | 0.4 |
| | C | 11 | 290 | 21000 | 26 | 1400 | 4900 | n/a | n/a |
| | B | 1.1 | 240 | 30000 | 8.1 | 900 | 3300 | 27.2 | 0.7 |

Table A.2: Summary of chemical sequential extraction results in μg $g^{-1}$.

| Step | Extractant | Description | Compounds | SR1 | SR2 | SR3 | SR4 | SR5 | SR6 | A | D | F | E |
|---|---|---|---|---|---|---|---|---|---|---|---|---|---|
| 1 | DI | Water-soluble | $HgCl_2$, $HgSO_4$ | 3.36 | 6.13 | 1.15 | 1.98 | 3.16 | 33.1 | 0.353 | 7.5 | 0.401 | 0.847 |
| 2 | 0.01M HCl + 0.1M CH3COOH | Stomach Acid | HgO, $HgSO_4$ | 0.75 | 0.64 | 3.42 | 2.11 | 1.83 | 11.1 | 0.141 | 0.558 | 0.042 | 0.081 |
| 3 | 1 M KOH | Organo-complexed | $Hg_2Cl_2$, $CH_3Hg$ | 2.64 | 2.06 | 0.6 | 2.27 | 0.98 | 13 | 0.424 | 3.74 | 6.04 | 5.6 |
| 4 | 12 M HNO3 | Elemental | $Hg_2Cl_2$, $Hg^0$ | 6.93 | 29.6 | 11 | 50.1 | 8.18 | 18.9 | 5.83 | 76.2 | 12.4 | 17.1 |
| 5 | Aqua Regia | Hg Sulfides | HgS, HgSe, HgAu | 27.5 | 27.2 | 8.83 | 35.6 | 31.1 | 310 | 0.511 | 125 | 1.21 | 5.8 |
| Total | | | | 41.18 | 65.63 | 25 | 92.06 | 45.25 | 386.1 | 7.26 | 213 | 20.1 | 29.4 |

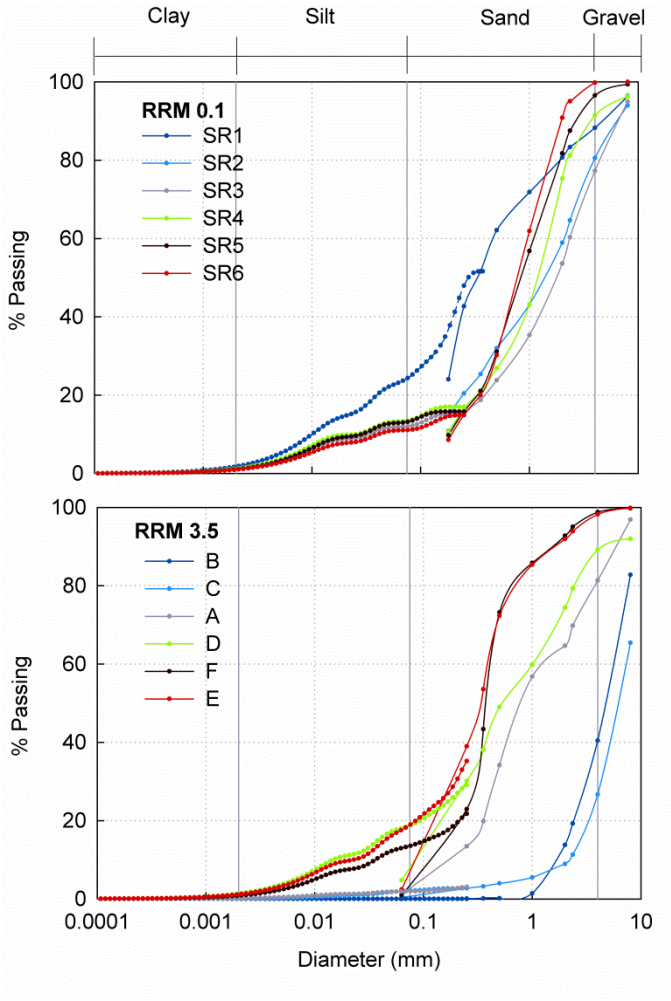


Figure A.1: Grain size distribution curves

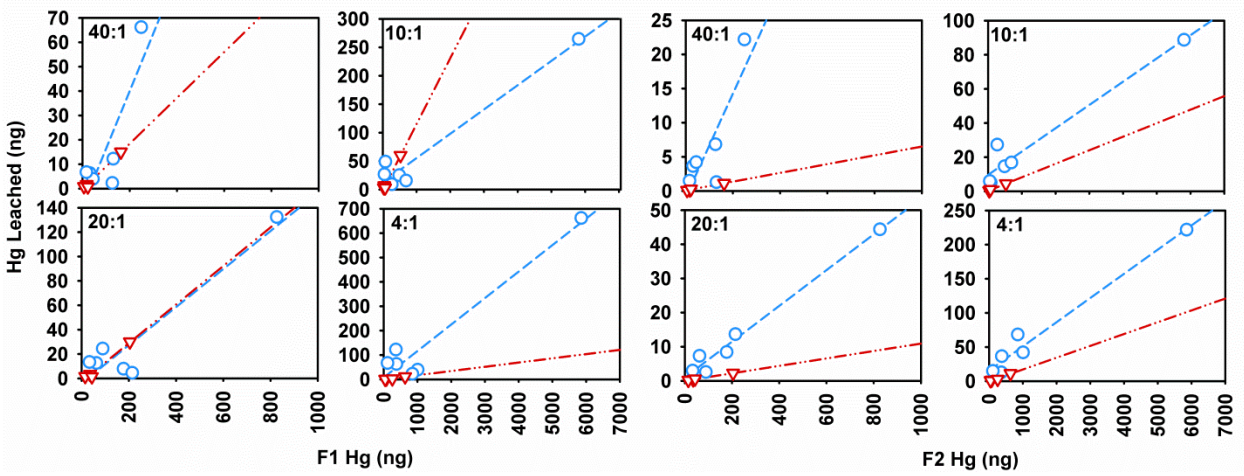


Figure A.2: Correlation plots for resuspension experiments vs sediment masses of water-soluble (F1) and stomach acid soluble (F2) fractions. ○ indicates samples for RRM 0.1, and ▽ indicates samples for RRM 3.5.

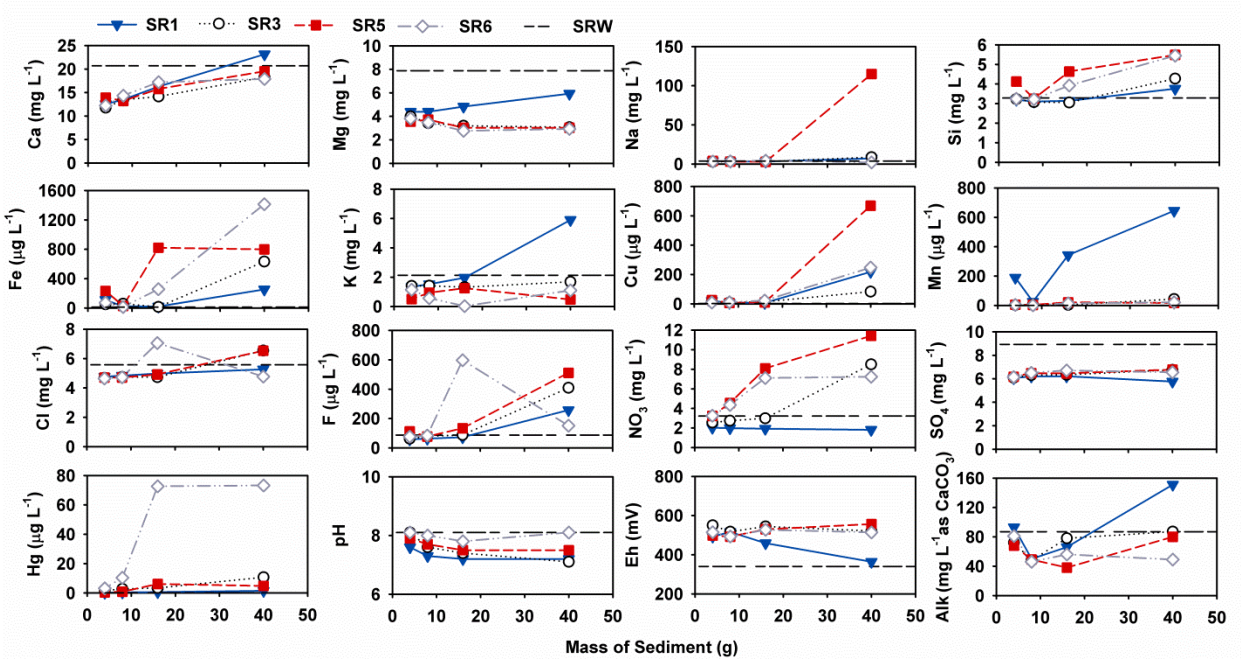


Figure A.3: Supernatant water chemistry from the sediment resuspension experiments.

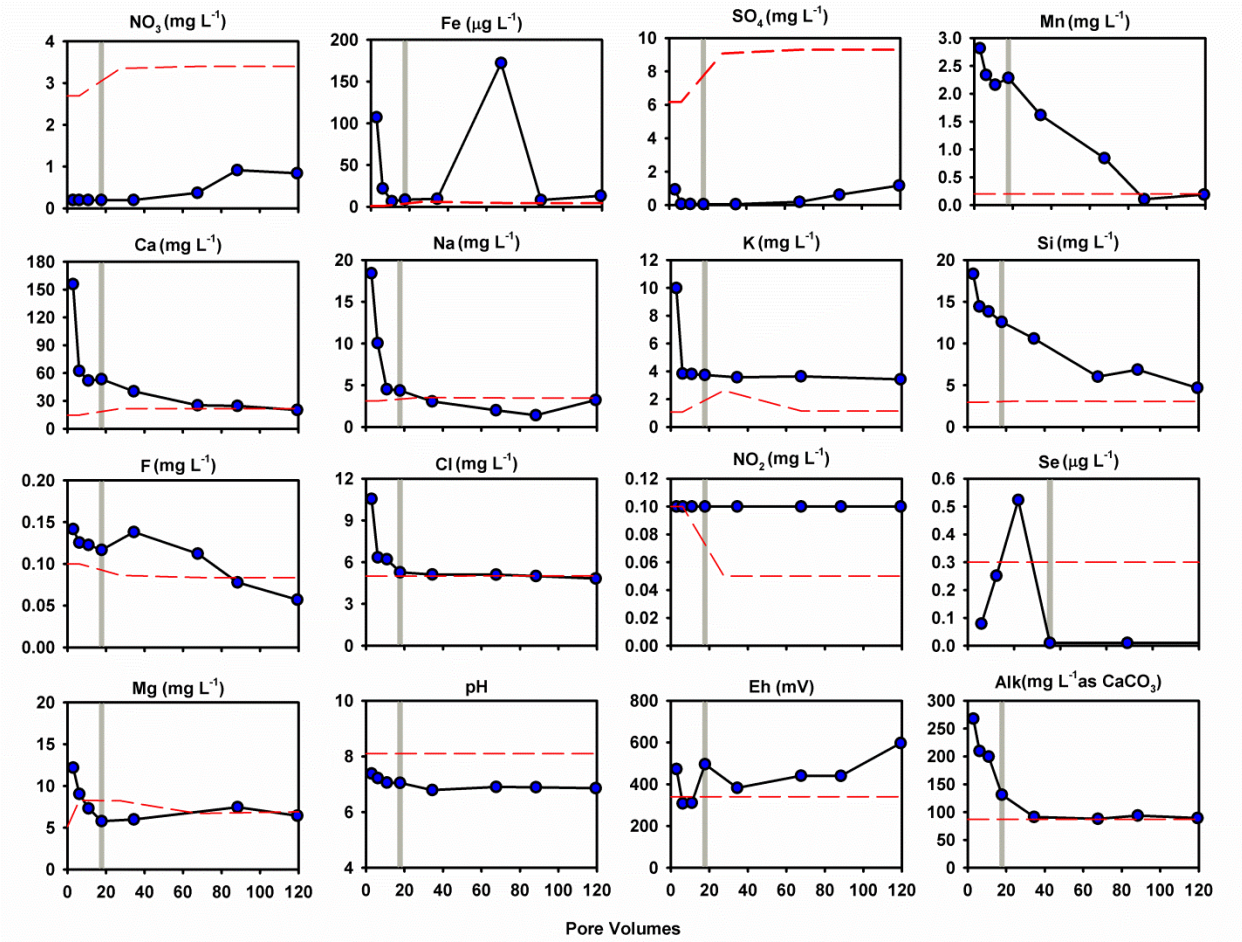


Figure A.4: Water chemistry for SR1 column effluent. Dashed red line represents the SRW influent, the grey bar represents the increase in pump speed from 1 pore volume to 3 pore volumes, and the blue circles represent SR1 column effluent.

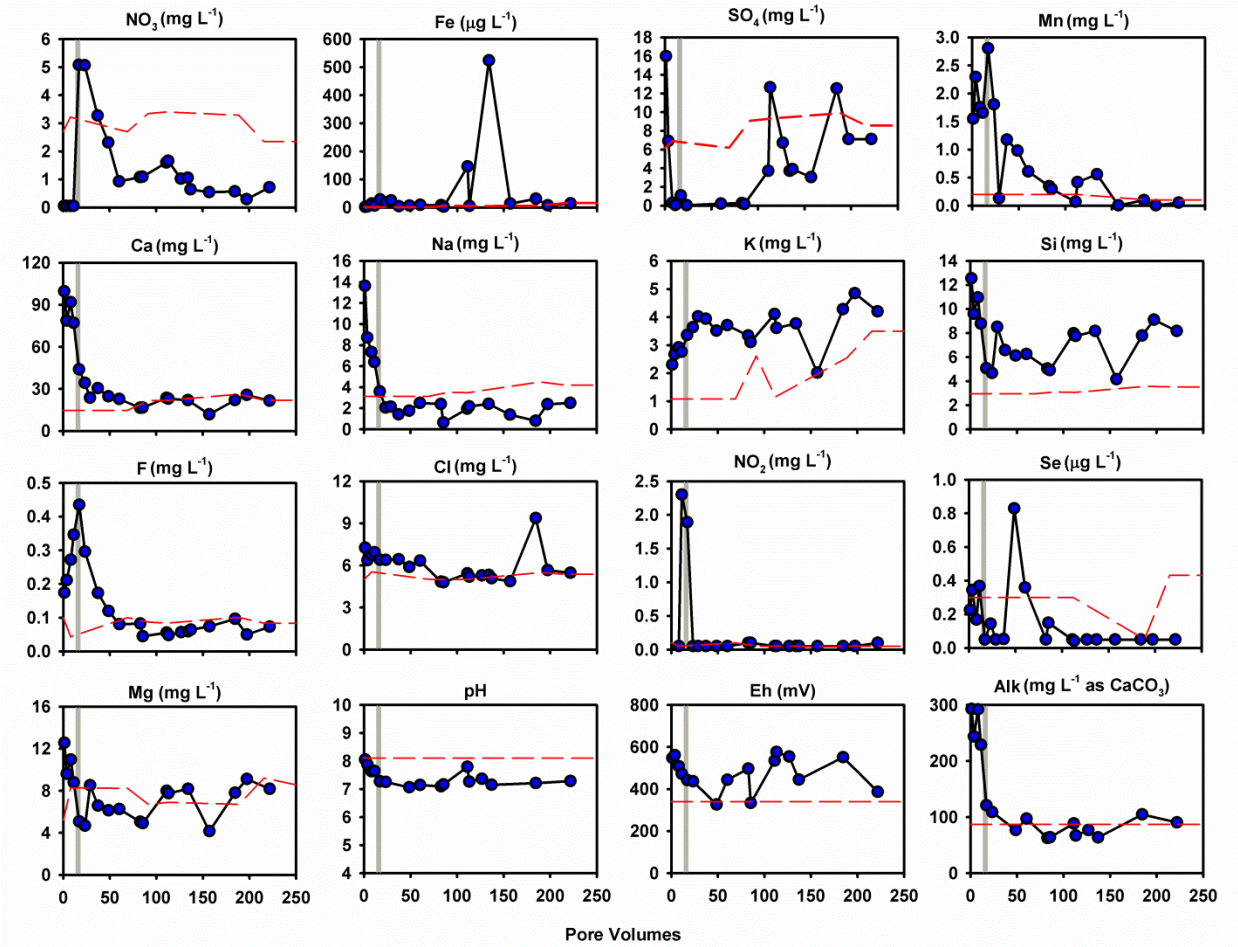


Figure A.5: Water chemistry for SR3 column effluent

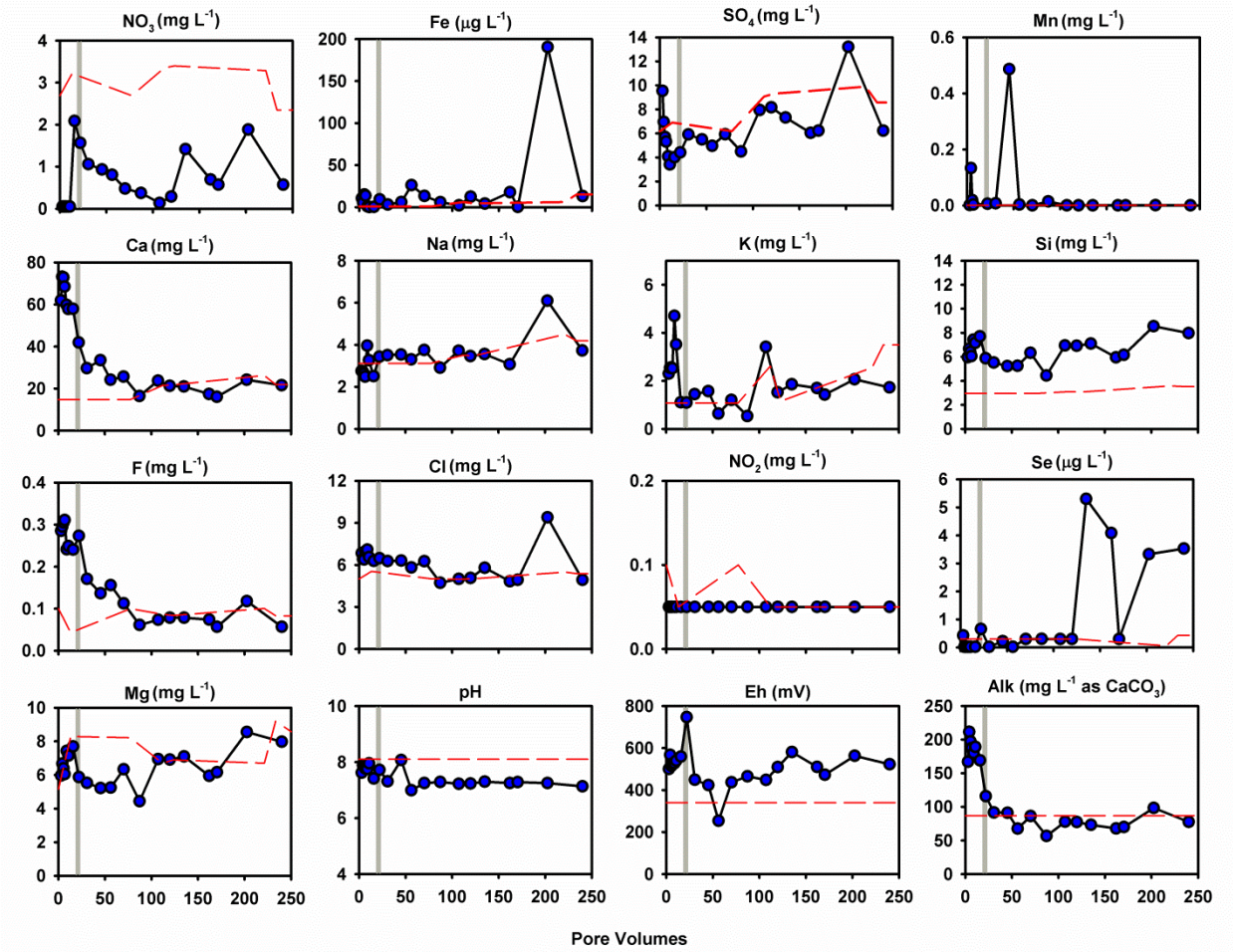


Figure A.6: Water chemistry for SR5 column effluent

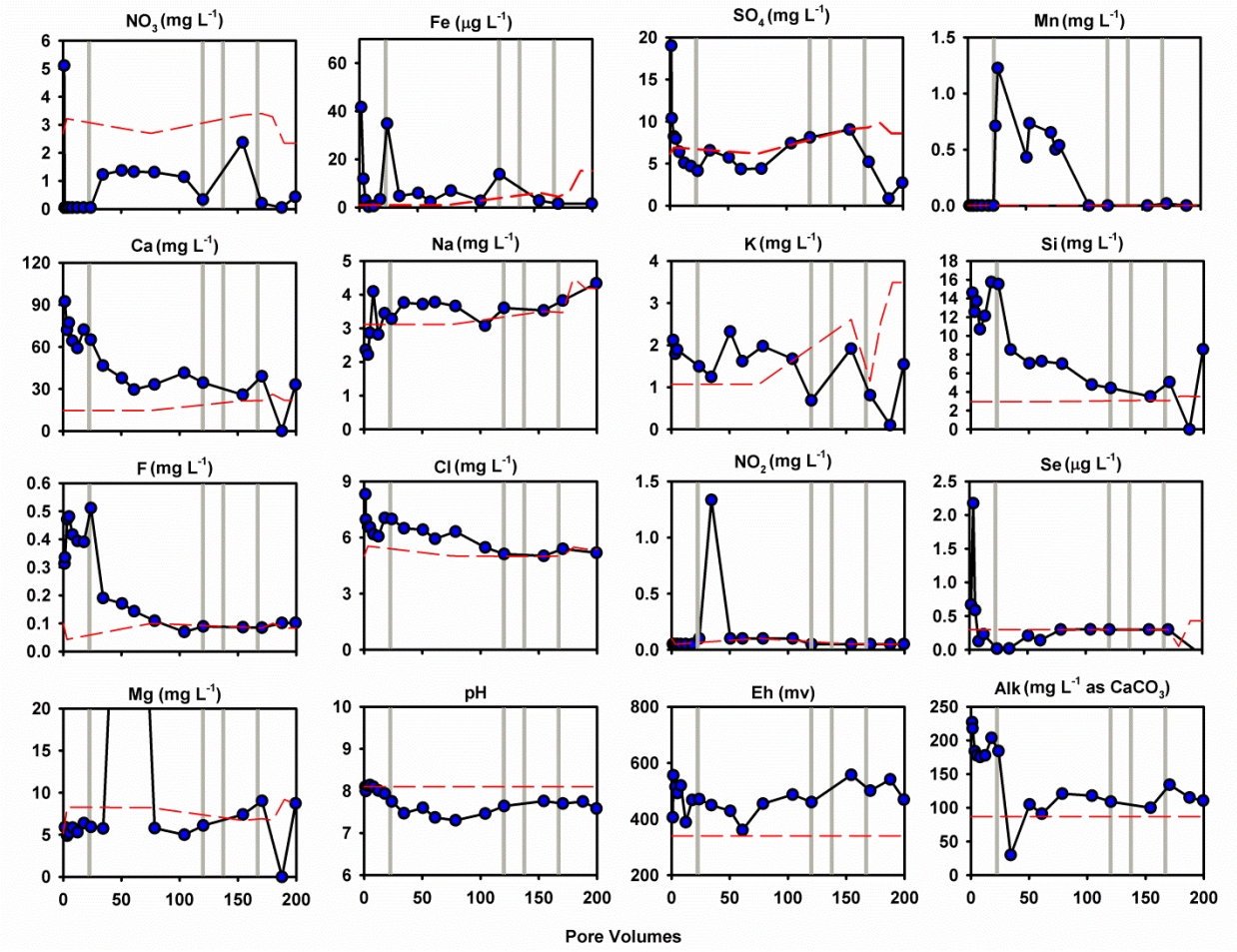


Figure A.7: Water chemistry for SR6 column effluent

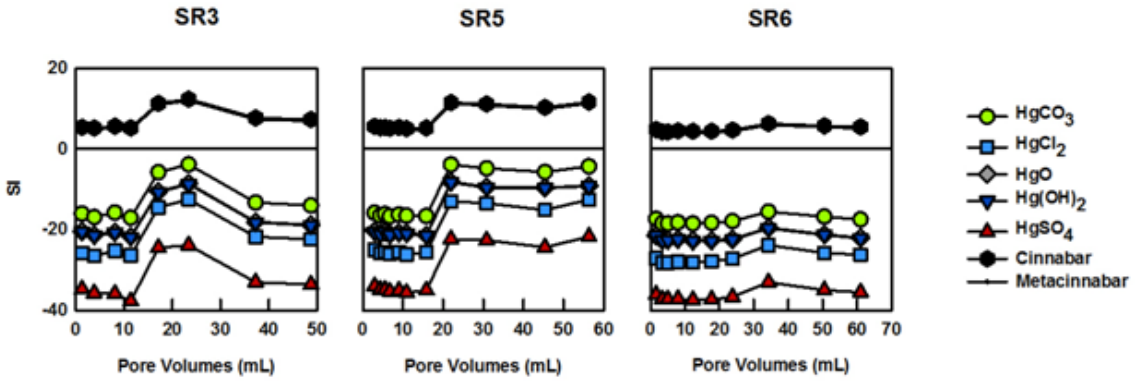


Figure A.8: Saturation indices for Hg compounds in the SR3, SR5 and SR6 column effluent.

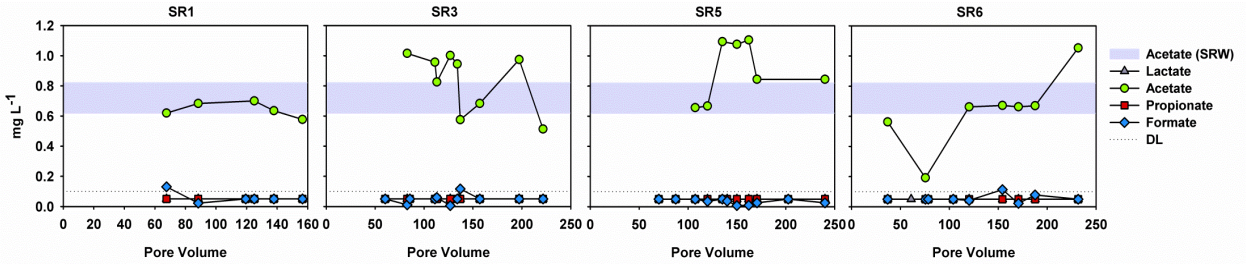


Figure A.9: Concentrations of organic acids in column effluent and SRW

# **Appendix B:** *Supplementary Information for Chapter 3*

Table B.1: Summary of sediment amendment batch experiment water chemistry.

| | Units | SRW | SRW +SR4 | Thiol II | GAC | ZVI | S | ATP | MRM | ATP +Thiol II | ZVI+S | ZVI +ATP | S +ATP | S +MRM |
|---|---|---|---|---|---|---|---|---|---|---|---|---|---|---|
| **pH** | | 8.03 | 7.97 | 4.81 | 8.4 | 7.68 | 7.09 | 8.35 | 7.57 | 7.18 | 6.34 | 8.25 | 7.39 | 8.61 |
| **Eh** | **mV** | 285 | 417 | 304.2 | 406.3 | 275.4 | 443.9 | 397.8 | 394.4 | 285.1 | 463.5 | 424 | 306.1 | 353.8 |
| **Alk** | **$mgL^{-1}$ $CaCO_3$** | 65.5 | 140.0 | 53.1 | 129.2 | 109.5 | 61.8 | 151.2 | 99.9 | 205.0 | 21.1 | 141.4 | 72.5 | 12.7 |
| **Hg** | **$ngL^{-1}$** | 5 | 2036 | 5 | 34 | 308 | 494 | 227 | 169 | 141 | 226 | 301 | 244 | 112 |
| **NO3** | **$mgL^{-1}$** | 4.0 | 30.4 | 26.4 | 13.4 | 19.8 | 0.2 | 29.7 | 3.0 | 0.2 | < 0.2 | 25.9 | 8.8 | < 0.2 |
| **Mn** | **$\mu gL^{-1}$** | 0.2 | 0.6 | 6.0E+04 | 0.5 | 4.1 | 48.2 | 0.3 | 1.8 | 5.5E+03 | 39.5 | 0.7 | 16.4 | 6.1 |
| **Fe** | **$\mu gL^{-1}$** | 9.7 | 9.4 | 1.1E+06 | 13.7 | 25.9 | 14.9 | 7.6 | 6.3 | 21.2 | 13.9 | 9.4 | 36.4 | 9.4 |
| **SO4** | **$mgL^{-1}$** | 7.6 | 9.8 | 19.0 | 65.8 | 9.4 | 163.1 | 13.1 | 130.5 | 309.9 | 284.2 | 10.7 | 235.5 | 293.2 |
| **Cl** | **$mgL^{-1}$** | 6.0 | 5.9 | 15.4 | 11.6 | 5.9 | 6.2 | 6.5 | 412.4 | 7.4 | 6.1 | 6.2 | 6.3 | 227.2 |
| **S** | **$mgL^{-1}$** | 2.8 | 3.8 | 5.1E+03 | 23.0 | 4.1 | 51.8 | 5.2 | 43.0 | 180.3 | 90.7 | 4.6 | 76.3 | 95.5 |
| **Ca** | **$mgL^{-1}$** | 20.9 | 46.5 | 397.7 | 33.4 | 39.8 | 70.0 | 34.8 | 110.2 | 149.6 | 100.3 | 42.1 | 78.8 | 120.5 |
| **Mg** | **$mgL^{-1}$** | 7.5 | 5.4 | 41.3 | 21.3 | 5.0 | 8.4 | 21.4 | 16.9 | 80.2 | 11.8 | 17.3 | 28.4 | 15.9 |
| **K** | **$mgL^{-1}$** | 1.0 | 4.4 | 9.4 | 12.5 | 3.0 | 2.9 | 3.7 | 5.3 | 5.8 | 3.1 | 4.2 | 19.7 | 4.4 |
| **Na** | **$mgL^{-1}$** | 4.2 | 3.9 | 8.4 | 12.4 | 3.5 | 4.0 | 5.4 | 187.2 | 5.1 | 5.0 | 4.5 | 7.1 | 101.1 |
| **Si** | **$mgL^{-1}$** | 3.3 | 6.7 | 75.7 | 3.4 | 5.5 | 7.5 | 4.6 | 6.6 | 9.3 | 9.4 | 4.7 | 7.1 | 8.6 |
| **Ni** | **$\mu gL^{-1}$** | 0.9 | 2.3 | 837.2 | 0.6 | 0.9 | 1.5 | 0.8 | 1.1 | 3.2 | 2.5 | 1.2 | 1.5 | 2.8 |
| **Se** | **$\mu gL^{-1}$** | 0.0 | 0.3 | 6.9 | 2.9 | 2.0 | 2.2 | 2.9 | 3.2 | 2.1 | 1.8 | 2.1 | 3.9 | 3.9 |
| **Zn** | **$\mu gL^{-1}$** | 2.4 | 1.3 | 2.4E+03 | 2.2 | 2.0 | 3.5 | 2.1 | 1.2 | 3.3 | 11.0 | 2.6 | 5.2 | 6.0 |
| **Al** | **$\mu gL^{-1}$** | 4.3 | 4.2 | 5.7E+03 | 37.9 | 3.3 | 2.1 | 1.6 | 0.9 | 5.8 | 0.8 | 3.5 | 15.4 | 1.6 |
| **As** | **$\mu gL^{-1}$** | 1.8 | 0.1 | 4.0 | 2.4 | 1.7 | 0.3 | 2.7 | 2.1 | 1.2 | 1.2 | 2.5 | 1.8 | 1.9 |

Table B.2: Elemental weight % as determined by EDAX for raw reactive materials prior to amending with sediment.

| | ATP | MRM | ZVI | ZVI+S | CL2 | Thiol II | GAC |
|---|---|---|---|---|---|---|---|
| **C** | - | - | - | - | 84 | - | 85 |
| **O** | 40 | 10 | 51 | 19 | 12 | 19 | 7 |
| **Al** | 8 | 1 | - | - | 0.1 | - | 0.2 |
| **K** | 1 | - | - | - | 0.2 | - | |
| **Ca** | 1 | - | - | - | 0.3 | - | 2 |
| **Au** | 8 | - | 7 | 2 | 3 | 6 | 6 |
| **Si** | 31 | 2 | - | - | - | - | 0.1 |
| **Mg** | 6 | - | - | - | - | - | 1.3 |
| **S** | - | 87 | - | 63 | - | 75 | - |
| **Fe** | 5 | - | 42 | 16 | - | - | - |

# **Appendix C:** *Quality Assurance / Quality Control (QA/QC)*

Table C.1: Internally and externally analyzed total aqueous Hg concentrations for a) column effluent experiments and b) sediment resuspension experiments.

| | Sample ID | Date | PV | Company | External THg (ng $L^{-1}$) | Internal THg (ng $L^{-1}$) |
|---|---|---|---|---|---|---|
| **A) Column Effluent Samples** | | | | | | |
| SR1 | ACC1-2 | 19-Oct-10 | 1 | Quicksilver | 78 | 99 |
| | ACC1-51 (0.1f) | 02-Aug-11 | 91 | UWO | 33 | 33 |
| | ACC1-51 (2) f | 02-Aug-11 | 91 | UWO | 32 | 33 |
| | ACC1-51 (5000MWCO) | 02-Aug-11 | 91 | UWO | 21 | 47 |
| | ACC1-51 unf | 02-Aug-11 | 91 | UWO | 31 | 36 |
| | ACC1-61 | 27-Oct-11 | 132 | UWO | 18 | 41 |
| SR3 | ACC3-41 | 06-Oct-10 | 49 | Quicksilver | 2770 | 3379 |
| | ACC3-58 | 06-Apr-11 | 113 | UWO | 320 | 313 |
| | ACC3-62 | 19-Jul-11 | 156 | UWO | 175 | 397 |
| SR5 | ACC5-104 | 05-Oct-11 | 197 | UWO | 20 | 47 |
| | ACC5-51 | 06-Oct-10 | 56 | Quicksilver | 104 | 204 |
| | ACC5-72 f | 22-Feb-11 | 107 | UWO | 31 | 58 |
| | ACC5-95 (0.1f) | 02-Aug-11 | 174 | UWO | 13 | 13 |
| | ACC5-95 (2) f | 02-Aug-11 | 174 | UWO | 22 | 28 |
| | ACC5-95 unf | 02-Aug-11 | 174 | UWO | 29 | 58 |
| SR6 (1) | ACC6-112 | 27-Oct-11 | 218 | UWO | 335 | 680 |
| | ACC6-47 | 10-Jun10 | 61 | Quicksilver | 3780 | 4669 |
| | ACC6-84 f | 28-Mar-11 | 171 | UWO | 1013 | 889 |
| SR6 (2) | LC6-13 | 26-Jul-11 | 17 | UWO | 6556 | 11566 |
| | LC6-14 (0.1f) | 03-Aug-11 | 21 | UWO | 8059 | 7868 |
| | LC6-14 (5000MWCO) | 03-Aug-11 | 21 | UWO | 3035 | 1693 |
| | LC6-14 f | 03-Aug-11 | 21 | UWO | 8683 | 9435 |
| | LC6-14 unf | 03-Aug-11 | 21 | UWO | 9307 | 13657 |
| SR3 Treatment | ACCL2-36 unf | 3-Aug-11 | 64 | UWO | 47 | 3 |
| | ACCL2-36 0.1f | 3-Aug-11 | 64 | UWO | 8 | 2 |
| | ACCL2-36 0.45f | 3-Aug-11 | 64 | UWO | 10 | 3 |
| SR6 Treatment | ATCCL2-16 | 04-Oct-11 | 22 | UWO | 70 | 70 |
| | ATCCL2-22 | 31-Oct-11 | 33 | UWO | 82 | 109 |
| Anaerobic SR6 | ANC6-3 | 22-Jul-11 | 3 | UWO | 16000 | 21469 |
| | ANC6-5 (0.1f) | 3-Aug-11 | 6 | UWO | 10983 | 13831 |
| | ANC6-5 (2) f | 3-Aug-11 | 6 | UWO | 12239 | 16539 |
| | ANC6-5 (5000MWCO) | 3-Aug-11 | 6 | UWO | 887 | 1189 |
| | ANC6-5 unf | 3-Aug-11 | 6 | UWO | 6779 | 18672 |
| | ANC6-10 | 23-Aug-11 | 13 | UWO | 8595 | 12046 |

| | Sample ID | Date | PV | Company | External THg (ng $L^{-1}$) | Internal THg (ng $L^{-1}$) |
|---|---|---|---|---|---|---|
| | ANC6-15 | 09-Sep-11 | 20 | UWO | 279 | 339 |
| | ANC6-22 | 03-Oct-11 | 30 | UWO | 6012 | 7556 |
| | ANC6-25 | 14-Oct-11 | 34 | UWO | 703 | 944 |
| | ANC6-27 | 20-Oct-11 | 36 | UWO | 763 | 772 |
| | ANC6-29 | 03-Nov-11 | 41 | UWO | 628 | 733 |
| **B) Resuspension Supernatant Samples** | | | | | | |
| SR1 | AET3M-SR1B | 29-Jan-10 | - | SGS | 1000 | 1300 |
| | AET4M-SR1A | 09-Nov-09 | - | SGS | 1000 | 300 |
| SR3 | AET2-SR3A | 06-Oct-09 | - | SGS | 12000 | 14600 |
| | AET3M-SR3A-20R | 26-Jan-10 | - | SGS | 2000 | 2700 |
| | AET5M-SR3A-R10 | 26-Jan-10 | - | SGS | 1000 | 300 |
| SR5 | AET5M-SR5A | 13-Nov-09 | - | SGS | 1000 | 1212 |
| | AET7-SR5A | 17-Jul-09 | - | SGS | 8000 | 7200 |
| SR6 | AET3M-SR6A-R10F | 13-Nov-09 | - | SGS | 65000 | 72000 |
| | AET3-SR6A | 15-Jul-09 | - | SGS | 108000 | 119000 |
| | AET4M-SR6A | 13-Nov-09 | - | SGS | 7000 | 6980 |
| | AET4-SR6A-R10A | 17-Jul-09 | - | SGS | 6000 | 4300 |
| | AET5M-SR6A | 13-Nov-09 | - | SGS | 4000 | 4300 |
| | AET5M-SR6A-R10 | 07-Jan-10 | - | SGS | 1000 | 2770 |
| | AET7-SR6A | 17-Jul-09 | - | SGS | 110000 | 125600 |
| | AET8-SR6A | 16-Jul-09 | - | SGS | 58000 | 97100 |

Table C.2: Internally and externally analyzed total solid-phase Hg concentrations for riverbank sediment samples.

| Sediment Sample | THg (µg $g^{-1}$) | |
|---|---|---|
| | Sediment Digestion (SGS) | Sequential Extraction (Frontier) |
| SR-6 | 280 | 386 |
| SR-5 | 29 | 45 |
| SR-4 | 75 | 92 |
| SR-3 | 24 | 25 |
| SR-2 | 56 | 66 |
| SR-1 | 13 | 41 |
| SR-E | 44 | 29 |
| SR-F | 24 | 20 |
| SR-D | 187 | 213 |
| SR-A | 22 | 7 |

Table C.3: Charge balance errors for a) column effluent and b) treatment batch experiment solutions.

| **A) Column Experiments** | | | | | | | |
|---|---|---|---|---|---|---|---|
| ACC1 (PV) | CBE (%) | ACC3 (PV) | CBE (%) | ACC5 (PV) | CBE (%) | ACC6 (PV) | CBE (%) |
| 2.9 | 36.1 | 1.3 | 10.3 | 2.9 | 9.9 | 1.6 | 36.2 |
| 6.2 | 9.3 | 3.8 | 8.9 | 4.3 | 43.2 | 3.4 | 17.3 |
| 10.9 | 1.2 | 8.1 | 8.2 | 5.5 | 17.7 | 5.0 | 14.0 |
| 17.8 | 20.6 | 11.4 | 11.0 | 6.7 | 10.8 | 8.0 | 5.3 |
| 34.5 | 25.7 | 17.1 | 7.0 | 9.0 | 9.2 | 12.3 | -1.5 |
| 67.6 | 8.5 | 23.4 | 0.7 | 10.9 | 4.9 | 17.7 | 7.1 |
| 88.4 | 3.3 | 60.2 | 11.4 | 15.8 | 7.0 | 34.3 | 18.0 |
| 119.4 | 2.6 | 82.7 | -11.1 | 22.0 | 12.8 | 50.5 | 80.9 |
| | | 85.5 | 5.8 | 30.8 | 12.2 | 61.0 | 1.9 |
| | | 111.1 | 19.7 | 56.3 | 14.3 | | |
| | | 113.1 | 0.8 | 70.2 | 6.9 | | |
| | | 134.0 | 18.4 | 87.3 | 22.4 | | |
| | | 157.0 | -17.6 | 107.3 | 11.7 | | |
| | | 184.6 | 9.6 | 119.9 | 6.4 | | |
| | | 197.3 | 6.0 | 135.1 | 6.6 | | |
| | | 221.7 | 4.1 | 162.1 | 4.0 | | |
| | | | | 170.5 | -3.9 | | |
| | | | | 202.5 | -0.5 | | |
| | | | | 240.0 | 10.4 | | |
| | | | | | | | |
| **B) Treatment Batch Experiments** | | | | | | | |
| SRW | 5.2 | | | | | | |
| SRW+SR4 | -23.2 | | | | | | |
| THIOL II | 90.5 | | | | | | |
| GAC | -5.8 | | | | | | |
| ZVI | -15.5 | | | | | | |
| S | -2.1 | | | | | | |
| ATP | -14.4 | | | | | | |
| MRM | -3.4 | | | | | | |
| THIOL II + ATP | 22.5 | | | | | | |
| ZVI+S | -1.6 | | | | | | |
| ZVI+ATP | -9.0 | | | | | | |
| S+ATP | 1.5 | | | | | | |
| S+MRM | -4.0 | | | | | | |

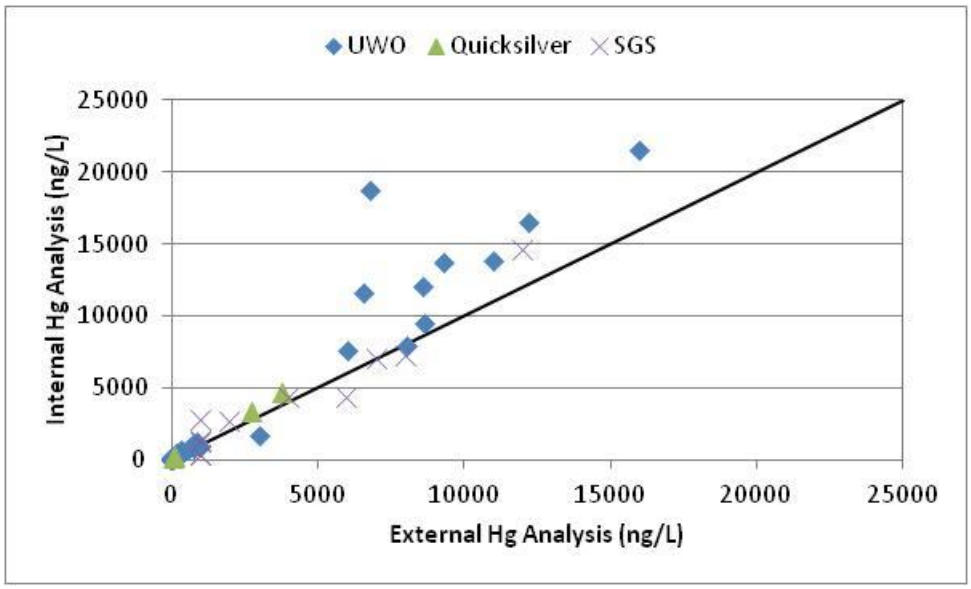


Figure C.1: Correlation of internal (University of Waterloo) versus external laboratory total aqueous Hg concentrations.